Esther Bonacker

Perturbed Projection Methods in Convex Optimization – Applied to Radiotherapy Planning

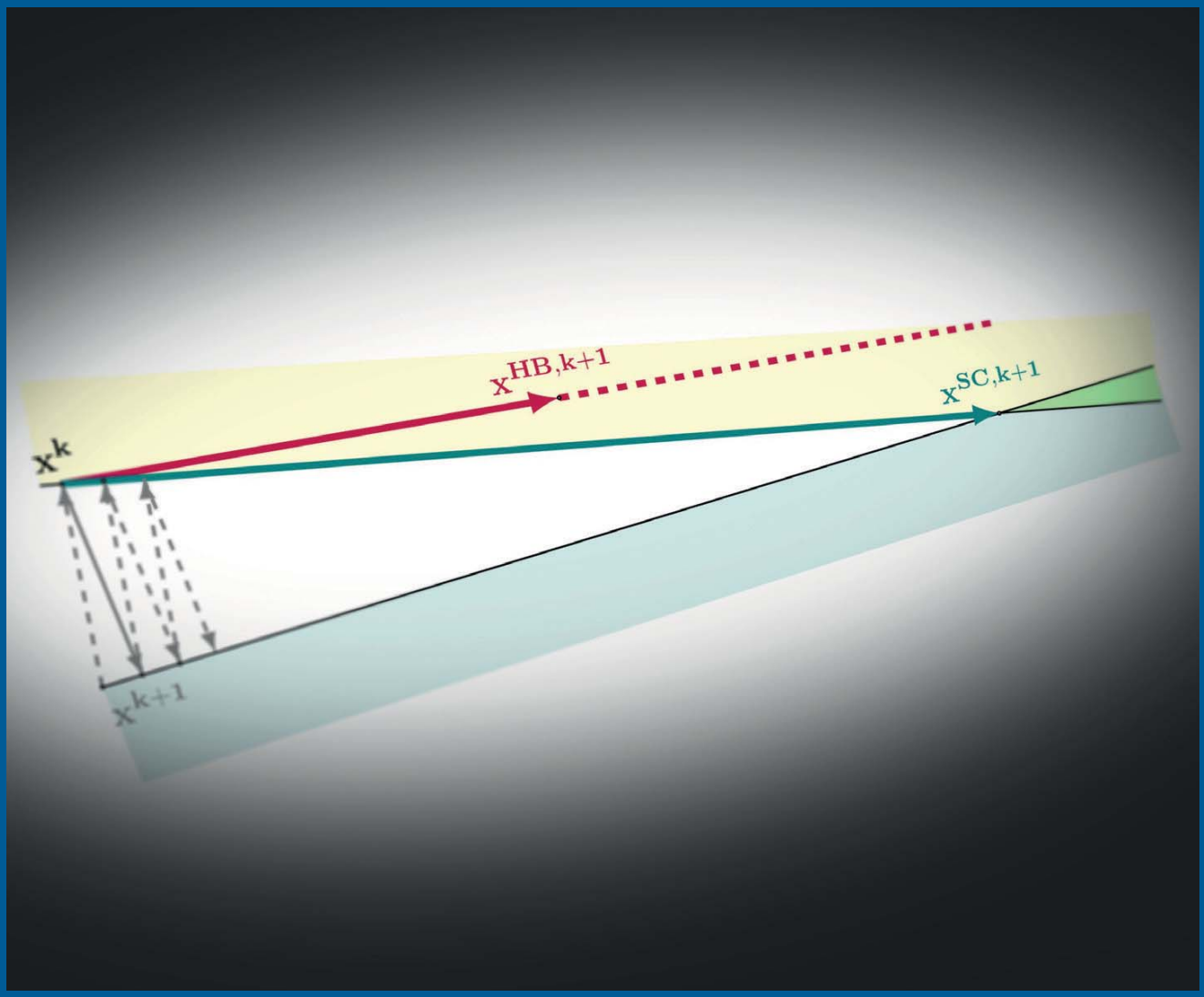

Technische Universität Kaiserslautern

Fraunhofer ITWM

Fraunhofer-Institut für
Techno- und Wirtschaftsmathematik ITWM

Perturbed Projection Methods in Convex Optimization – Applied to Radiotherapy Planning

Esther Bonacker

FRAUNHOFER VERLAG

Kontakt:
Fraunhofer-Institut für Techno- und Wirtschaftsmathematik ITWM
Fraunhofer-Platz 1
67663 Kaiserslautern
Telefon +49 631/31600-0
Fax +49 631/31600-1099
E-Mail info@itwm.fraunhofer.de
URL www.itwm.fraunhofer.de

Bibliografische Information der Deutschen Nationalbibliothek
Die Deutsche Nationalbibliothek verzeichnet diese Publikation in der Deutschen Nationalbibliografie; detaillierte bibliografische Daten sind im Internet über http://dnb.d-nb.de abrufbar.
ISBN (Print): 978-3-8396-1529-4

D 386

Zugl.: Kaiserslautern, TU, Diss., 2019

Titelbild: © Esther Bonacker

Druck: Mediendienstleistungen des
Fraunhofer-Informationszentrum Raum und Bau IRB, Stuttgart

Für den Druck des Buches wurde chlor- und säurefreies Papier verwendet.

Fraunhofer-Informationszentrum Raum und Bau IRB
Postfach 80 04 69, 70504 Stuttgart
Nobelstraße 12, 70569 Stuttgart
Telefon 07 11 9 70-25 00
Telefax 07 11 9 70-25 08
E-Mail verlag@fraunhofer.de
URL http://verlag.fraunhofer.de

Perturbed projection methods in convex optimization – applied to radiotherapy planning

Vom Fachbereich Mathematik der
Technischen Universität Kaiserslautern
zur Verleihung des akademischen Grades
Doktor der Naturwissenschaften
(Doctor rerum naturalium, Dr. rer. nat.)
genehmigte

Dissertation

von

Esther Bonacker

1.Gutachter: Prof. Dr. Karl-Heinz Küfer
2.Gutachter: Prof. Yair Censor

Datum der Disputation: 11. Juli 2019

D386

Danksagung

Die vorliegende Arbeit ist mit finanzieller Unterstützung der Abteilung Optimierung des Fraunhofer Instituts für Techno- und Wirtschaftsmathematik ITWM in Kaiserslautern entstanden.

Mein besonderer Dank gilt meinem Doktorvater Prof. Dr. Karl-Heinz Küfer für seine Unterstützung und wertvollen Anregungen während der Anfertigung meiner Dissertation sowie für die Möglichkeit ein herausforderndes und überaus interessantes Thema bearbeiten zu können. Für viele fachliche Diskussionen und Hilfe beim Einstieg in die umfangreiche Anwendungsthematik meiner Arbeit bedanke ich mich ganz herzlich bei Dr. Philipp Süss und Dr. Katrin Teichert. Ein großer Dank gebührt auch meinen Kolleginnen und Kollegen der Abteilung Optimierung im Fraunhofer ITWM für die positive Arbeitsatmosphäre und ihre Hilfsbereitschaft bei jeglichen Belangen sowie Jasmin Kirchner für ihre wertvolle Unterstützung bei organisatorischen Aufgaben.

Ich war während der vergangenen vier Jahre in der glücklichen Situation, nicht nur am Fraunhofer ITWM, sondern auch von Dr. Aviv Gibali am ORT Braude College in Israel betreut zu werden. Ihm danke ich sehr herzlich für die positive und konstruktive Zusammenarbeit bei unseren gemeinsamen Publikationen, viele interessante fachliche Diskussionen, hilfreiche Anregungen sowie für seine warmherzige Gastfreundschaft bei meinen Aufenthalten in seinem Heimatland Israel.

Für das Korrekturlesen meiner Arbeit und wertvolle Anregungen zur Darstellung der Inhalte meiner Arbeit danke ich vielmals meinen Kolleginnen und Kollegen Dr. Cristina Collicott, Helene Krieg, Rasmus Schröder, Tobias Seidel, Dr. Philipp Süss, Dr. Katrin Teichert und Dr. Christian Weiß. Helene Krieg und Tobias Seidel gebührt darüber hinaus eine besondere Auszeichnung für unermüdliche Diskussionen über Skalarprodukte und Hyperebenen.

Nicht zuletzt danke ich von Herzen meinen Eltern und Freunden, deren Zuspruch, Geduld und Unterstützung es mir ermöglicht haben, an dieser Arbeit über mich hinauszuwachsen.

Abstract

This thesis is motivated by the treatment planning problem in intensity modulated radiation therapy (IMRT). The IMRT planning problem, like many others arising in real life applications, is a convex constrained multicriteria optimization problem. In this thesis we tackle the task of minimizing multiple objective functions in two different ways. We either optimize them in a lexicographic way, ranked according to their importance, or accumulate the objectives in a weighted sum. Both approaches yield one or several convex single criteria optimization problems. Our strategy to solve the resulting single criteria optimization problems in an approximate way is to translate them into a sequence of convex feasibility problems via the level set scheme and then solve each feasibility problem using projection methods.

Characteristics of some real life problems, in particular IMRT treatment planning, are challenging to this strategy. Our focus in this thesis are two of these challenges. Depending on the correlation of the objective functions a solution of one lexicographic optimization level picked by the solution algorithm might be far less favorable with respect to the objective function of the next level than a different solution. Additionally, projection methods often exhibit zigzagging behavior when the problem is ill-conditioned. Both phenomena lead to slow convergence of the overall procedure.

To mitigate these disadvantages, we exploit the fact that projection methods are bounded perturbation resilient. We accelerate lexicographic optimization via superiorization, which is a special kind of perturbation, with respect to the objective function of the next optimization level. The zigzagging behavior of the projection methods is avoided by three new perturbations we introduce. Two of these perturbations use gradient information from previous iterates in the spirit of k-step methods. The third perturbation uses the approach of surrogate constraint methods combined with relaxed, averaged projections.

We study both the theoretical and computational impact of the suggested perturbed iteration schemes. The most important new theoretical result presented in this context states that the third perturbation guarantees a significantly bigger minimum progress per iteration than the simultaneous subgradient projection method when subsequent simultaneous projection steps are strongly opposing.

We demonstrate our methods on linear examples and also apply them to nonlinear optimization problems arising from IMRT treatment planning on cases where the tumor is situated in the head-neck area. We present two different choices of superiorization parameter sets suited to yield fast convergence for each case individually or robust behavior for all four cases. Furthermore we illustrate that the anti-zigzag perturbations can significantly accelerate the convergence of the projection methods. For the IMRT optimization problems the perturbed projection methods find an approximate solution within up to 84.1% fewer iterations than the unperturbed methods while at the same time achieving objective function values which are up to 5.2% lower.

Contents

1 Introduction

One of the most important methods in modern cancer treatment is intensity modulated radiation therapy (IMRT). For this method it is crucial that the dose is targeted in such a way that the tumor volume receives high dose values while surrounding healthy tissue is spared as much as possible. The IMRT treatment is carried out using high energy photon beams, which are produced by a linear accelerator and delivered the the patient's body by multiple beams coming from different directions. With so-called multi-leaf collimators the fluence intensities emerging from the beam surface can be modulated in order to shape the resulting dose distribution in the patient's body in such a way that tumor volumes are irradiated with a sufficiently high dose to destroy the tumor and at that the same time surrounding healthy organs are spared as much as possible.

Mathematical optimization in IMRT treatment planning has been a long-standing and fruitful area of research [17, 67, 35, 24, 39, 36, 45, 46, 57]. Different branches of this research are concerned with various aspects of optimizing treatment plans. The IMRT optimization problem as phrased it in this thesis is to find values of fluence intensities for an individual patient, which result in a dose distribution that best fulfills the clinical goals formulated by the physician. Since there are usually several goals and some goals can be in conflict with each other, the decision of which treatment plan should be chosen must be based on multiple relevant criteria.

Translated to mathematics finding a good IMRT treatment plan corresponds to solving a constrained multicriteria optimization problem. We use convex functions to model the IMRT planning problem and therefore consider it in this thesis as a convex constrained multicriteria optimization problem.

A priori it is not clear what it means to minimize more than one objective function. There are numerous ways to tackle this question, see e.g. [48]. In this thesis we present two approaches, which are similar in one main aspect: The multicriteria problem is transformed into one ore more single criteria problems.

The first approach is very common: We accumulate the objectives in a new function, for example a weighted sum. If the accumulation keeps the convexity intact, we end up with a single criteria optimization problem. Often the function accumulating the values of the objective functions is chosen as a weighted sum. If multiple of these single criteria optimization problems with different weights for the accumulating weighted sum are solved to optimality, we get multiple points of the so-called pareto front, which is the set of all pareto optimal solutions to the multicriteria optimization problem. The standard procedure in modern IMRT planning software used in clinics is to calculate multiple points on the pareto front and to offer the treatment planner to choose from these solutions or combinations of them. However, the multitude of possible solutions and the high dimensionality of the pareto front are often challenging to grasp.

The second approach is lexicographic optimization, which requires an importance-ranking on the objective functions. This ranking, the so-called lexicographic order, is often known in an

intuitive way by the IMRT treatment planners and can be used together with lexicographic optimization to simplify the decision process. According to the lexicographic order, several single criteria constrained optimization problems, which are called optimization levels, are formulated. In the first optimization level the most important objective function is to be minimized under the constraints of the original multicriteria problem. In the second level the second most important objective is minimized under the original constraints plus the constraint that the value of the most important objective function does not deviate at all or only by a small amount from its minimum value from the first level. The procedure continues in this way until all levels are solved.
When applying either of these approaches to optimization problems arising from IMRT planning, one typically encounters several difficulties, two of which are the focus of this thesis.
The first challenge is the ill-conditionedness of IMRT optimization problems, which has been discussed e.g. in [1, 12], together with the fact that adjacent volumes in the patient's body often have conflicting dose prescriptions. The tumor volume for example requires a high uniformly distributed dose while the maximum dose in the spinal cord may not exceed a certain threshold if severe side effects are to be avoided. Due to physical reasons the dose falloff over small distances is limited, which leads to a situation where it is impossible to fulfill these conflicting dose prescriptions at the same time and we encounter strongly opposing gradients of the functions corresponding to the goals of fulfilling the dose prescriptions. Under these circumstances many optimization algorithms, especially those which rely only on first order derivative information, exhibit zigzagging behavior and therefore slow convergence.
The second challenge arises in lexicographic optimization if the set of solutions to one of the optimization levels has more than one element. In that case it may happen that a solution algorithm picks a solution for one level, that is unfavorable with respect to the objective function of the next. On the other hand a n alternative solution to the former level may have been closer to the optimum of the latter one. This phenomenon, too, may lead to slow convergence.

In this thesis we use the level set scheme [32] to solve single criteria optimization problems. This scheme transforms a convex optimization problem into a sequence of convex feasibility problems, by introducing a decreasing sequence of upper bounds on the objective function. Thereby the objective function is transformed into in additional constraint and the problem of minimizing the objective function is translated into finding elements of the intersection of the feasible sets corresponding to each constraint. The feasibility problems are then solved by a suitable algorithmic operator. Our choices for this operator are two different projection methods: The cyclic and the simultaneous subgradient projection method.
Projection methods are desirable in this context, because they are not only a successful class of algorithms to solve convex feasibility problems, but also bounded perturbation resilient. Bounded perturbation resilience is a relatively general concept introduced in [11] for general mathematical problems and iterative operators, which are suited to solve them. An iterative operator being bounded perturbation resilient means that the iteration process can be disturbed in one of two ways at each step: By adding a bounded perturbation vector to either the iterate to which the operator then is applied or to the result of applying the operator to the unperturbed iterate. If for a given starting point the sequence of iterates generated by the unperturbed iteration scheme converges to a solution of the mathematical problem, the perturbed iteration scheme will do so as well.

For each described difficulty we present a way to mitigate it by exploiting the bounded perturbation resilience of projection methods in a way which is innovative in the field of IMRT optimization.

The first way is superiorization, which is a recently developed methodology [38]. It is a special way of using perturbations where they steer the sequence of iterates into a direction, which is advantageous with respect to a so-called superiorization function. We utilize this approach to steer the iteration process of the simultaneous subgradient projection method used in lexicographic optimization into a direction, which is favorable with respect to the objective function of the next optimization level. Thereby we aim to find a solution of the current optimization level, which is close to the minimizer(s) of the next level.

The second way of using perturbations we present is as anti-zigzag strategy. We derive them from methods, which are known to alleviate zigzagging behavior and use those ideas to formulate perturbations, which can be used to do the same. In this thesis we present perturbations which use the approaches of the heavy ball method by Polyak [56], the Nesterov Acceleration Method [52] and a method by Dudek [30], which blends the idea of surrogate constraint methods with relaxed, averaged projections.

Our numerical results demonstrate that our strategies can indeed mitigate the two aforementioned challenges in IMRT optimization: We are able to accelerate the convergence of the lexicographic optimization process by at least 4.6% and at most 33.8% (with an average of 12.2%) by using superiorization. Also the perturbed projection methods using our anti-zigzag perturbations converge faster than their unperturbed counterparts the majority of times. The perturbed simultaneous subgradient projection method finds the solution with the minimal objective value after 15.9-86.7% (with an average of 41.5%) of the number of iterations its unperturbed counterpart needs.

Our theoretical results imply that the worst case progress made by the perturbed simultaneous subgradient projection method using the surrogate constraint perturbation is significantly bigger than the worst case progress made by its unperturbed counterpart when the subsequent simultaneous subgradient projection steps are strongly opposing.

The remainder of this thesis is organized as follows.

In Chapter 2 we briefly introduce the methods and concept applied in this thesis. We focus on the level set scheme, projection methods, perturbations in general and in the special form of superiorization. Furthermore we present some new theoretical results on perturbations and bounded perturbation resilient operators.

Details on IMRT and modeling the IMRT optimization problem in a mathematical way are presented in Chapter 3. We describe briefly how the dose distribution resulting from the chosen fluence intensity values is calculated, which functions we use to evaluate the dose distribution inside a specific volume and elaborate on which difficulties arise in IMRT optimization due to the physical circumstances of the procedure itself.

In Chapter 4 the aforementioned difficulty in lexicographic optimization is addressed. Here, we use superiorization to find solutions of the current optimization level, which are also favorable with respect to the objective function of the next level. In Section 4.1 we elaborate on how to implement the idea of lexicographic optimization and superiorization in an algorithm we call superiorized lexicographic optimization. In Section 4.2 we present numerical results from a linear problem to illustrate the mechanism of our method and also results from the nonlinear setting of IMRT optimization.

In Chapter 5 we present the second way of using perturbations to alleviate difficulties arising in IMRT optimization: As anti-zigzag strategy. We begin the chapter with a detailed description of our algorithm, which we call the perturbed level set scheme. In Section 5.2 we then illustrate and quantify the zigzagging behavior we encounter in IMRT optimization. In Section 5.3 we introduce three new perturbations developed by us and show that they are bounded. In Section 5.4 we prove theoretical results on the convergence of the perturbed simultaneous subgradient projection method. Numerical results are presented in Section 5.6, both for a linear feasibility problem in order to illustrate the methods and for IMRT optimization problems. We also compare the actual convergence of the methods to the theoretical results presented before in Section 5.4. Finally, in Section 5.7 we elaborate on the computational effort needed to apply the perturbed simultaneous subgradient projection in IMRT optimization compared to its unperturbed counterpart.
We conclude in Chapter 6 with a summary and a short outlook on possible future research directions.

2 Mathematical preliminaries

2.1 The general multicriteria convex constrained optimization problem

In many applications we encounter the problem of minimizing multiple convex functions $f_s : \mathbb{R}^n \to \mathbb{R}, s \in S = \{1, ..., r\}$ such that convex constraints $g_j : \mathbb{R}^n \to \mathbb{R}, j \in J = \{1, ..., m\}$ are fulfilled.

$$\begin{aligned} &\text{Minimize } F(x) := (f_s)_{s \in S} \\ &\text{s.t. } g_j(x) \leq 0 \qquad \forall j \in J \end{aligned} \tag{2.1}$$

where $F(x)$ is the vector of the values $f_s(x)$ for all $s \in S$.
It is not clear a priori what it means to minimize multiple objective functions. A survey on strategies to solve a multicriteria optimization problem can be found e.g. in [48]. In what follows we present two of these strategies.

2.1.1 As single criteria problem

One approach is to transform the multi objective problem into a single objective problem by accumulating the values of the functions f_s using a function $\Phi : \mathbb{R}^r \to \mathbb{R}$ such that $\Phi(F(x))$ is again a convex function. Φ can e.g. be a weighted sum of $f_s(x)$ or the norm of the vector $F(x)$.

$$\begin{aligned} &\text{Minimize } \Phi(F(x)) \\ &\text{s.t.} \quad g_j(x) \leq 0 \qquad \forall j \in J \end{aligned} \tag{2.2}$$

In the following we will use the notation $\Phi(x)$ as abbreviation for $\Phi(F(x))$ if it is clear that we refer to the vector $F(x)$.
There exist many optimization methods, which are able to solve a single objective optimization problem, see e.g. [4]. The method to solve (2.2) we are going to consider in this work is the level set scheme, which is presented in Section 2.2.

2.1.2 As lexicographic problem

A different approach is lexicographic optimization (LO). In classical LO we preserve the multi objective nature of the original problem by defining an importance-ranking the functions f_s. Then we minimize the functions following that order under the given constraints g_j in so-called optimization levels. After having minimized a function f_s in one level we impose an

additional constraint for the next level, which ensures that the objective function value with respect to f_s of subsequent solutions do not deviate from the previously found minimum of f_s by more than a given tolerance. This procedure continues until all optimization levels are solved.
In this work, however, we consider a more general setting for the formulation of the optimization problems. Here, we gather the functions f_s in priority groups $S_\mu \subseteq S, \mu = 1, ..., M$, which are ranked from most to least important. We accumulate the values of the functions contained in each priority group, similar to (2.2), and then proceed in the sense of classical LO.
The priority groups $\{S_\mu\}_{\mu=1}^{M}$ are a partition of the index set S, i.e.

$$\bigcup_{\mu=1}^{M} S_\mu = S \quad \text{and} \quad S_\mu \cap S_\gamma = \emptyset \quad \text{for } 1 \leq \mu \neq \gamma \leq M. \tag{2.3}$$

If the sets S_μ are singletons for all $\mu = 1, ..., M$, this setting obviously reduces to the classical LO problem.
The vectors $F_\mu := (f_s)_{s \in S_\mu}$ contain the function values $f_s(x)$ with $s \in S_\mu$ for all $\mu = 1, ..., M$. The functions

$$\Phi_\mu : \mathbb{R}^{r_\mu} \to \mathbb{R} \tag{2.4}$$

with $r_\mu = |S_\mu|$ and $\Phi_\mu(F_\mu(x))$ convex are the functions used to accumulate these values, similar to Φ in (2.2).
To solve the lexicographic optimization problem means to subsequently solve the optimization levels μ for all $\mu = 1, ..., M$. Each optimization level is a single criteria optimization problem

$$\begin{aligned} &\text{Minimize } \Phi_\mu(F_\mu(x)) \\ &\quad \text{s.t.} \qquad g_j(x) \leq 0 \qquad \forall j \in J \\ &\qquad\quad \Phi_\gamma(F_\gamma(x)) \leq \Phi_\gamma^* + \delta_\gamma \quad \forall \gamma \in \{1, ..., \mu - 1\} \end{aligned} \tag{2.5}$$

where $\Phi_\gamma^* = \Phi_\gamma(x^{*,\gamma})$ are the minimum values found for each Φ_γ in the previous optimization levels at the respective points $x^{*,\gamma}$. The parameters $\delta_\gamma \in \mathbb{R}_{\geq 0}, \gamma = 1, ..., \mu - 1$ allow a little room for the solving algorithm to improve the value of the current objective.
In the following we will use the notation $\Phi_\mu(x)$ as abbreviation for $\Phi_\mu(F(x))$ if it is clear that we refer to the vector $F_\mu(x)$ of the values $f_s(x)$ for all $s \in S_\mu$.
Using LO we transform the multicriteria optimization problem into M constrained single criteria problems with $1 \leq M \leq r$.

2.2 From optimization to feasibility problem: The level set scheme

We consider the general constrained convex optimization problem (2.2) and reformulate it into an equivalent *epigraph form*

$$\begin{aligned} &\text{Minimize } t \\ &\text{s.t. } \Phi(x) - t \leq 0 \\ &\qquad g_j(x) \leq 0 \quad \forall j \in J. \end{aligned} \tag{2.6}$$

We denote the optimal value of (2.6) by t^*. We assume that $t^* \in \mathbb{R}$ is finite and that there exists a point x^* with $\Phi(x^*) = t^*$, which is feasible for (2.6). The solution x^* of (2.6) is of course also a solution to the general single objective optimization problem (2.2).
The approach of the level set scheme to solve (2.6) and thus (2.2) in an approximate way is to transform it into a sequence of convex feasibility problems, see also [5, Subsection 2.1.2].

Definiton 1
The general formulation of a *convex feasibility problem* (CFP) is

$$\text{Find } x \in C := \bigcap_{i \in I} C_i \tag{2.7}$$

where $C_i := \{x \in \mathbb{R}^n \mid \varphi_i(x) \leq 0\}$ and the functions φ_i are convex for all $i \in I$.

In the following we describe the *level set scheme* [32]. We use a decreasing sequence $\left\{t^l\right\}_{l=1}^{L}$. This sequence (and also L) is not known a priori. The first element $t^1 = \infty$ is fixed and every subsequent element of the sequence is determined later during the iteration process. We define the functions

$$\varphi_i^l(x) := \begin{cases} \Phi(x) - t^l & i = 1 \\ g_{i-1}(x) & i = 2, ..., m+1. \end{cases} \tag{2.8}$$

Then we attempt to solve the CFP $\boldsymbol{P}^l$:

$$\text{Find } x \in C^l = \bigcap_{i \in I} C_i^l \tag{2.9}$$

with $C_i^l := \left\{x \in \mathbb{R}^n \mid \varphi_i^l(x) \leq 0\right\}$ and $I = \{1, ..., m+1\}$.
If $C^l \neq \emptyset$, a solution of $\boldsymbol{P}^l$ found by a suitable algorithmic operator $\boldsymbol{T}$ is denoted by x_l^*. Now t^{l+1} is calculated according to a user defined update rule, for example

$$t^{l+1} = \Phi(x_l^*) - \varepsilon_l \tag{2.10}$$

$$\text{or} \quad t^{l+1} = \Phi(x_l^*)(1 - \varepsilon_l) \tag{2.11}$$

where $\{\varepsilon_l\}_{l=1}^{L-1}$ is some user chosen sequence with $\varepsilon_l > 0$ for all $l = 1, ..., L-1$. Using t^{l+1} the next CFP $\boldsymbol{P}^{l+1}$ is formulated and the iteration proceeds.

By L we denote the first index for which the problem $\boldsymbol{P}^L$ is infeasible. We consider the solution x^*_{L-1} of the previous CFP to be the result of the level set scheme and terminate the procedure. If the chosen reduction strategy for t^l is (2.10), x^*_{L-1} is an ε_{L-1}-optimal solution of (2.2) in the sense that

$$\begin{aligned} \Phi(x^*_{L-1}) &\leq \Phi(x^*) + \varepsilon_{L-1} \\ g_j(x^*_{L-1}) &\leq 0 \qquad \forall j \in J. \end{aligned} \tag{2.12}$$

If strategy (2.11) is selected, x^*_{L-1} is still a ε-optimal solution in the sense of (2.12), but with $\varepsilon = \Phi(x^*_{L-1})\varepsilon_{L-1}$.

2.3 Solving feasibility problems: Projection methods

One successful class of algorithmic operators for solving CFPs is the class of projection methods. These are iterative algorithms that use projections onto individual sets in order to find an element of a set which is derived from the individual sets, e.g. the intersection or an image set under some transformation. These methods exploit the fact that in general projections onto the individual sets are easier to perform than projections onto derived sets. Projection methods possess desirable convergence properties and come in various algorithmic structures some of which are particularly suitable for parallel computing [16, 22, 68]. A special case of a CFP is the linear feasibility problem $Ax = b$. For this problem, an illustration of different projection methods and their different algorithmic structures can be found in [19].
In this paper we present two different projection methods as options for the operator $\boldsymbol{T}$ which solves the CFPs arising from the level set scheme. Both methods rely only on first order (sub)gradient information of the functions φ_i defining the feasible sets and are therefore a particularly attractive choice if second derivatives of φ_i are computationally expensive to evaluate or not even defined. The first option is the cyclic subgradient projection method, which is also used in combination with the level set scheme in [32]. Like some other projection methods, it utilizes the concept of control sequences. These are sequences $\{i(\nu)\}_{\nu=0}^{\infty}$, which determine an ordering of the indices of the sets C_i mentioned in (2.7). The sort of control sequence used by the cyclic subgradient projection method is defined below.

Definiton 2
The sequence $\{i(\nu)\}_{\nu=0}^{\infty}$ is called a *cyclic control sequence*, if $i(\nu) = (\nu \bmod n) + 1$, where n is the number of sets in (2.7).

The *cyclic subgradient projection* method can be written as algorithmic operator $\boldsymbol{T}$ in the following way:
Let $x^0 \in \mathbb{R}^n$ be an arbitrary starting point. Given the current iterate x^k, the next iterate x^{k+1} can be calculated via

$$x^{k+1} = \boldsymbol{T}(x^k) = x^k + \lambda_k p(x^k) \tag{2.13}$$

with

$$p(x^k) = -\frac{\max\{0, \varphi_{i(k)}(x^k)\}}{\|\xi^k\|^2}\xi^k \tag{2.14}$$

where ξ^k is an arbitrary element of the subdifferential $\partial\varphi_i(x^k)$ of φ at x^k, $\lambda_k \in [\epsilon_1, 2-\epsilon_2]$ are relaxation parameters for arbitrary $\epsilon_1, \epsilon_2 \in (0, 1]$ and $\{i(k)\}$ is a cyclic control sequence.

The second option we present for the algorithmic operator $\boldsymbol{T}$ is the *simultaneous subgradient projection* method. We can write it in terms of $\boldsymbol{T}$ as follows:
Let $x^0 \in \mathbb{R}^n$ be an arbitrary starting point. Given the current iterate x^k, the next iterate x^{k+1} can be calculated via

$$x^{k+1} = \boldsymbol{T}(x^k) = x^k + \lambda_k p(x^k) \tag{2.15}$$

with

$$p(x^k) := -\sum_{i\in I} w_i(x^k)\frac{\max\{0, \varphi_i(x^k)\}}{\|\xi^k\|^2}\xi^k \tag{2.16}$$

where ξ^k is an arbitrary element of the subdifferential $\partial\varphi_i(x^k)$ of φ at x^k, $w_i(x^k) \geq 0$ are weights with $\sum_{i\in I} w_i = 1$ and $\lambda_k \in [\epsilon_1, 2-\epsilon_2]$ are relaxation parameters for arbitrary $\epsilon_1, \epsilon_2 \in (0, 1]$.
If the functions φ_i are differentiable at x^k, the subgradient is of course replaced in both methods by the gradient $\nabla\varphi_i(x^k)$.

Detecting the inconsistency of a CFP $\boldsymbol{P}$, i.e. $C = \emptyset$ where C is the set of solutions of $\boldsymbol{P}$, is in general not a trivial task. The strategy we use in our computations is to assume that $\boldsymbol{P}$ has no solutions when we haven't found any within $n_{\max}$ iterations. While this criterion is simple (yet computationally expensive) to evaluate, it yields no statement about the proximity to the optimal solution. Alternatives are presented e.g. in [42, 43, 44, 23].
For simplicity, we use in the following the notation $\bar{p}(x^k) := p(x^k)/\|p(x^k)\|$, refer to the simultaneous subgradient projection method simply as simultaneous projection and to the cyclic subgradient projection method as cyclic projection.
The convergence proof of the level set scheme [32, Theorem 3.6] relies on using a finite convergence method. We can transform both the cyclic and the simultaneous projection to fulfill this property using the approach of [26]. Note that [32, Theorem 3.6], in contrast to convergence proofs for other finite convergent projection methods, e.g. [18], is not based on the assumption that the Slater Condition holds. In our context this means that we do not rely on the existence of $x \in \mathbb{R}^n$ with $\varphi_i(x) < 0$ for all $i \in I$ for the level set scheme to converge.

2.4 Perturbing the iteration process

2.4.1 Bounded perturbation resilience

Perturbations can be applied to any iterative operator $\boldsymbol{T}$ which generates a sequence $\{x^k\}_{k=0}^{\infty}$ via $x^{k+1} = \boldsymbol{T}(x^k)$. A central concept in the context of perturbations is *bounded perturbation*

resilience. This concept is defined in [11] in a general way, i.e. for a general mathematical problem $\boldsymbol{P}$ and an algorithmic operator $\boldsymbol{T}$, which is suited to solve $\boldsymbol{P}$.

In [28, 29] the concept of bounded perturbation resilience is considered with the problem $\boldsymbol{P}$ being the variational inequality problem. The operators $\boldsymbol{T}$ used to solve $\boldsymbol{P}$ in [28, 29] are the extragradient method, the subgradient extragradient method and the projection and contraction method. In [31, 41] the problem is the bioluminescence imaging problem, which can be phrased as a constrained optimization problem, and the operator used to solve it is the expectation maximization method. For a detailed overview and more examples see [15]. In this thesis, the problem $\boldsymbol{P}$ is a convex feasibility problem and $\boldsymbol{T}$ can be read as one of the projection methods we presented before.

Definiton 3
Consider a problem $\boldsymbol{P}$, an algorithmic operator $\boldsymbol{T}$ and a starting point x^0 such that the sequence $\{x^k\}_{k=0}^{\infty}$, generated by $x^{k+1} = \boldsymbol{T}(x^k)$ converges to a solution of $\boldsymbol{P}$. $\boldsymbol{T}$ is called *bounded perturbation resilient* if any sequence $\{y^k\}_{k=0}^{\infty}$ with $y^0 = x^0$ generated using either *inner perturbations* via

$$y^{k+1} = \boldsymbol{T}(y^k + \beta_k b^k) \qquad \forall k \geq 0 \tag{2.17}$$

or using *outer perturbations* via

$$y^{k+1} = \boldsymbol{T}(y^k) + \beta_k b^k \qquad \forall k \geq 0 \tag{2.18}$$

where $\beta_k b^k$ are bounded perturbations (i.e. $\beta_k \in \mathbb{R}_{\geq 0}$ for all $k \geq 0$, $\sum_{k=0}^{\infty} \beta_k < \infty$, $b^k \in \mathbb{R}^n$ and $\|b^k\| \leq M \in \mathbb{R}$ for all $k \geq 0$) also converges to a solution of $\boldsymbol{P}$.

Both the cyclic and the simultaneous projection method are known to be bounded perturbation resilient [20].

2.4.2 Superiorization

One variant of perturbations is the *superiorization methodology* [38]. It was recently developed as a framework for algorithms that lie conceptually between feasibility-seeking and optimization algorithms. Superiorization is designed to find a solution to a CFP which is superior with respect to a given function ψ compared to the solution obtained by a classical feasibility seeking algorithmic operator. An extensive source for current research on superiorization is "Superiorization and Perturbation Resilience of Algorithms: A Bibliography compiled and continuously updated"by Yair Censor. In particular, [37] and [14] are recent reviews of interest.

Definiton 4
Given a function $\psi : \mathbb{R}^n \to \mathbb{R}$ and a point $z \in \mathbb{R}^n$, we say that a vector $d \in \mathbb{R}^n$ is *nonascending* for ψ at z if and only if $\|d\| \leq 1$ and there is a $\delta > 0$ such that for all $\lambda \in [0, \delta]$ we have $\psi(z + \lambda d) \leq \psi(z)$.

Definiton 5
Let $\boldsymbol{T}$ be an algorithmic operator suited to solve a convex feasibility problem (2.7) by producing a sequence $\{x^k\}_{k=0}^{\infty}$ via the iteration scheme $x^{k+1} = \boldsymbol{T}(x^k)$ which converges to a solution of (2.7).
Let $\psi : \mathbb{R}^n \to \mathbb{R}$ be a given convex and continuously differentiable function.
The *superiorized iteration scheme* of $\boldsymbol{T}$ (with respect to ψ) is

$$\begin{aligned} y^0 &= x^0 \\ y^{k+1} &= \boldsymbol{T}(y^k + \beta_k d^k) \end{aligned} \tag{2.19}$$

where d^k is nonascending for ψ at y^k, $\beta_k \in \mathbb{R}_{\geq 0}$ and $\sum_{k=0}^{\infty} \beta_k < \infty$.

One option for d^k, as it is used in [38], is

$$d^k = \begin{cases} -\dfrac{\nabla\psi(y^k)}{\left\|\nabla\psi(y^k)\right\|} & \text{if } \nabla\psi(y^k) \neq \vec{0} \\ 0 & \nabla\psi(y^k) = \vec{0}. \end{cases} \tag{2.20}$$

If the solution set C of the feasibility problem contains several elements, the superiorized version of $\boldsymbol{T}$ obtains a solution that is potentially superior with respect to ψ to the solution achieved by the basic algorithmic operator $\boldsymbol{T}$.

2.5 New results about perturbations

2.5.1 The relation of inner and outer perturbations

In this section we explore the relation of iteration sequences resulting from methods using inner and outer perturbations concerning their convergence behavior.
First, we are extending Proposition 5 from [21] to include the simultaneous subgradient projection method (2.15) as operator $\boldsymbol{T}$.
Let

$$b^k := \begin{cases} \tilde{b}^k & \text{if } c(x^k) = \text{ true} \\ 0 & \text{otherwise} \end{cases} \tag{2.21}$$

be perturbation vectors where $c : \mathbb{R}^n \to \{\text{false, true}\}$ is a function that gives a condition, which determines whether or not to perturb the current iterate.

Consider the sequences $\{y^k\}_{k=0}^{\infty}$ generated using outer perturbations and $\{z^k\}_{k=0}^{\infty}$ using inner perturbations, which are defined as follows:

$$y^{k+1} = \boldsymbol{T}(y^k) + b^k \tag{2.22}$$

and

$$\begin{cases} z^0 = \boldsymbol{T}(y^0) \\ z^{k+1} = \boldsymbol{T}(z^k + b^k) \end{cases} \tag{2.23}$$

with $y^0 \in \mathbb{R}^n$.

Proposition 1. *Suppose that $\{b^k\}_{k=0}^{\infty}$ is a sequence in $\mathbb{R}^n$ satisfying $\lim_{k\to\infty} b^k \to \vec{0}$. If $\{y^k\}_{k=0}^{\infty}$ as defined in (2.22) converges weakly to some y^*, then also $\{z^k\}_{k=0}^{\infty}$ as defined in (2.23) converges weakly to y^* and vice versa. If $\{y^k\}_{k=0}^{\infty}$ converges strongly, then $\{z^k\}_{k=0}^{\infty}$ converges strongly to the same limit and vice versa.*

Proof.
We show that by induction $y^{k+1} = z^k + b^k$ for all $k \in \mathbb{N} \cup \{0\}$. The rest of the statement follows from the proof of Proposition 5 in [21].

k=0 Show that $y^1 = z^0 + b^0$.

$$z^0 + b^0 = \boldsymbol{T}(y^0) + b^0 = y^1 \qquad \text{according to (2.23) and (2.22)}$$

Induction step Show that $y^k = z^{k-1} + b^{k-1} \Rightarrow y^{k+1} = z^k + b^k$.

$$\begin{aligned} z^k + b^k &= \boldsymbol{T}(z^{k-1} + b^{k-1}) + b^k && \text{according to (2.23)} \\ &= \boldsymbol{T}(y^k) + b^k = y^{k+1} && \text{according to (2.22)} \end{aligned}$$

□

Proposition 1 implies that inner and outer perturbations of the simultaneous projection method using the same perturbation vectors b^k as described before can be used interchangeably with regard to weak and strong convergence.

In Section 5.3 we present three perturbations developed by us and formulate them both as inner and outer perturbation. In contrast to (2.22) and (2.23), we do not use the same perturbation vectors b^k for both formulations there. Instead we define the inner and outer perturbation scheme as follows. We assume specific choices of λ_k, β_k, which will be explained in more detail, and present a result regarding the convergence of the sequence of iterates produced by methods using these perturbations.

Let again $\boldsymbol{T}$ be an iterative operator producing a sequence $\{x^k\}_{k=0}^{\infty}$ via the scheme $x^{k+1} = \boldsymbol{T}(x^k)$ with

$$\boldsymbol{T}(x) = x + \lambda(x)p(x) \tag{2.24}$$

where $p(x)$ is either the simultaneous (2.16) or the cyclic projection step (2.14). Note that $\lambda : \mathbb{R}^n \to [\epsilon_1, 2 - \epsilon_2)$ with arbitrary $\epsilon_1, \epsilon_2 \in (0, 1]$ is a function here.
Let $c : \mathbb{R}^n \to \{\text{false, true}\}$ and $\tilde{c} : \mathbb{R}^n \times \mathbb{R}^n \to \{\text{false, true}\}$ with

$$\tilde{c}(y^k, y^{k-1}) := \neg c(y^{k-1}) \wedge c(y^k). \tag{2.25}$$

be functions, which determine, whether perturbation is applied in a certain iteration with $k \geq 1$. $\tilde{c}(y^k, y^{k-1})$ is by construction only true, if $c(y^{k-1})$ is false and $c(y^k)$ is true. Assume that $\|p(y^k)\| < q \in \mathbb{R}$ for all $k \geq 0$.

Definiton 6
Let $\{y^k\}_{k=0}^{\infty}$ be the sequence of iterates produced by the *outer perturbation scheme*, which is defined as follows.

$$\begin{cases} y^0 = x^0 \\ y^{k+1} = \boldsymbol{T}(y^k) + \beta_k b^k \end{cases} \tag{2.26}$$

where $\{\beta_k\}_{k=0}^{\infty}$ is a sequence with $\beta_k \in \mathbb{R}_{\geq 0}$ for all $k \geq 0$ and $\sum_{k=0}^{\infty} \beta_k < \infty$,

$$b^k = \begin{cases} \tilde{b}^k - \lambda(y^k)p(y^k) & \text{if } \tilde{c}(y^k, y^{k-1}) = \text{ true} \\ 0 & \text{otherwise} \end{cases} \tag{2.27}$$

and the sequence $\{b^k\}_{k=0}^{\infty}$ is bounded.

Definiton 7
Let $\{z^k\}_{k=0}^{\infty}$ be the sequence of iterates produced by the *inner perturbation scheme*, which is defined as follows.

$$\begin{cases} z^0 = x^0 \\ z^{k+1} = \boldsymbol{T}(z^k + \beta_k b^k) \end{cases} \tag{2.28}$$

where $\{\beta_k\}_{k=0}^{\infty}$ is a sequence with $\beta_k \in \mathbb{R}_{\geq 0}$ for all $k \geq 0$ and $\sum_{k=0}^{\infty} \beta_k < \infty$,

$$b^k = \begin{cases} \tilde{b}^k & \text{if } c(z^k) = \text{ true} \\ 0 & \text{otherwise} \end{cases} \tag{2.29}$$

and the sequence $\{b^k\}_{k=0}^{\infty}$ is bounded.

Now let

$$\beta_k = \begin{cases} 1 & k \leq K \\ 0 & k > K \end{cases} \tag{2.30}$$

for some $K \in \mathbb{N}$. Choosing β_k like this means that for $k > K$ no more perturbations will be applied. In our computations we choose K as the maximum number $n_{\max}$ of iterations allowed for the projection method to solve a CFP arising from the level set scheme.

Lemma 2. *If $y^0 = z^0$ and $\{\beta_k\}_{k=0}^{\infty}$ is chosen as in (2.30), the following statements are true.*

(a) If for some $l < K$ it holds that $c(z^k) =$ false for all $k = 0, ..., l-1$ and $c(z^l) =$ true, we have $z^k = y^k$ for all $k = 0, ..., l$.

(b) $\{z^k\}_{k=0}^{\infty} \subseteq \{y^k\}_{k=0}^{\infty}$.

(c) For all $z^k \in \{z^k\}_{k=0}^{\infty}$ exists $N \in \mathbb{N}_0, 0 \leq N \leq K$ such that $z^k = y^{k+N}$.

Proof.
Statement (a) follows directly from equations (2.29) and (2.27).
Now suppose that l with $0 \leq l < K$ is the first iteration index where the condition for applying perturbations is fulfilled. This means that $c(z^l) = \tilde{c}(y^l, y^{l-1}) =$ true and $c(z^k) = \tilde{c}(y^k, y^{k-1}) =$ false for all $k < l$. We know from (a) that then $z^k = y^k$ for all $k = 0, ..., l$.
We have $\beta_l = 1$ because $l < K$. The iteration schemes give us

$$\begin{aligned} z^{l+1} &= \boldsymbol{T}(z^l + \beta_l b^l) \\ &= \boldsymbol{T}(y^l + b^l) \end{aligned}$$

and

$$\begin{aligned} y^{l+1} &= \boldsymbol{T}(y^l) + \beta_l(b^l - \lambda(y^l)p(y^l)) \\ &= y^l + (1 - \beta_l)\lambda(y^l)p(y^l) + \beta_l b^l \\ &= y^l + b^l. \end{aligned}$$

$c(y^l) =$ true, so $\tilde{c}(y^{l+1}, y^l) =$ false, no matter what $c(y^{l+1})$ is. Therefore $b^{l+1} = 0$ and the following iterate is an unperturbed one.

$$\begin{aligned} y^{l+2} &= \boldsymbol{T}(y^{l+1}) \\ &= \boldsymbol{T}(y^l + b^l) = z^{l+1} \end{aligned}$$

Because λ depends on the iterate (and not on the iteration index) and $y^{l+2} = z^{l+1}$, we get

$$\begin{aligned} z^{l+2} &= \boldsymbol{T}(z^{l+1}) = z^{l+1} + \lambda(z^{l+1})p(z^{l+1}) \\ &= y^{l+2} + \lambda(y^{l+2})p(y^{l+2}) \\ &= \boldsymbol{T}(y^{l+2}) = y^{l+3} \end{aligned}$$

assuming that $c(z^{l+1}) = \text{false}$. Otherwise, the same argument as before holds. Statement (b) follows from this. Before any perturbations are applied, the number N from statement (c) is 0. Each time perturbations are applied in an iteration, N increases by 1.

□

Proposition 3. *Suppose that $\{\beta_k\}_{k=0}^{\infty}$ is chosen as in (2.30) and $\{b^k\}_{k=0}^{\infty}$ is a bounded sequence in $\mathbb{R}^n$. If $\{y^k\}_{k=0}^{\infty}$ converges weakly to some y^*, then also $\{z^k\}_{k=0}^{\infty}$ converges weakly to y^* and vice versa. If $\{y^k\}_{k=0}^{\infty}$ converges strongly, then $\{z^k\}_{k=0}^{\infty}$ converges strongly to the same limit and vice versa.*

Proof.
It follows from Lemma 2(c) that there exists $0 \leq N \leq K$ such that $z^k = y^{k+N}$ for all $k = l, ...\infty$ for some $l \in \mathbb{N}_0$. □

Proposition 3 implies that inner and outer perturbations in combination with both the simultaneous and cyclic projection method using the perturbation vectors (2.29) or (2.27) can be used interchangeably with regard to weak and strong convergence.

2.5.2 Bounded perturbation resilience of perturbed iteration schemes

In this section we explore the effects of bounded perturbations when they are applied to an iteration scheme, which is already perturbed.
Let again $\boldsymbol{P}$ be a mathematical problem in a Hilbert space $\mathcal{H}$ and $\boldsymbol{T} : \mathcal{H} \to \mathcal{H}$ be a bounded perturbation resilient operator designed to solve $\boldsymbol{P}$, which generates a sequence $\{x_k\}_{k=0}^{\infty}$ for via

$$x^{k+1} = \boldsymbol{T}(x^k)$$

with x^0 being an arbitrary starting point.

Outer perturbations

Denote by $\hat{\boldsymbol{T}}$ any operator, which is $\boldsymbol{T}$ used with arbitrary bounded outer perturbations $\hat{\beta}_k\hat{b}_k$. It produces a sequence $\{y^k\}_{k=0}^{\infty}$ via

$$\begin{aligned} y^0 &= x^0, \\ y^{k+1} &= \hat{\boldsymbol{T}}(y^k) \\ &= \boldsymbol{T}(y^k) + \hat{\beta}_k\hat{b}_k. \end{aligned} \tag{2.31}$$

Note that the sequences $\{\hat{\beta}_k\}_{k=0}^{\infty}, \{\hat{b}^k\}_{k=0}^{\infty}$ can either be independent of the iterates y^k or depend on them. In the following we will write $\hat{\beta}_k, \hat{b}^k$ as functions of y^k and thereby also cover the case when they do not depend on y^k as the special case of $\hat{\beta}_k, \hat{b}^k$ being constant functions over $\mathbb{R}^n$. For the perturbations to be bounded, they need to fulfill the properties

$$\sum_{k=0}^{\infty} \hat{\beta}_k(y^k) < \infty$$
$$\hat{\beta}_k \geq 0 \text{ for all } k \geq 0$$

and

$$\|\hat{b}^k(y^k)\| \leq \hat{M} \in \mathbb{R} \text{ for all } k \geq 0$$

for any sequence of vectors $\{y^k\}_{k=0}^{\infty}$.
Denote by $\check{\boldsymbol{T}}$ any operator, which generates a sequence $\{z^k\}_{k=0}^{\infty}$ via

$$\begin{aligned} z^0 &= x^0, && (2.32)\\ z^{k+1} &= \check{\boldsymbol{T}}(z^k) \\ &= \hat{\boldsymbol{T}}(z^k) + \check{\beta}_k(z^k)\check{b}^k(z^k), && (2.33) \end{aligned}$$

where $\check{\beta}_k\check{b}^k$ are arbitrary bounded perturbations, i.e.

$$\check{\beta}_k(z^k) \geq 0 \qquad \forall k \geq 0$$
$$\sum_{k=0}^{\infty} \check{\beta}_k(z^k) < \infty$$

and

$$\|\check{b}^k(z^k)\| < \check{M} \in \mathbb{R} \qquad \forall k \geq 0.$$

Proposition 4. *Any operator $\check{\boldsymbol{T}}$ as defined in* (2.33) *can be written as an operator $\hat{\boldsymbol{T}}$ as defined in* (2.31) *with:*

$$\begin{aligned} z_0 &= x_0, \\ z_{k+1} &= \check{\boldsymbol{T}}(z_k) \\ &= \boldsymbol{T}(z_k) + \bar{\beta}_k(z_k)\bar{b}^k(z_k) && (2.34) \end{aligned}$$

for some bounded perturbations $\bar{\beta}_k(z_k)\bar{b}^k(z_k)$.

Proof.
$z_0 = x_0$ is fulfilled by (2.32).

$$\begin{aligned} z_{k+1} &= \check{\boldsymbol{T}}(z_k) \\ &= \hat{\boldsymbol{T}}(z_k) + \check{\beta}_k(z^k)\check{b}^k(z^k) \\ &= \boldsymbol{T}(z_k) + \hat{\beta}_k(z^k)\hat{b}^k(z^k) + \check{\beta}_k(z^k)\check{b}^k(z^k) \\ &= \boldsymbol{T}(z_k) + \bar{\beta}_k(z^k)\bar{b}^k(z^k) \end{aligned}$$

where $\bar{\beta}_k(z^k) := \hat{\beta}_k(z^k) + \check{\beta}_k(z^k)$ and $\bar{b}_k(z^k) := \hat{b}^k(z^k) + \check{b}^k(z^k)$.
Now we show that $\bar{\beta}_k(z^k)\bar{b}^k(z^k)$ are bounded perturbations.

$$\begin{aligned} \bar{\beta}_k(z^k) &= \hat{\beta}_k(z^k) + \check{\beta}_k(z^k) \\ &\geq 0 \end{aligned}$$

$$\begin{aligned} \sum_{k=0}^{\infty} \bar{\beta}_k(z^k) &= \sum_{k=0}^{\infty} \hat{\beta}_k(z^k) + \check{\beta}_k(z^k) \\ &= \sum_{k=0}^{\infty} \hat{\beta}_k(z^k) + \sum_{k=0}^{\infty} \check{\beta}_k(z^k) \\ &< \infty \end{aligned}$$

$$\begin{aligned} \|\bar{b}_k(z^k)\| &= \|\hat{b}^k(z^k) + \check{b}^k(z^k)\| \\ &\leq \|\hat{b}^k(z^k)\| + \|\check{b}^k(z^k)\| \\ &\leq \hat{M} + \check{M} =: \tilde{M} \end{aligned}$$

□

Inner perturbations

Denote again by $\hat{\boldsymbol{T}}$ any operator, which is $\boldsymbol{T}$ used with arbitrary bounded inner perturbations $\hat{\beta}_k\hat{b}_k$. It produces a sequence $\{y^k\}_{k=0}^{\infty}$ via

$$\begin{aligned} y^0 &= x^0 \\ y^{k+1} &= \hat{\boldsymbol{T}}(y^k) \\ &= \boldsymbol{T}(y^k + \hat{\beta}_k(y^k)\hat{b}^k(y^k)), \end{aligned} \tag{2.35}$$

where $\hat{\beta}_k(y^k)\hat{b}^k(y^k)$ are bounded perturbations, i.e.

$$\begin{aligned} \hat{\beta}_k(y^k) &\geq 0 \qquad \forall k \geq 0 \\ \sum_{k=0}^{\infty} \hat{\beta}_k(y^k) &< \infty \end{aligned}$$

and

$$\|\hat{b}^k(y^k)\| < \hat{M} \in \mathbb{R} \qquad \forall k \geq 0$$

for any sequence of vectors $\{y^k\}_{k=0}^{\infty}$.
Denote again by $\check{\boldsymbol{T}}$ any operator, which generates a sequence $\{z^k\}_{k=0}^{\infty}$ via

$$\begin{aligned} z^0 &= x^0, && (2.36)\\ z^{k+1} &= \check{\boldsymbol{T}}(z^k) \\ &= \hat{\boldsymbol{T}}(z^k + \check{\beta}_k(z^k)\check{b}^k(z^k)), && (2.37) \end{aligned}$$

where $\check{\beta}_k(z^k)\check{b}^k(z^k)$ are bounded perturbations, i.e.

$$\check{\beta}_k(z^k) \geq 0 \qquad \forall k \geq 0$$
$$\sum_{k=0}^{\infty} \check{\beta}_k(z^k) < \infty$$

and

$$\|\check{b}^k(z^k)\| < \check{M} \in \mathbb{R} \qquad \forall k \geq 0$$

for any sequence of vectors $\{z^k\}_{k=0}^{\infty}$.

Proposition 5. *Any operator $\check{\boldsymbol{T}}$ as defined in* (2.37) *can be written as an operator $\hat{\boldsymbol{T}}$ as defined in* (2.35) *with:*

$$\begin{aligned} z_0 &= x_0, \\ z_{k+1} &= \check{\boldsymbol{T}}(z_k) \\ &= \boldsymbol{T}(z_k + \bar{\beta}_k(z_k)\bar{b}^k(z_k)) && (2.38) \end{aligned}$$

for some bounded perturbations $\bar{\beta}_k(z_k)\bar{b}^k(z_k)$.

Proof.
$z^0 = x^0$ is fulfilled by (2.36).

$$\begin{aligned} z^{k+1} &= \check{\boldsymbol{T}}(z^k) \\ &= \hat{\boldsymbol{T}}(z^k + \check{\beta}_k(z^k)\check{b}^k(z^k)) \\ &= \boldsymbol{T}\left(z^k + \check{\beta}_k(z^k)\check{b}^k(z^k) + \hat{\beta}_k\left(z^k + \check{\beta}_k(z^k)\check{b}^k(z^k)\right)\hat{b}^k\left(z^k + \check{\beta}_k(z^k)\check{b}^k(z^k)\right)\right) \\ &= \boldsymbol{T}(z^k + \bar{\beta}_k(z^k)\bar{b}^k(z^k)) \end{aligned}$$

where $\bar{\beta}_k(z^k) := \check{\beta}_k(z^k) + \hat{\beta}_k\left(z^k + \check{\beta}_k(z^k)\check{b}^k(z^k)\right)$ and $\bar{b}^k(z^k) := \check{b}^k(z^k) + \hat{b}^k\left(z^k + \check{\beta}_k(z^k)\check{b}^k(z^k)\right)$.

Now we show that $\bar{\beta}_k(z^k)\bar{b}^k(z^k)$ are bounded perturbations.

$$\begin{aligned}\bar{\beta}_k(z^k) &= \check{\beta}_k(z^k) + \hat{\beta}_k\left(z^k + \check{\beta}_k(z^k)\check{b}^k(z^k)\right)\\ &\geq 0 + 0 = 0\end{aligned}$$

$$\begin{aligned}\sum_{k=0}^{\infty}\bar{\beta}_k(z^k) &= \sum_{k=0}^{\infty}\check{\beta}_k(z^k) + \hat{\beta}_k\left(z^k + \check{\beta}_k(z^k)\check{b}^k(z^k)\right)\\ &= \sum_{k=0}^{\infty}\check{\beta}_k(z^k) + \sum_{k=0}^{\infty}\hat{\beta}_k\left(z^k + \check{\beta}_k(z^k)\check{b}^k(z^k)\right)\\ &< \infty + \infty = \infty\end{aligned}$$

$$\begin{aligned}\|\bar{b}^k(z^k)\| &= \|\check{b}^k(z^k) + \hat{b}^k\left(z^k + \check{\beta}_k(z^k)\check{b}^k(z^k)\right)\|\\ &\leq \|\check{b}^k(z^k)\| + \|\hat{b}^k\left(z^k + \check{\beta}_k(z^k)\check{b}^k(z^k)\right)\|\\ &\leq \check{M} + \hat{M} =: \tilde{M} \qquad \forall k \geq 0\end{aligned}$$

□

Propositions 4 and 5 imply that if a bounded perturbation resilient operator $\boldsymbol{T}$ starting from a point x^0 produces a sequence of iterates $\{x^k\}_{k=0}^{\infty}$, which converges to a solution of the problem $\boldsymbol{P}$, the operator $\boldsymbol{T}$ can be perturbed by bounded inner or outer perturbations an arbitrary number of times and, starting from the same point $y^0 = x^0$, the perturbed operator will produce a sequence of iterates $\{y^k\}_{k=0}^{\infty}$, which also converges to a solution of $\boldsymbol{P}$.

3 Optimization in IMRT planning

3.1 IMRT planning

One of the most important treatment options in modern clinical oncology is intensity modulated radiation therapy (IMRT). This tool helps physicians to achieve their aim of destroying the tumor tissue by irradiation while sparing surrounding healthy tissue as much as possible. These aims are formulated as so-called clinical goals. One goal could be for example to ensure that 95% of the tumor volume is exposed to a dose of at least 60 Gy or that the spinal cord is not exposed to dose values higher than 45 Gy. Multiple clinical goals for different biological structures are gathered in so called clinical protocols, see e.g. [55].
There are usually several goals and some goals can be in conflict with each other due to physical limitations like the proximity of the tumor to healthy organs and the attainable decrease of the dose values over a given distance. The decision of which treatment plan should be chosen must therefore be based on multiple relevant criteria.
The most common device to produce the radiation field in IMRT is a linear accelerator. The accelerator gantry can be rotated around the couch on which the patient is positioned in order to irradiate the patient's body from different angles. The couch can be rotated as well to allow for a treatment field, which is tilted with respect to the vertical axis of the couch. The radiation modulation in IMRT is accomplished by a multileaf collimator (MLC). It has multiple pairwise opposing leaves, which can move independently to cover the beam surface and thus block a fraction of the radiation. The modulated intensity values resulting from this process are gathered in intensity maps.
In clinical practice, there exist two different delivery modes. For dynamic delivery, the gantry moves while emitting radiation, while for static or step-and-shoot delivery it stops at certain angles and only emits radiation from these angles. In this thesis we only consider static delivery.

3.2 The optimization problem in IMRT planning

An IMRT treatment plan consists of multiple parameters describing the patient treatment. We gather these parameters in three main groups, of which we consider one to be the optimization variables in the IMRT planning problem we discuss in this thesis.
The first group of parameters is the delivery scheme, which describes the radiation modality, energies and fractionation. We consider these parameters fixed in this context.
The second parameter group is the beam arrangement which describes the angles of the couch relative to the gantry angles as well as the rotation of the gantry and the number of beams. The optimization of these parameters unfortunately is a global optimization problem [10, 47]. Even the optimization of the orientation of beams and the fluence intensity at the same time is an non-convex problem for which solvers tend to get stuck in local optima

[7]. Therefore, the number of beams in practice is chosen using empirical experience and heuristics without a guarantee for optimality. In this work, we assume these parameter to be fixed as well.
The third group of parameters are the intensity maps for each beam. The IMRT planning problem, it is considered it in this thesis, is to determine these intensity maps, i.e. a set of fluence intensity values that causes a dose distribution in the patient's body which will fulfills clinical goals as well as possible.

3.3 Modeling the IMRT optimization problem

In order to optimize the fluence intensity values applied in IMRT treatment, one has to be able to predict their impact in terms of dose distribution. Insights into the physics of dose deposits in tissue and the development of 3D dose calculation algorithms yielded the option to accomplish this prediction via virtual radiotherapy planning. This method offers a virtual simulation of the dose distribution using CT images of an individual patient and the configurations of the linear accelerator.

3.3.1 Dose calculation

Dose kernel

The dose $d(r)$ received at a point r in the patient's body can be calculated using a smooth dose kernel $\kappa(r, s)$ [54]. The kernel describes the absorbed energy at a point r under unit energy fluence from the point s on the undiscretized beam surface S.

$$d(r) = \int_S \kappa(r, s) \cdot x(s) ds \tag{3.1}$$

Discretization

The model for the IMRT optimization problem used in this thesis is based on three discretizations.
First, the beam surface is discretized into so-called beamlets, which are small rectangular parts of the beam surface. The length of the vertical side of these rectangles results from the width of the collimator leafs. The other one stems from a horizontal discretization of the beam surface width. The fluence intensity is assumed to be constant over one beamlet.
Second, the volume of the patient's body is discretized into small cuboid-shaped voxels. The resolution of this discretization is limited by the quality of the underlying medical images. The dose value received by one voxel is assumed to be constant.
Third, the kernel is discretized into an operator $\boldsymbol{D}$, which maps the beamlet intesity values $x \in \mathbb{R}_{\geq 0}$ to voxel dose values. We assume that this discretization represents the true physical absorption well enough for clinical purposes. $\boldsymbol{D}$ is also called dose matrix. Each row corresponds to one voxel and each column describes the dose values resulting from unit energy fluence of one beamlet.

Calculating the dose vector d, which contains the dose values received by each voxel, resulting from the fluence values x now reformulates to

$$d = \boldsymbol{D}x. \tag{3.2}$$

Due to physical reasons, the vector x of fluence intensity values is restricted to be non-negative.

3.3.2 Dose evaluation functions

To evaluate and improve how well a dose distribution fulfills the previously defined clinical goals we need a measurement for it the form of a mathematical function. All clinical goals refer to a biological structure, which, from a mathematical point of view, is a set $\mathcal{O}$ of indices corresponding to the voxels contained in the biological structure. By $d_i = \langle a_i, x \rangle$ we denote the dose value received by the voxel with index i, where a_i is the i-th row of $\boldsymbol{D}$.
For the evaluation of a treatment plan cumulative dose volume histograms (DVH) are a common tool among physicians. Those consist of curves for each biological structure, which depict what volume percentage of the structure receives at least which dose. An intuitive approach for constraints are DVH constraints, which require the curve of a given structure to pass above or below a certain point and are often used in clinical protocols, see e.g. [55]. They translate for example to "At most 5% of the myelon volume should receive a dose greater or equal than 45 Gy". Unfortunately, constraints of this type are mathematically unfavorable, because they result in a non-convex feasible region and therefore a global optimization problem. Optimization problems of this type require either significantly more computational effort to be solved or one has to accept, that a solution found by an optimization algorithm could be only a local optimum with no measure of how the objective function value of the local optimum differs from the one of the global optimum.
To circumvent these disadvantages, convex substitute functions have been devised, which indirectly influence the shape of the DVH curves.

Lower tail penalty function The lower tail penalty function penalizes dose values of d corresponding to the structure $\mathcal{O}$ which fall below a given threshold $L \in \mathbb{R}$.

$$f(d, \mathcal{O}) = \frac{1}{|\mathcal{O}|} \sum_{i \in \mathcal{O}} \max(0, L - d_i)^p \quad p \in [1, \infty) \tag{3.3}$$

Upper tail penalty function The upper tail penalty function penalizes dose values of d corresponding to the structure $\mathcal{O}$ which exceed a given threshold $U \in \mathbb{R}$.

$$f(d, \mathcal{O}) = \frac{1}{|\mathcal{O}|} \sum_{i \in \mathcal{O}} \max(0, d_i - U)^p \quad p \in [1, \infty) \tag{3.4}$$

Mean upper tail penalty function The mean upper tail penalty function is used to keep the mean dose values below a given threshold $M \in \mathbb{R}$, which is a less strict way of avoiding overdosage than using the upper tail penalty function.

$$f(d, \mathcal{O}, d^{ref}) = \left(\max \left\{ \left(1/|\mathcal{O}| \sum_{i \in \mathcal{O}} d_i \right) - M, 0 \right\} \right)^p \quad p \in [1, \infty) \tag{3.5}$$

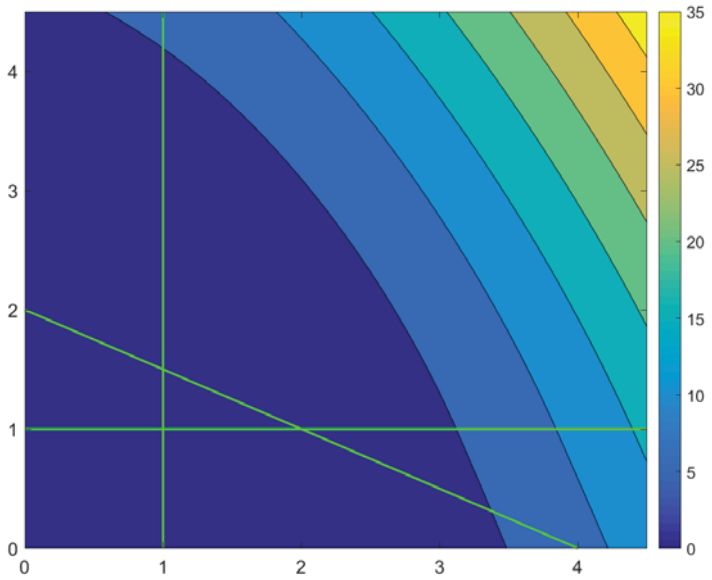

Figure 3.1: 2D example for the upper tail penalty function. The green lines represent the hyperplanes separating feasible (towards the origin) from infeasible half-spaces. Isolines of the upper tail penalty function values are given according to the color map.

Another approach to evaluate the quality of a dose distribution is to consider its biological impact. The biological impact is quantified using statistical data on tumor control probability and normal tissue complication probability [65, Chapter 5]. Similar to DVH constraints, these functions cause the optimization problem to be non-convex and are therefore substituted by the equivalent uniform dose (EUD) function introduced by [9], which is convex.

Equivalent uniform dose (EUD) The EUD function penalizes dose values of d corresponding to the structure $\mathcal{O}$ which deviate from 0.

$$f(d, \mathcal{O}) = \frac{1}{|\mathcal{O}|} \sum_{i \in \mathcal{O}} d_i^p \quad p \in (-\infty, 1) \cup (1, \infty) \tag{3.6}$$

Negative values for p are used for tumor volumes and positive values for healthy structures.

Tumor conformity The tumor conformity function is used to ensure an even dose distribution within the tumor volume. It penalizes dose values of d corresponding to the structure $\mathcal{O}$ which deviate from a given reference value.

$$f(d, \mathcal{O}, d^{ref}) = \frac{1}{|\mathcal{O}|} \sum_{i \in \mathcal{O}} |d^{ref} - d_i|^p \quad p \in [1, \infty) \tag{3.7}$$

All of these functions take into account the system of linear (in)equalities resulting from $d_i = \langle a_i, x \rangle$ being less/ greater or equal than a right hand side value determined by the function parameters, where $i \in \mathcal{O}$. The functions measure the distance of the vector x to the (separating) hyperplanes corresponding to the linear (in)equalities in a nonlinear way. Figure 3.1 illustrates this concept with a simple 2D example.

The given functions do not represent a complete list of dose evaluation functions used in clinical applications. A more complete survey of such functions can be found in [58] and [61].

3.4 Challenges in IMRT optimization

The dose matrix $\boldsymbol{D}$ is calculated based on a CT image of the individual patient. Each matrix row corresponds to one voxel in the CT image and multiplying an individual matrix row with a vector x of fluence intensities yields the virtually simulated dose received by the corresponding voxel. To ensure a sufficient accuracy of the treatment plan the resolution of the CT image has to be high, which leads to a dose matrix with an enormous number of rows. Additionally, the change of the dose over a small distance is relatively small and therefore voxels in close proximity typically correspond to very similar matrix rows. Enhancing the resolution of the CT image increases the number of similar matrix rows, which also increases the condition number of the dose matrix.
The majority of the computational effort in IMRT optimization is spent on evaluating the dose and the gradients of the dose evaluation functions. The effort for both tasks grows with the number of dose matrix rows and therefore the computational effort grows with the resolution of the CT image. To counteract this phenomenon clustering techniques have been proposed in [59, 63], which exploit the fact that very similar matrix rows result in evenly similar dose values. By accumulating these rows and only breaking up the accumulations when needed, some of the effort for calculating almost redundant dose information can be saved.
In this thesis, however, we concern ourselves not with this challenge, but with the second effect of the high CT resolution we mentioned before, the high condition number of the dose matrix, in combination with the conflict between adjacent volumes with opposing dose prescriptions.
The high condition number causes the inverse problem of finding a vector of fluence intensities corresponding to a given dose distribution to be ill-posed and therefore harder to solve.
On a macro level the conflicting clinical goals lead to objective functions of the multicriteria optimization problem, which are often correlated in a positive or negative way. When lexicographic optimization is applied to solve the multicriteria optimization problem, objective functions are minimized successively according to their priority. Depending on the priority ranking of the objectives, it may happen that the distance of a solution to an optimization level from the set of solutions to the next level is large, while other solutions lie closer to this set.
On a more detailed level the conflicting clinical goals translate to adjacent voxels corresponding to similar dose matrix rows which have conflicting dose prescriptions. Those prescriptions often cannot be fulfilled at the same time because the change of the dose per spatial unit is limited by physical laws. Therefore their conflict is present during the whole iteration process and becomes more and more prominent during the end phase of the optimization process when other goals, which are attainable at the same time, are already fulfilled. Voxels of the described type contribute almost parallel but opposing directions to the individual gradients of the dose evaluation functions. This often results in zigzagging behavior of gradient based optimization methods, for example projection methods, which gets more severe over the course of the optimization process.

Both the bad starting point for subsequent lexicographic optimization levels and the zigzagging behavior lead to slow convergence of the overall optimization procedure. In Chapters 4 and 5 we present methods which each address one of these challenges.

4 Perturbations as superiorization

The use of superiorization in the context of IMRT optimization has been suggested in several publications. In [38, 25] the algorithmic operator is designed to find a solution that satisfies a set of constraints on the dose values and the superiorization function is chosen as an additional merit function, in these cases the total variation of the vector of fluence intensities. In [33] the IMRT optimization problem is translated into a sequence of convex feasibility problems via the level set scheme. The resulting feasibility problems are solved using projection methods. Superiorization is applied with respect to the objective function of the original optimization problem when its decrease is detected to be slow.
In this chapter we consider convex lexicographic optimization problems and explore how superiorization can help to accelerate the process of solving them. In lexicographic optimization we solve so-called levels of optimization, which are single criteria optimization problems. In each optimization level μ we choose a subset of objective functions and accumulate them using a single function Φ_μ, such that the accumulation still is a convex function. In our case we choose Φ_μ to be a weighted sum of the objective function values. We then minimize $\Phi_\mu(x)$ under the given constraints $g_j(x) \leq 0$ for all $j \in J$ plus the constraints that the values of the accumulation functions $\Phi_\gamma, \gamma = 1, ..., \mu - 1$ deviate from the minimal values Φ_γ^* of previous optimization levels only by a small amount δ_γ. The tolerances δ_γ allow the solution algorithm some freedom to move into a descent direction of Φ_μ.
Similar to [33] we solve each optimization level via the level set scheme. We also use projection methods, in our case the simultaneous subgradient projection method, as algorithm to solve the arising convex feasibility problems. Our choice of te superiorization function, however, differs from the one made in [33].
As described in Section 3.4 it may happen that the solver picks a solution of one level, which is unfavorable with respect to the objective of the next level, depending on the choice of the objective function(s) to be minimized in each optimization level. Therefore we choose $\Phi_{\mu+1}(F_{\mu+1}(x))$ as superiorization function $\psi(x)$ in optimization level μ and in this way steer the solver into a direction, which is favorable for the subsequent optimization level. If the set of solutions to the current optimization level μ has more than one element, this process can lead to a solution of optimization level μ, which is closer to a solution of level $\mu + 1$ than the solution of level μ achieved by the unsuperiorized algorithm and thus accelerate the convergence of the overall process.

4.1 The superiorized lexicographic optimization scheme

In this section we combine concepts introduced in Chapter 2 to derive our approach. We consider the multicriteria optimization problem (2.1) and define the priority groups S_μ and weights $\{w_s\}_{s \in S_\mu}$, $\mu = 1, ..., M$. We then translate it into a LO problem like (2.5). Each optimization level μ is a single objective optimization problem with the objective function $\Phi_\mu = \sum_{s \in S_\mu} w_s f_s$, which we convert into its equivalent epigraph form

$$\begin{aligned} &\text{Minimize } t && (4.1)\\ &\quad \text{s. t. } \Phi_\mu(x) - t \leq 0 \\ &\qquad g_j(x) \leq 0 \qquad\qquad \forall j \in J \\ &\qquad \Phi_\gamma(x) \leq \Phi^*_\gamma + \delta_\gamma \qquad \gamma = 1, ..., \mu - 1 \end{aligned}$$

with $\delta_\gamma \geq 0$ for all $\gamma < \mu$. Following the level set scheme we transform the epigraph representation (4.1) into a sequence $\{\boldsymbol{P}^{l,\mu}\}_{l=1}^{L}$ of CFPs. For this procedure we use a decreasing sequence $\{t^{l,\mu}\}_{l=1}^{L}, t_1 = \infty$ which is constructed during the process of solving the sequence of CFPs. The first element for $\mu = 1$ is $t^{1,1} = \infty$, for $\mu \geq 1$ we choose $t^{1,\mu} = 0.99 \cdot \Phi_\mu(x^{*,\mu-1})$ where $x^{*,\mu-1}$ is the solution of the previous optimization level $\mu - 1$. Subsequent elements $t^{l,\mu}$ are chosen as $t^{l,\mu} = 0.99 \cdot \Phi(x^*_{l-1,\mu})$ where $x^*_{l-1,\mu}$ is the solution of the previously solved problem $\boldsymbol{P}^{l-1,\mu}$. Each problem $\boldsymbol{P}^{l,\mu}$ is of the form

$$\text{Find } x \in C^{l,\mu} := \bigcap_{i \in I_\mu} C_i^{l,\mu} \tag{4.2}$$

where $C_i^{l,\mu} := \{x \in \mathbb{R}^n \mid \varphi_i^{l,\mu}(x) \leq 0\}$ and

$$\varphi_i^{l,\mu} := \begin{cases} \Phi_\mu(x) - t^{l,\mu} & i = 1 \\ g_{i-1}(x) & i = 2, ..., m+1 \\ \Phi_{i-(m+1)}(x) - \Phi^*_{i-(m+1)} - \delta_{i-(m+1)} & i = m+2, ..., m+\mu \text{ if } \mu > 1. \end{cases} \tag{4.3}$$

The set of indices i of the functions φ_i is denoted by I_μ with $|I_\mu| = m + \mu$.
We solve each CFP $\boldsymbol{P}^{l,\mu}$ using the simultaneous subgradient projection method as the basic algorithm $\boldsymbol{T}$.

Let $\hat{S} \subseteq \bigcup_{\gamma=\mu+1}^{M} S_\gamma$ be a subset of indices contained in the subsequent priority groups $S_{\mu+1}, \cdots, S_M$ and let $\hat{w}_s$ be weights to the corresponding objective functions.
Then, after having successfully solved K CFPs $\boldsymbol{P}^{l,\mu}$ we include superiorization with respect to $\psi(x) := \sum_{s \in \hat{S}} \hat{w}_s f_s$ by defining d^k as in (2.20) with x^k and setting

$$x^{k+1} = x^k + \beta_k d^k \tag{4.4}$$

where $\beta_k \geq 0$ for all $k \geq 0$ such that $\sum_{k=0}^{\infty} \beta_k < \infty$ and $\psi(x^k + \beta_k d^k) \leq \psi(x^k)$, meaning that d^k is nonascending for ψ at x^k.
In the following we refer to this method as *superiorized lexicographic optimization* (SLO).

4.1.1 Implementation

In this section we show pseudo code of the algorithms we implemented to solve the IMRT optimization problems. Algorithm 1 implements the lexicographic optimization problem turned into a sequence of convex feasibility problems and Algorithm 2 implements the superioriation methodology.

In the following paragraph we give some details about the submethods mentioned in the pseudocode.

`findFeasibleSolution(`t`)` tries to solve the CFP (4.2) with $t = t^{l,\mu}$ within $n_{\max}$ iterations. If this is successful, it returns [x, true] with $x \in C^{l,\mu}$. If this is not successful, the method returns [x, false] with $\Phi_\mu(x) \leq \tilde{t} \leq t^{l-1,\mu}, \tilde{t} > t^{l,\mu}$ and $x \in C_i^{l,\mu}$ for all $i = 2, ..., m + \mu$. $\tilde{t}$ is the smallest upper bound for Φ_μ that the algorithm was able to find a feasible solution for.

`reduce(`$\Phi_\mu(x)$`)` returns a new upper bound $t^{l+1,\mu}$ for Φ_μ that is smaller than $\Phi_\mu(x)$ according to a predefined strategy like (2.10) or (2.11). In our computations we used (2.11) with $\varepsilon_l = 0.01$.

`addConstraint(`Φ_μ^*`)` adds $\Phi_\mu(x) \leq \Phi_\mu^* + \delta_\mu$ to the set of constraints.

`supDirection(`x`)` returns the direction of superiorization at x. In our calculations we used superiorization with respect to the objective function $\Phi_{\mu+1}$ of the following optimization level.

Algorithm 1 Lexicographic level set scheme

```
1: μ = 1
2: x = x^0
3: while μ ≤ M do
4:     if μ == 1 then
5:         t = ∞
6:     else
7:         t = reduce(φ_μ(x))
8:     end if
9:     levelIsSolved = false
10:    counter = 0
11:    while ¬ levelIsSolved do
12:        [x, feasibleSolutionFound] = findFeasibleSolution(t)
13:        counter++
14:        if feasibleSolutionFound then
15:            if t == t_min then
16:                levelIsSolved = true
17:                φ*_μ = φ_μ(x)
18:                addConstraint(φ*_μ)
19:                μ++
20:            else
21:                if μ < M && counter (mod K) == 0 then
22:                    x = superiorize()
23:                end if
24:                t = reduce(φ_μ(x))
25:            end if
26:        else
27:            levelIsSolved = true
28:            φ*_μ = φ_μ(x)
29:            addconstraint(φ*_μ)
30:            μ++
31:        end if
32:    end while
33: end while
```

Algorithm 2 superiorize

```
1: coefficientBigEnough = true
2: base ∈ (0, 1)
3: λ = 0
4: while λ < Λ && coefficientBigEnough do
5:     direction = supDirection(x)
6:     loop = true
7:     exponent = 1
8:     while loop && coefficientBigEnough do
9:         coefficient = base^exponent
10:        x_sup = x + coefficient · direction
11:        if x_sup ≥ 0 && φ_{μ+1}(x_sup) ≤ φ_{μ+1}(x) then
12:            x = x_sup
13:            loop = false
14:            λ++
15:        else
16:            if coefficient > minStepsize then
17:                exponent++
18:            else
19:                coefficientBigEnough = false
20:            end if
21:        end if
22:    end while
23: end while
```

4.2 Results

4.2.1 Demonstrating superiorization: A linear optimization problem

We demonstrate the mechanism of superiorization and how it can be useful for lexicographic optimization on the following linear example.

Example 6. *Solve the multicriteria optimization problem*

$$\begin{aligned} \textit{Minimize } F(x) = \begin{pmatrix} f_1(x) \\ f_2(x) \\ f_3(x) \end{pmatrix} &= \begin{pmatrix} -8x_1 - 12x_2 \\ -14x_1 - 10x_2 \\ -x_1 - x_2 \end{pmatrix} \\ \textit{s.t. } 2x_1 + x_2 - 150 &\leq 0 \\ 2x_1 + 3x_2 - 300 &\leq 0 \\ 4x_1 + 3x_2 - 360 &\leq 0 \\ -x_1 - 2x_2 + 120 &\leq 0 \\ -x_1 &\leq 0 \\ -x_2 &\leq 0 \end{aligned} \tag{4.5}$$

in a lexicographic way with $S_1 = \{1\}, S_2 = \{2\}, S_3 = \{3\}$, $\Phi_1(F_1(x)) = f_1(x), \Phi_2(F_2(x)) = f_2(x), \Phi_3(F_3(x)) = f_3(x)$ *and* $\delta_1 = \delta_2 = 0$.

The optimal solution $x^* = (x_1^*, x_2^*)$ (in the lexicographic sense) is $(30, 80)$ with

$$\begin{aligned} F(x^*) &= (\Phi_1(x^*), \Phi_2(x^*), \Phi_3(x^*)) \\ &= (f_1(x^*), f_2(x^*), f_3(x^*)) \\ &= (-1200, -1220, -110). \end{aligned}$$

We stopped the optimization process at the iterate x^k if $\|F(x^k) - F(x^*)\| \leq 10^{-2}$. In the following, points are given with precision 10^{-2}. In this example calculating the gradients and projections is computationally very cheap, but for IMRT cases gradient- and dose-evaluations consume most of the computation time, so we compare the number of projections and gradient evaluations.

Figure 4.1 shows the feasible region and the trajectories of the iterates of the classical and the superiorized LO for the starting point $x^0 = (0, 47.5)$.
Both methods first seek feasibility and find the point $(5, 57.5)$. In optimization level 1, the classical level set scheme minimizes with respect to Φ_1 only and ends up at the solution $x^{*,1} = (23.08, 84.63)$ of the first optimization level with $\Phi_1^* = \Phi_1(x^{*,1}) = -1200$ using 327 projections and 327 gradient calculations. Additionally, it needs another 260 projections and 518 gradient evaluations to find out that it cannot improve Φ_1 any further while staying feasible. In optimization level 2, the classical LO preserves $\Phi_1(x^k) = \Phi_1^*$ for all subsequent iterates x^k and minimizes Φ_2 under this additional condition. It arrives at the solution $x^{*,2} = (30, 80)$ of optimization level 2 after a total of 4743 projections and 9107 gradient calculations. It cannot improve any further with respect to Φ_3 and has found the optimal solution.

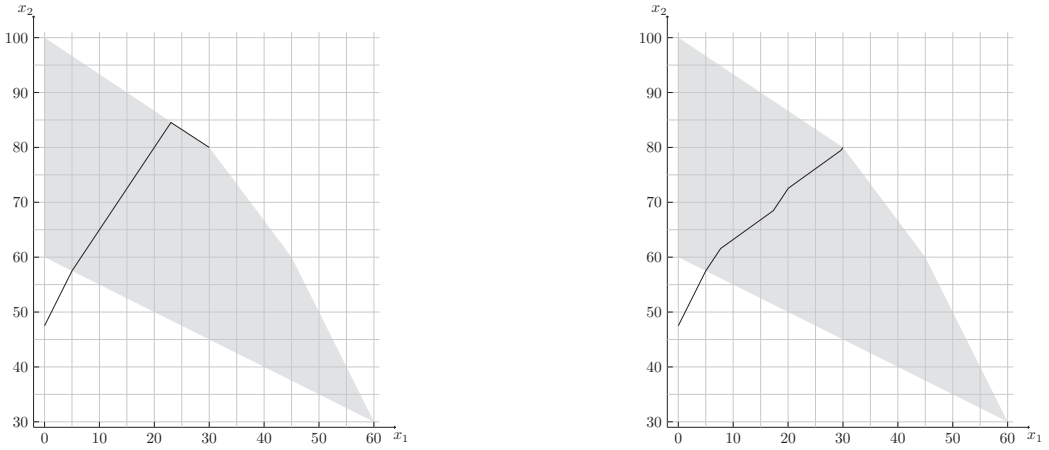

(a) unsuperiorizedLO **(b)** superiorizedLO

Figure 4.1: Trajectories for unsuperiorized and superiorized LO. The set of feasible solutions is shown in light gray.

The superiorized lexicographic optimization minimizes Φ_1 in optimization level 1 but uses superiorization with respect to Φ_2. It arrives at the solution $x^{*,1} = (30, 80)$ of optimization level 1 after 108 projections and 144 gradient calculations, 34 of which were needed for the superiorization. Using superiorized LO we get already sufficiently close to x^* in optimization level 1.

4.2.2 Applying superiorization in practice: IMRT optimization

IMRT optimization model

Table 4.1 shows the functions we chose to formulate the optimization model of the first of the head neck cases according to [55]. The other cases were treated similarly, depending on the individual geometry of the tumor tissue.
Non-tumor Tissue 1 denotes the three-dimensional margin of 1 cm around the lymphatic drainage pathways (which provide the largest of the target volumes and contain both PTV 60 and PTV 70). Non-tumor Tissue 2 is the tissue that consists of everything but the lymphatic drainage pathways and Non-tumor Tissue 1.
These structures are introduced to reduce the radiation to non-tumor tissue, especially to areas which are not covered by any of the organs at risk. Additionally, it offers an incentive to the optimization algorithm to reduce the dose values of the organs at risk that lie outside of the lymphatic drainage pathways even below the prescribed maximum or maximum mean dose values.
In optimization level μ we minimize the objective function $\Phi_\mu = \sum_{s \in S_\mu} w_s f_s$.

Numerical results

From the formulae (3.3.2)–(3.3.2) of the utilized functions it is clear that the minimal value we can hope to achieve for any of the Φ_μ is 0. Thus we considered an optimization level μ to be solved, if for some $l > 0$ a solution x_l^* of the CFP $\boldsymbol{P}^l$ fulfills $\Phi_\mu(x_l^*) \leq t_{\min} := 10^{-8}$. Then $x^{*,\mu} = x_l^*$ and $\Phi_\mu^* = \Phi_\mu(x_l^*)$.

Table 4.1: Evaluation functions of the structures under consideration gathered in different priority groups.

planning structure $\mathcal{O}$	function	parameters	priority group
PTV 70	lower tail penalty	$L = 66.5$	constraint
PTV 70	upper tail penalty	$U = 80.5$	constraint
PTV 70	mean upper tail penalty	$M = 73.5$	constraint
Myelon	upper tail penalty	$U = 45$	constraint
PTV 60	lower tail penalty	$L = 57.5$	I_1
Eye right	upper tail penalty	$U = 45$	I_1
Eye left	upper tail penalty	$U = 45$	I_1
Optic nerve right	upper tail penalty	$U = 50$	I_1
Optic nerve left	upper tail penalty	$U = 50$	I_1
Parotis left	mean upper tail penalty	$M = 26$	I_1
Lymphatic drainage	lower tail penalty	$L = 47.5$	I_2
Parotis right	mean upper tail penalty	$M = 26$	I_2
Brain	upper tail penalty	$U = 60$	I_2
Brainstem	upper tail penalty	$U = 52$	I_2
Larynx	mean upper tail penalty	$M = 45$	I_2
Esophagus	mean upper tail penalty	$M = 45$	I_2
Oral cavity	mean upper tail penalty	$M = 40$	I_2
Non-tumor Tissue 2	mean upper tail penalty	$M = 5$	I_2
Plexus right	upper tail penalty	$U = 63$	I_3
Plexus left	upper tail penalty	$U = 63$	I_3
Mandible	upper tail penalty	$U = 75$	I_3
Inner ear right	upper tail penalty	$U = 45$	I_3
Inner ear left	upper tail penalty	$U = 45$	I_3
Lips	upper tail penalty	$U = 30$	I_3
Non-tumor Tissue 1	mean upper tail penalty	$M = 20$	I_3

What requires most of the computational effort with IMRT cases are multiplications of the dose matrix $\boldsymbol{D}$ with the fluence vector x which occur when we evaluate the dose or calculate the objective function gradient for a given x. The number of these multiplications is what we use here as units to measure progress, i.e., reduction of objective function values, of the classical and the superiorized LO.

In Algorithm 1 and 2 in Subsection 4.1.1 parameters K and Λ occur, which determine the behavior of the method. K is the number of CFPs that have to be solved successfully before superiorization is applied and Λ is the maximum number of superiorization steps that are taken. If the superiorization step size is smaller than a predefined threshold or the maximum number of steps is reached, the superiorization stops and we solve the next CFP.

In Tables 4.2 and 4.3 we first present results we achieved by trying different parameter sets (K, Λ) and then picking for each case individually the set that resulted in the fastest convergence of the algorithm, measured in the number of multiplications. We refer to the sets of parameters picked according to this strategy as $(\hat{K}, \hat{\Lambda})$ and call the superiorized lexicographic optimization scheme using these parameter sets "fast SLO". All values presented in the tables in this section are rounded to 10^{-4}.

The results presented in Table 4.2 show that fast SLO results in equal or lower objective values than unsuperiorized LO within less multiplications. In Table 4.3 we see that fast SLO produces solutions of the single optimization levels with potentially lower objective values of the subsequent objective functions than unsuperiorized LO. Fast SLO thus offers a better starting point to the single optimization levels than unsuperiorized LO which reduces the overall number of multiplications.

$\Phi_\mu^* = \Phi_\mu(x^{*,\mu})$ denotes the value of Φ_μ at the solution $x^{*,\mu}$ of optimization level μ obtained using the classical LO. $\hat{\Phi}_\mu^* = \Phi_\mu(\hat{x}^{*,\mu})$ denotes the value of Φ_μ at the solution $\hat{x}^{*,\mu}$ of optimization level μ obtained using the superiorized LO with the parameter set $(\hat{K}, \hat{\Lambda})$.
N_j^k is the number of multiplications needed by the classical LO to solve optimization levels $j+1$ to level k. $N := N_0^M = \sum_{j=0}^{M-1} N_j^{j+1}$ is the total number of multiplications needed to solve the entire lexicographic optimization problem. Analogously, $\hat{N}_j^k$ denotes the number of multiplications needed by the superiorized LO with $(\hat{K}, \hat{\Lambda})$ to solve optimization levels $j+1$ to$k$ and $\hat{N} := \sum_{j=0}^{M-1} \hat{N}_j^{j+1}$.
For our calculations we chose $\delta_\mu = 0.1\Phi_\mu^*$ for the classical LO and $\delta_\mu = 0.1\hat{\Phi}_\mu^*$ for the superiorized LO.

Table 4.2: Optimal objective value and total multiplication number ratios for $(\hat{K}, \hat{\Lambda})$. Fast SLO achieves lower or equal objective values than unsuperiorized LO within fewer multiplications. The notation $1^\Diamond$ means that we solved the optimization level, meaning that the objective function value has dropped below 10^{-8}.

	$\hat{\Phi}_1^*/\Phi_1^*$	$\hat{\Phi}_2^*/\Phi_2^*$	$\hat{\Phi}_3^*/\Phi_3^*$	$\hat{N}/N$
case 1	$1^\Diamond$	0.9598	0.9923	0.8998
case 2	$1^\Diamond$	0.9743	0.9960	0.6612
case 3	$1^\Diamond$	0.9996	1.0000	0.9210
case 4	$1^\Diamond$	0.9708	0.9941	0.8959

Table 4.3: Multiplication numbers per optimization level and objective values of starting points for $(\hat{K}, \hat{\Lambda})$. Fast SLO produces solutions of the single optimization levels with potentially lower objective values of the subsequent objective functions than unsuperiorized LO.

	$\hat{N}_0^1/N_0^1$	$\hat{N}_1^2/N_1^2$	$\hat{N}_2^3/N_2^3$	$\Phi_2(\hat{x}^{*,1})/\Phi_2(x^{*,1})$	$\Phi_3(\hat{x}^{*,2})/\Phi_3(x^{*,2})$
case 1	1.6521	0.5669	0.9895	0.3741	0.9856
case 2	1.4066	0.3588	1.0065	0.3682	1.0008
case 3	1.0403	0.8594	1.0000	0.5625	1.0075
case 4	0.3818	1.0536	0.8591	0.8196	0.9939

It is not clear a priori how to choose values for K and Λ for a given problem. Therefore we aimed to find a robust set of parameters that yields good results for all four IMRT cases and could possibly be applied for other IMRT head neck cases as well. We refer to this set

of parameters as $(\check{K}, \check{\Lambda})$ and call the superiorized lexicographic optimization scheme using this parameter sets "robust SLO". The results for the robust parameter set are presented in Table 4.4 and 4.5.
The results in Table 4.4 show that robust SLO achieves comparable objective values to unsuperiorized LO within fewer multiplications. In Table 4.5 we see that robust SLO, too, produces solutions of the single optimization levels with potentially lower objective values of the subsequent objective functions than unsuperiorized LO. Like fast SLO, robust SLO also offers a better starting point to the single optimization levels than unsuperiorized LO, which again reduces the overall number of multiplications.

Following the previous notation $\check{\Phi}^*_\mu = \Phi_\mu(\check{x}^{*,\mu})$ is the value of Φ_μ at the solution $\check{x}^{*,\mu}$ of optimization level μ obtained using the superiorized LO with $(\check{K}, \check{\Lambda})$.
$\check{N}^k_j$ denotes the number of multiplications needed by the superiorized LO with $(\check{K}, \check{\Lambda})$ to solve optimization levels $j+1$ to k and $\check{N} := \sum_{j=0}^{M-1} \check{N}^{j+1}_j$.

Table 4.4: Optimal objective value and total multiplication number ratios for $(\check{K}, \check{\Lambda})$. Robust SLO achieves comparable objective values to unsuperiorized LO within fewer multiplications. The notation $1^\Diamond$ means that we solved the optimization level, meaning that the objective function value has dropped below 10^{-8}.

	$\check{\Phi}^*_1/\Phi^*_1$	$\check{\Phi}^*_2/\Phi^*_2$	$\check{\Phi}^*_3/\Phi^*_3$	$\check{N}/N$
case 1	$1^\Diamond$	1.0046	1.0002	0.9177
case 2	$1^\Diamond$	1.0020	1.0043	0.8877
case 3	$1^\Diamond$	0.9829	0.9969	0.9541
case 4	$1^\Diamond$	1.0245	1.0071	0.8859

Table 4.5: Multiplication numbers per optimization level and objective values of starting points for $(\check{K}, \check{\Lambda})$. Robust SLO produces solutions of the single optimization levels with potentially lower objective values of the subsequent objective functions than unsuperiorized LO.

	$\check{N}^1_0/N^1_0$	$\check{N}^2_1/N^2_1$	$\check{N}^3_2/N^3_2$	$\Phi_2(\check{x}^{*,1})/\Phi_2(x^{*,1})$	$\Phi_3(\check{x}^{*,2})/\Phi_3(x^{*,2})$
case 1	1.1825	0.6972	0.9849	0.3916	1.0008
case 2	0.7447	0.8409	0.9999	0.5194	1.0058
case 3	1.1320	0.9029	0.9999	0.5530	1.0007
case 4	1.2453	0.8575	0.8664	0.4959	1.0103

In Figure 4.2 we present the cumulative DVH of case 1 with the dose distribution resulting from the solution of superiorized LO with the robust parameter set $(\check{K}, \check{\Lambda})$.
The underlying dose matrix was created using CERR [27]. Note that the dose calculation via the dose matrix, which is used in the optimization algorithm, provides only an approximation to the dose values calculated by CERR which are depicted in Figure 4.2. Thus the DVH curves show e.g. that dose values below 66.5 Gy occur in the PTV70 even though in the optimization the mathematical constraint ensuring that this does not happen is not violated.

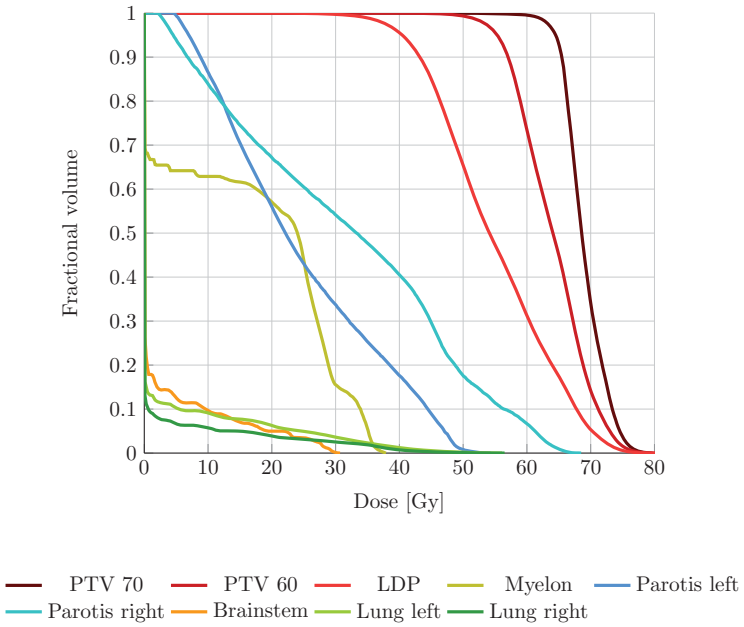

Figure 4.2: DVHs resulting from solution dose of robustly superiorized LO.

In Figure 4.3 we present the objective values of Φ_1, Φ_2 and Φ_3 plotted against the number of dosematrix-vector-multiplications for case 1. To show the fundamental behavior of the superiorization method we intentionally did not give any actual numbers in the plots in Figure 4.3.
In Figure 4.3a and 4.3b we see how Φ_2 increases while we minimize Φ_1 in level 1 using classical LO. We also see how the superiorization with respect to Φ_2 disturbs the minimization of Φ_1 and leads to N_0^1 being smaller than $\hat{N}_0^1$. Figure 4.3b shows that $\hat{x}^{*,1}$ is a better starting point for the minimization of Φ_2 in level 2 than $x^{*,1}$ because its objective value of Φ_2 is significantly lower. This results in $\hat{N}_1^2$ being notably smaller than N_1^2.
Due to the correlation of the clinical goals there are relatively few CFPs to be solved in optimization level 2 for all cases. When superiorization is applied (both with optimal and robust (K, Λ)) we even get so close to the minimum of Φ_2 at the end of level 1 that for these parameter sets the CFP in level 2 turns inconsistent within less than $\hat{K}$ or $\check{K}$ reductions of $t^{l,2}$. Therefore no superiorization is applied in level 2 and the objective value of Φ_3 is about the same for fast SLO, robust SLO and unsuperiorized LO.
As we can see from Figure 4.3c superiorization with respect to Φ_2 during level 1 can – depending on the correlation of the objective functions – reduce the value of Φ_3 and $\hat{N}_2^3$.
Similar behavior can be observed for the superiorized LO that uses the robust parameter set $(\check{K}, \check{\Lambda})$.

4.3 Discussion

In this chapter we phrased a convex multicriteria optimization problem as a convex lexicographic optimization problem. We combined this multicriteria optimization technique with the superiorization methodology to accelerate the convergence by steering the algorithm towards solutions of the optimization levels, which are favorable for the next level. We applied

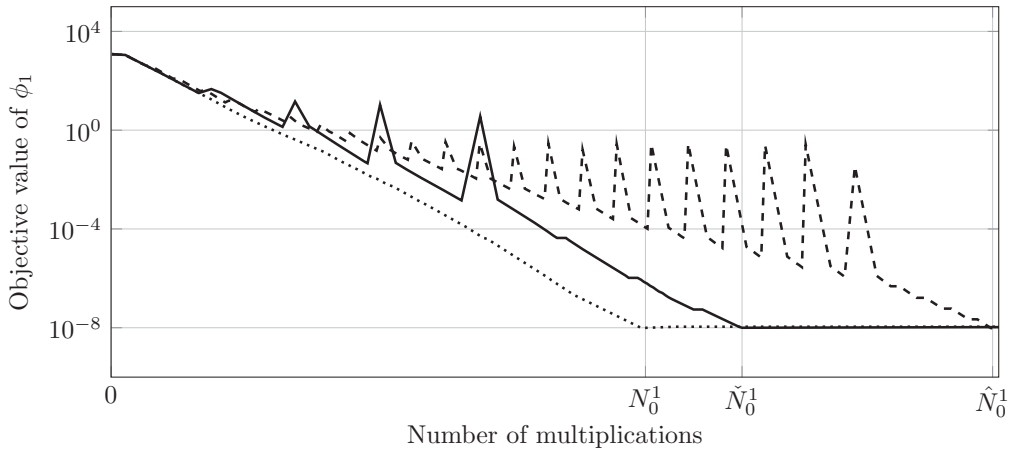

(a) Values of Φ_1 for robust SLO, fast SLO and unsuperiorized LO.

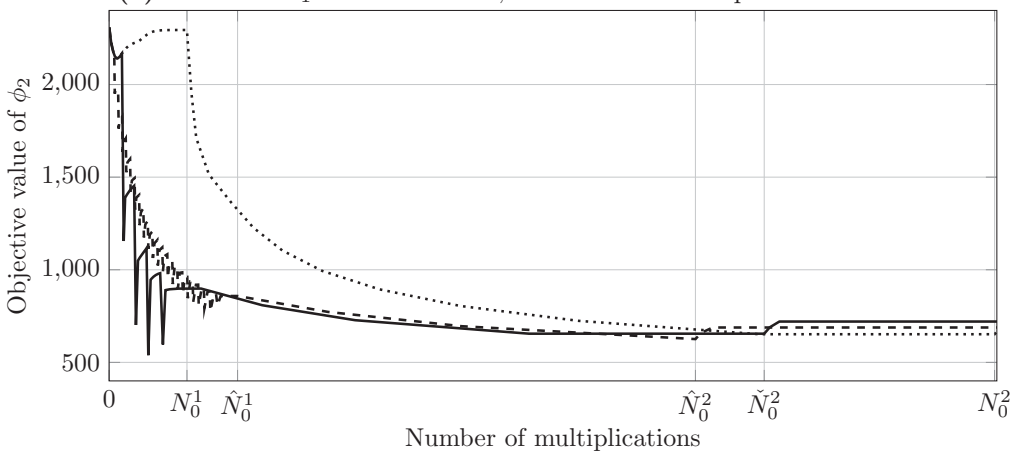

(b) Values of Φ_2 for robust SLO, fast SLO and unsuperiorized LO.

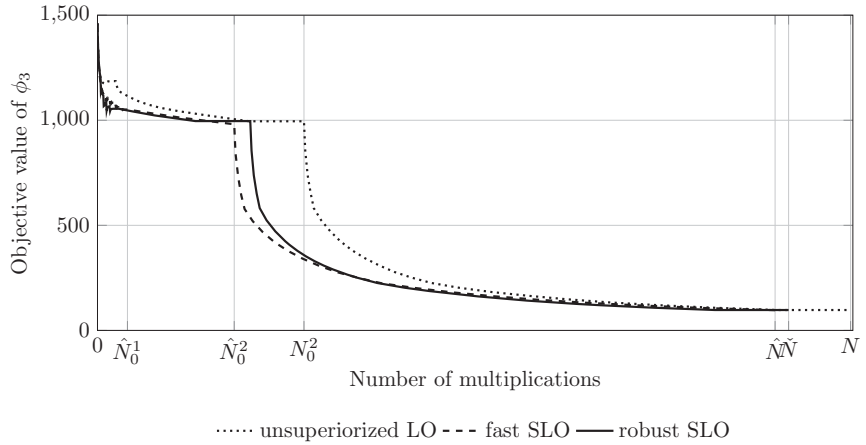

(c) Values of Φ_2 for robust SLO, fast SLO and unsuperiorized LO.

robust SLO fast SLO unsuperiorized LO

Figure 4.3: Superiorization perturbs the optimization of Φ_1. Superiorization applied in level 1 offers a starting point with significantly lower value of Φ_2 and accelerates the optimization of Φ_2. No superiorization is applied in level 2 and SLO and unsuperiorized LO perform similarly. Due to the acceleration in level 2 the overall number of multiplications is lower for SLO.

our approach to IMRT optimization problems and in the process included a priori knowledge of the decision maker about the priorities of different clinical goals.
We solved each optimization level by transforming it via the level set scheme into a sequence of convex feasibility problems. We then used the simultaneous subgradient projection method to solve each feasibility problem and perturbed this process according to previously chosen parameters by superiorization with respect to the objective function of the next optimization level.
We chose the unit to measure progress as multiplications of dose matrix and fluence vector, because these multiplications make up the vast majority of the computational effort in the optimization process. For the four IMRT head-neck cases we considered we determined two kinds of parameter sets in an experimental way. The first parameter set is chosen individually for each case such that the convergence was fast as possible. With this parameter set we are able to reduce the number of multiplications by at least 7.9% and at most 33.8% with an average of 15.6% The second set of parameters is chosen with the intention of determining one "robust" pair of values which works reasonably well for all cases. This choice results in a convergence acceleration of at least 4.6% and at most 11.4% with an average of 8.9%.
Choosing the superiorization parameters in an experimental way as we did is of course very time consuming and therefore not a practical approach for real world application. An interesting question for future research would be if robust parameters determined by experiments on large numbers of similar problems, i.e. with similar trade offs among the objective functions and the superiorization function(s), yield equally good results on further problems of the same group. If the superiorization parameters are chosen poorly the convergence of the overall procedure can happen to be delayed.
Our choice of the superiorization function ψ is of course not the only possible one. A weighted sum of different evaluation functions than we chose or a function that is not included in the lexicographic optimization model at all but contains information on some kind of a priori or meta knowledge, could be considered as well.

5 Perturbations as anti-zigzag strategy

In this chapter we explore a different way of using perturbations than in the previous one. Our approach is designed to address the zigzagging behavior resulting from the ill-conditionedness of the IMRT optimization problem and the conflicting clinical goals for neighboring volumes we described in Section 3.4.

Projection methods use subgradient or first order derivative information evaluated at the current iterate in order calculate the next iterate. In this aspect they are very similar to the Steepest Descent Method, which is the basis for many gradient-based solution procedures. Projection methods as well as the Steepest Descent Method suffer from zigzagging and thus slow convergence when they solve an ill-conditioned problem and gradients evaluated at subsequent iterates are strongly opposing. For the Steepest Descent Method there exist numerous strategies to improve the convergence in the context of unconstrained optimization like e.g. Conjugate Gradient Methods, the Newton method, quasi-Newton methods and many combinations and variations of these approaches, see e.g. [4]. The Newton method and various quasi-Newton methods use second order derivative information in the form of the inverse of the Hessian matrix or approximations of it. These approaches have found their way into constrained optimization in (quasi-Newton) SQP algorithms.

While sophisticated methods like these have desirable convergence properties and are applied successfully in many areas, in IMRT optimization even they are challenged by the degeneracy of the Hessian of the objective function, see e.g. [1, 12]. SQP algorithms often include a lot of overhead and parameters which need to be tuned and require specific properties of the functions used to model the optimization problem. Furthermore, calculating second order derivative information is extremely computationally expensive for IMRT optimization problems due to the size of the dose matrix. Therefore, our goal is to improve the convergence behavior of the comparably simple projection methods using again simple tools, which are computationally cheap to evaluate.

We borrow the ideas for developing these tools from inertial methods, which only require first oder derivative information of the current and the previous iterate, as well as from a method presented in [30], which combines the idea of surrogate constraint methods with relaxed, averaged projections. In Section 5.3 we present a detailed derivation of the perturbations developed by us.

5.1 The perturbed level set scheme

We now combine the concept of perturbations we presented in Section 2.4 and the level set scheme introduced in Section 2.2 into an algorithm we call the perturbed level set scheme.

To solve the constrained convex optimization problem (2.2)

$$\begin{aligned} &\text{Minimize } \Phi(x) \\ &\text{s.t.} \quad g_j(x) \leq 0 \qquad \forall j \in J \end{aligned}$$

we convert it into its epigraph representation (2.6)

$$\begin{aligned} &\text{Minimize } t \\ &\text{s.t. } \Phi(x) - t \leq 0 \\ &\qquad g_j(x) \leq 0 \quad \forall j \in J. \end{aligned}$$

Then we use the level set scheme to transform the epigraph representation into a sequence $\{\boldsymbol{P}^l\}_{l=1}^L$ of CFPs. For this procedure we use a decreasing sequence $\{t^l\}_{l=1}^L, t_1 = \infty$ which is constructed during the process of solving the sequence of CFPs. The first element is $t^1 = \infty$ and subsequent elements t^l are chosen as $t^l = \Phi(x_{l-1}^*)(1 - \varepsilon_{l-1})$ according to (2.11) where $\varepsilon_{l-1} = 0.01$ and x_{l-1}^* is the solution of the previous CFP $\boldsymbol{P}^{l-1}$. Each problem $\boldsymbol{P}^l$ is of the form

$$\text{Find } x \in C^l = \bigcap_{i \in I} C_i^l \tag{5.1}$$

with $C_i^l := \left\{x \in \mathbb{R}^n \mid \varphi_i^l(x) \leq 0\right\}, I = \{1, ..., m+1\}$ and

$$\varphi_i^l(x) := \begin{cases} \Phi(x) - t^l & i = 1 \\ g_{i-1}(x) & i = 2, ..., m+1. \end{cases}$$

Next we use the simultaneous (2.15) or cyclic projection (2.13) as operator $\boldsymbol{T}$ to solve each CFP $\boldsymbol{P}^l$. If the use of perturbations is specified, we use either the inner (2.28) or the outer perturbation scheme (2.26) defined in Section 2.5, which we recall here briefly for convenience.
We define functions $c : \mathbb{R}^n \to \{\text{false, true}\}$ and $\tilde{c} : \mathbb{R}^n \times \mathbb{R}^n \to \{\text{false, true}\}$ with

$$\tilde{c}(x^k, x^{k-1}) := \begin{cases} \neg\tilde{c}(x^{k-1}, x^{k-2}) \wedge c(x^k) & k > 1 \\ c(x^k) & k \leq 1 \end{cases}$$

which determine, whether an iteration is to be perturbed for $k \geq 1$. $\tilde{c}(x^k, x^{k-1})$ is by construction only true, if $\tilde{c}(x^{k-1}, x^{k-2})$ is false and $c(x^k)$ is true, i.e. if iteration $(k-1) \to k$ has not been perturbed and the condition c is fulfilled at x^k.
The sequence of iterates $\{x^k\}_{k=0}^\infty$ generated by the outer perturbation scheme is

$$x^{k+1} = \boldsymbol{T}(x^k) + \beta_k b^k$$

where $\{\beta_k\}_{k=0}^\infty$ is a sequence with $\beta_k \in \mathbb{R}_{\geq 0}$ for all $k \geq 0$ and $\sum_{k=0}^{\infty} \beta_k < \infty$,

$$b^k = \begin{cases} \tilde{b}^k - \lambda(x^k)p(x^k) & \text{if } \tilde{c}(x^k, x^{k-1}) = \text{ true} \\ 0 & \text{otherwise} \end{cases}$$

and the sequence $\{b^k\}_{k=0}^{\infty}$ is bounded.
Using the inner perturbation scheme the iterates $\{x^k\}_{k=0}^{\infty}$ are generated using the following rule:

$$x^{k+1} = \boldsymbol{T}(x^k + \beta_k b^k)$$

where again $\{\beta_k\}_{k=0}^{\infty}$ is a sequence with $\beta_k \in \mathbb{R}_{\geq 0}$ for all $k \geq 0$ and $\sum_{k=0}^{\infty} \beta_k < \infty$,

$$b^k = \begin{cases} \tilde{b}^k & \text{if } c(x^k) = \text{ true} \\ 0 & \text{otherwise} \end{cases}$$

and the sequence $\{b^k\}_{k=0}^{\infty}$ is bounded.
In Section 5.3 we give a more concrete form of the perturbation vectors b^k. There we define the Nesterov (5.22), the heavy ball (5.16) and the surrogate constraint perturbation (5.33), which we use in the outer perturbation scheme for our numerical results presented in Section 5.6.

5.2 Zigzagging of projection steps in IMRT optimization

In what follows we present observations from the unperturbed solving process of IMRT optimization problems via the level set scheme using the simultaneous projection as operator $\boldsymbol{T}$ to solve the arising CFPs as described in Section 5.1. Our observations illustrate and quantify the statement made in Section 3.4 that zigzagging behavior occurs in IMRT optimization. We demonstrate that during the whole solving process of an IMRT optimization problem, the simultaneous projection method moves in the majority of iterations in zigzagging directions, which lie almost only within a single plane whereas the decision variable space is about 2000-dimensional.
When we use the level set scheme presented in Section 2.2 to solve IMRT optimization problems together with the simultaneous projection (2.16) as operator $\boldsymbol{T}$ that solves the arising CFPs, we observe two phenomena in all of the IMRT cases we considered. In this section we present these two phenomena and quantify them to illustrate the behavior of the unperturbed simultaneous projection in IMRT optimization.
In this section we use the following notation. The index k of the iterates x^k generated in each consistent CFP $\boldsymbol{P}^l$ with $l = 1, ..., L-1$ goes from 1 to K_l, which makes x^{K_l} the last iterate and therefore a solution of $\boldsymbol{P}^l$. Note that we are referring to our implementation here, which means that $K_l \leq n_{\max}$ for all $l = 1, ..., L-1$, where $n_{\max}$ is the maximum number of iterations for the (both perturbed and unperturbed) projection methods to solve a CFP $\boldsymbol{P}^l$ arising from the level set scheme. When we want to specify from which CFP $\boldsymbol{P}^l$ an iterate results, we denote it by x_l^k. Thereby we can distinguish iterates from different CFPs, e.g. $\boldsymbol{P}^{l_1}$ and $\boldsymbol{P}^{l_2}$, by using the notation $x_{l_1}^k$ and $x_{l_2}^k$.

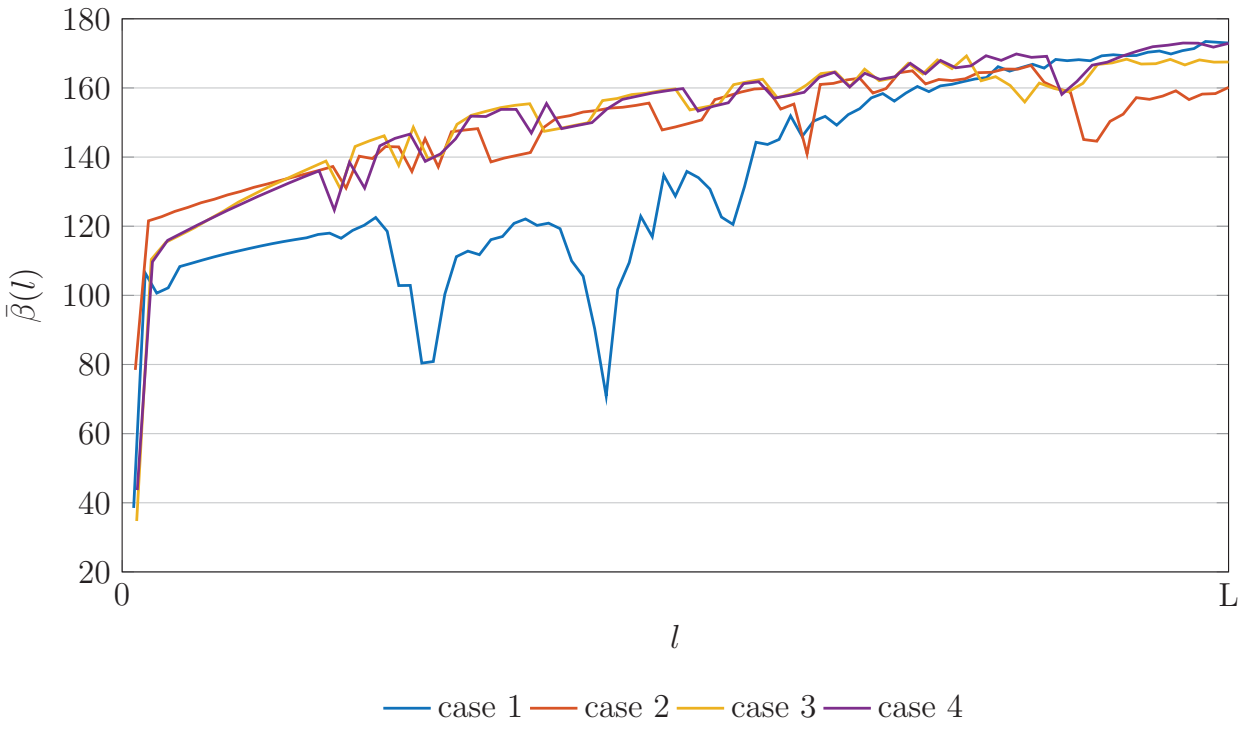

Figure 5.1: The value of $\bar{\beta}_l$ for all CFPs $\boldsymbol{P}^l$. $\bar{\beta}_l$ approaches 180° for increasing l.

Zigzagging

The first phenomenon we present is zigzagging projection steps, i.e.

$$\langle \bar{p}(x^k), \bar{p}(x^{k+1}) \rangle = -1 + \epsilon$$

for subsequent iterates x^k, x^{k+1} generated by $\boldsymbol{T}$, $\bar{p}(x) = p(x)/\|p(x)\|$ with p being the simultaneous projection step (2.16) and $0 < \epsilon \ll 1$. The zigzagging behavior tends to get more frequent and more severe over the course of the optimization process. We considered the mean value of

$$\beta(k, k+1, l) := \cos^{-1}\left(\langle \bar{p}(x_l^k), \bar{p}(x_l^{k+1}) \rangle\right)$$

over $k = 1, .., K_l - 2$ for each CFP $\boldsymbol{P}^l$ (5.1), which we denote by $\bar{\beta}(l)$ for $l = 1, ..., L-1$. Figure 5.1 shows how $\bar{\beta}(l)$ changes over the CFPs $\boldsymbol{P}^l$ for all four IMRT cases.
The total number of values of $\beta(k, l)$ occurring over all CFPs $\boldsymbol{P}^l$ for $l = 1, ..., L-1$ is $K_{\text{total}} := \sum_{l=1}^{L-1}(K_l - 2)$. Let $h(\beta)$ be the number of values $\beta(k, k+1, l)$ over all $k = 1, ..., K_l - 2$ and $l = 1, ..., L-1$ for which $\beta(k, k+1, l) \geq \beta$. In Figure 5.2 we present a diagram that shows the fraction

$$h(\beta)/K_{\text{total}} \tag{5.2}$$

for all four IMRT cases.
Figures 5.1 and 5.2 show that the majority of subsequent projection directions is strongly opposing and that the frequency of this phenomenon increases when l approaches $L-1$,

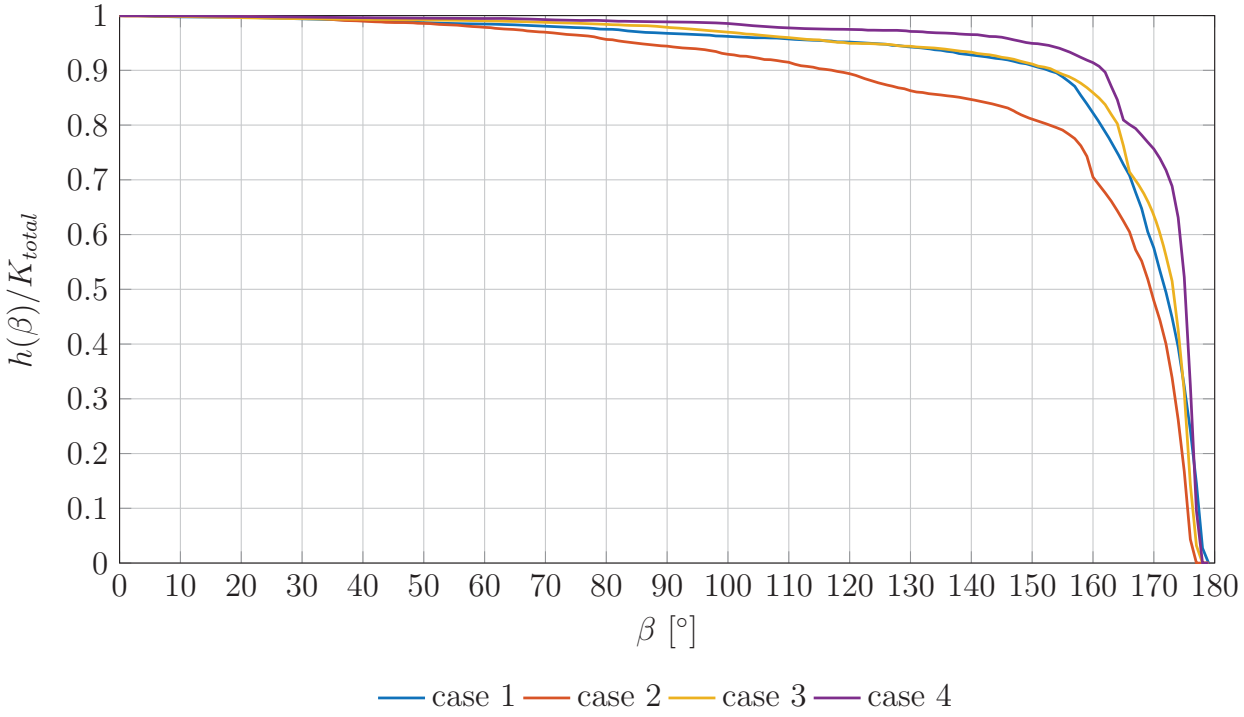

Figure 5.2: The fraction $h(\beta)/K_{\text{total}}$ (5.2) for all four IMRT cases. The majority of subsuquent projection steps is strongly opposing.

i.e. when the upper bounds t^l in the CFPs $\boldsymbol{P}^l$ approach $\Phi(x^*_{L-1})$ and the problems become harder to solve.

Movement within a plane

The second phenomenon we observe is that not only subsequent projection steps are often strongly opposing, but also that after some initial CFPs every other projection step points into almost the same direction. This means that from a certain point on the simultaneous projection moves through the about 2000-dimensional space of decision variables almost only in a subspace spanned by two vectors.
We denote by $\tilde{l}$ the index of the CFP $\boldsymbol{P}^{\tilde{l}}$ in which the zigzagging for the first time passes a certain threshold, i.e.

$$\cos^{-1}\left(\langle \bar{p}(x^k_{\tilde{l}}), \bar{p}(x^{k+1}_{\tilde{l}})\rangle\right) \geq 150°. \tag{5.3}$$

for any $k = 1, ..., K_{\tilde{l}} - 2$.

Normalized inner products of projection steps within each CFP

To quantify this observation we present a normalized cumulative histogram in Figure 5.3. For the values in this fFigure we calculated for each CFP $\boldsymbol{P}^l$ with $l = \tilde{l}, ..., L-1$ the values of

$$\beta(k, \hat{k}, l) := \cos^{-1}\left(\langle \bar{p}(x^k_l), \bar{p}(x^{\hat{k}}_l)\rangle\right) \tag{5.4}$$

for all $k = 1, ..., K_l - 2$ and all $k < \hat{k} \leq K_l - 1$.
For each CFP $\boldsymbol{P}^l$ the total number of these values is $K_{l,\text{total}} := (K_l - 2)(K_l - 1)/2$. Let $h(\beta, l)$ denote the number of values $\beta(k, \hat{k}, l)$ for which $\beta(k, \hat{k}, l) \geq \beta$.
We added the fractions $h(\beta, l)/K_{l,\text{total}}$ for all $\beta = 1°, 2°, ..., 180°$ and all $l = 1, .., L - 1$ and again normalized the result

$$H(\beta) := \left(\sum_{l=1}^{L-1} h(\beta, l)/K_{l,\text{total}} \right) /(L - 1), \tag{5.5}$$

which is depicted in Figure 5.3.
Figure 5.4 shows an normalized cumulative histogram of

$$\tilde{\beta}(k, \hat{k}, l) := \cos^{-1} \left(|\langle \bar{p}(x_l^k), \bar{p}(x_l^{\hat{k}}) \rangle| \right) \tag{5.6}$$

calculated in the same way as the data for Figure 5.3. Here, we denote by $\tilde{h}(\beta, l)$ the number of values $\tilde{\beta}(k, \hat{k}, l)$ for which $\tilde{\beta}(k, \hat{k}, l) \geq \beta$. The fraction

$$\tilde{H}(\beta) := \left(\sum_{l=1}^{L-1} \tilde{h}(\beta, l)/K_{l,\text{total}} \right) /(L - 1) \tag{5.7}$$

is depicted in Figure 5.4.
The histograms in Figures 5.3 and 5.4 tell us that for all four cases within the solving process of each CFP $\boldsymbol{P}^l$ (for $l \geq \tilde{l}$) in 80-90% of the iterations $\bar{p}(x^k)$ deviates from either $\bar{p}(x^{\hat{k}})$ or $-\bar{p}(x^{\hat{k}})$ by at most 30° with $k < \hat{k}$. Therefore one could say that the solving process of each CFP $\boldsymbol{P}^l$ is dominated by two directions, which are strongly opposing.

Normalized inner products of projection steps from last feasible CFP with all previous CFPs

Finally we want to know if the two directions dominating the solving process of each CFP are similar for several or even all CFPs. We therefore examine the normalized inner products $\langle \bar{p}(x_{L-1}^{\hat{k}}), \bar{p}(x_l^k) \rangle$ with $\hat{k} = 0, ..., K_{L-1}, k = 0, .., K_l$ for all $l = \tilde{l}, ..., L - 1$, of all directions used in the last feasible CFP $\boldsymbol{P}^{L-1}$ with all directions used in previous CFPs $\boldsymbol{P}^l$ after the zigzagging has passed the aforementioned threshold (5.3) for the first time in the CFP $\boldsymbol{P}^{\tilde{l}}$.
We consider the values

$$\beta(k, \hat{k}, l, L - 1) := \cos^{-1}(\langle \bar{p}(x_{L-1}^{\hat{k}}), \bar{p}(x_l^k) \rangle)$$

and

$$\tilde{\beta}(k, \hat{k}, l, L - 1) := \cos^{-1}(|\langle \bar{p}(x_{L-1}^{\hat{k}}), \bar{p}(x_l^k) \rangle|)$$

and generate from them two normalized cumulative histograms in the same way as for Figures 5.3 and 5.4 before.
In Figure 5.5 and 5.6 we present

$$H(\beta) := \left(\sum_{l=1}^{L-1} h(\beta, l)/K_{l,\text{total}} \right) /(L - 2) \tag{5.8}$$

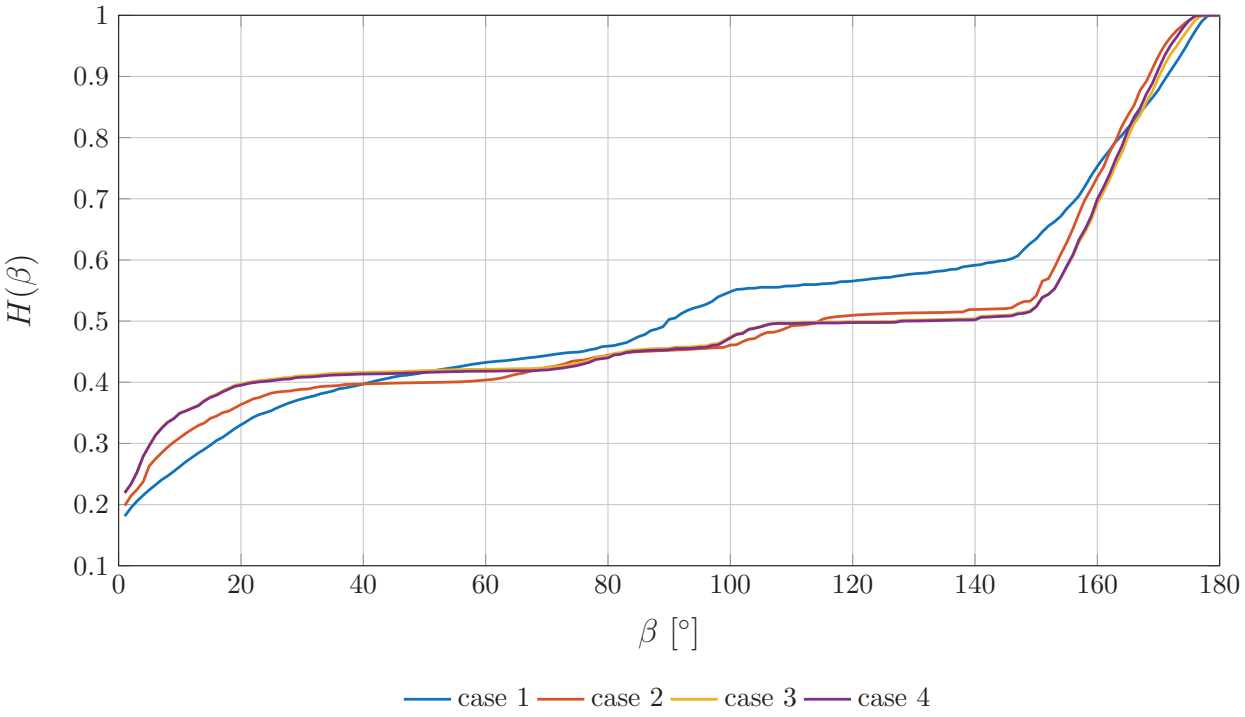

Figure 5.3: Normalized cumulative histogram of $\cos^{-1}(\langle \bar{p}(x_l^k), \bar{p}(x_l^{\hat{k}}) \rangle)$ over all $l = \tilde{l}, ..., L-1$.

and

$$\tilde{H}(\beta) := \left(\sum_{l=1}^{L-1} \tilde{h}(\beta, l) / K_{l,\text{total}} \right) / (L-2) \tag{5.9}$$

plotted against β.
The curves are very similar to those in Figures 5.3 and 5.4, which indicates that not only the solving process of each CFP is dominated by just two strongly opposing directions, but that these dominant directions do not change significantly over all CFPs once the zigzagging has passed the threshold (5.3) for the first time. From that point onwards the optimization process generates iterates, which deviate very little from one plane within an about 2000-dimensional decision variable space. These limitations are a strong indicator for slow convergence of the simultaneous projection method.

Simplified 2D simulation

To give the reader an impression of how a trajectory of iterates resulting from the solving process of one CFP $\boldsymbol{P}^l$ might look like we made a simplified 2D simulation based on the observations we mentioned before and the step lengths which occurred during the IMRT optimization. We chose the artificial starting point $(0, 0)$ and assumed that the iterates move only within the (x, y)-plane. Furthermore, we assumed that $\cos^{-1}(\langle \bar{p}(x_l^k), \bar{p}(x_l^{k-1}) \rangle) = 150°$ for all $k \geq 1$. We generated the iterates x^k according to these assumptions and the actual step lengths $\|p(x_{L-1}^k)\|$ occurring in the last feasible CFP $\boldsymbol{P}^{L-1}$ of one of the IMRT cases. Figure 5.7 shows the trajectory resulting from these simplifications.

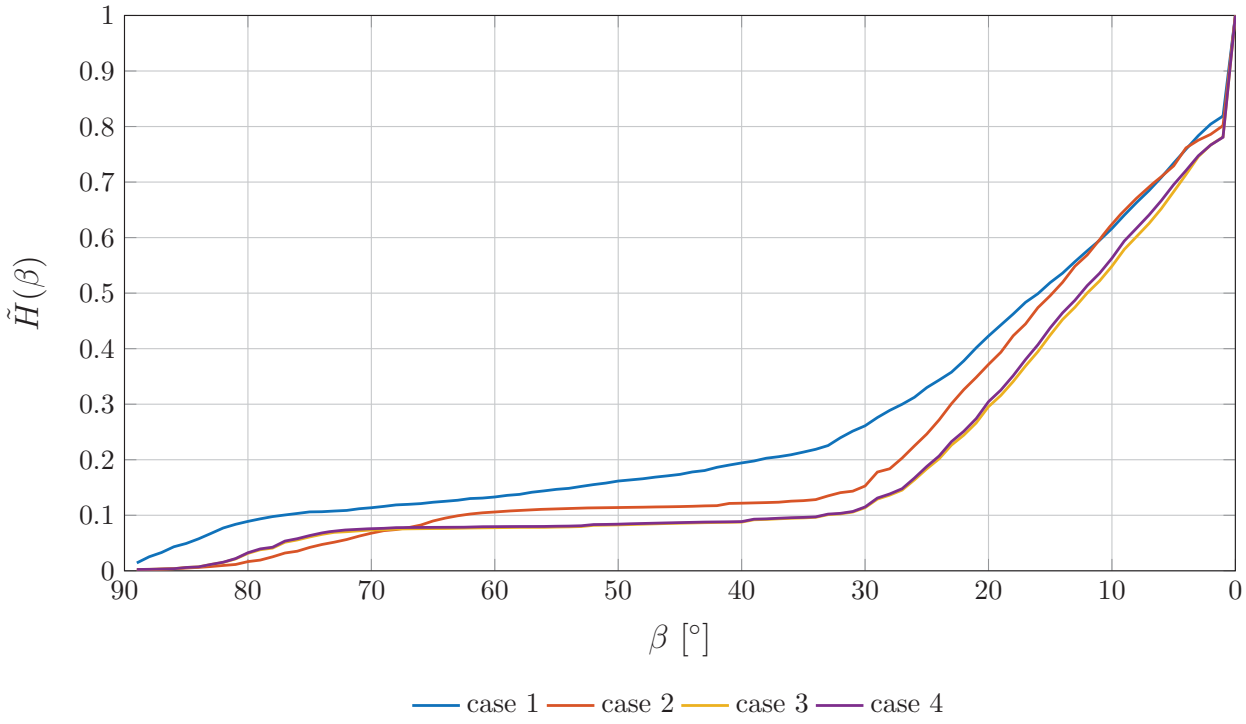

Figure 5.4: Normalized cumulative histogram of $\cos^{-1}(|\langle \bar{p}(x_l^k), \bar{p}(x_l^{\hat{k}})\rangle|)$ over all $l = \tilde{l}, ..., L-1$.

5.3 Three new variants of perturbations

In this Section we derive the three new variants of perturbations we developed in order to counteract the zigzagging behavior illustrated in the previous section. We briefly describe the methods we used as inspiration for our perturbations and formulate all three both as inner and outer perturbations. We prove that all three perturbations are bounded as described in Definition 3 in both formulations and can therefore be used together with the projection methods in the sense of their bounded perturbation resilience.

5.3.1 The heavy ball perturbation

The heavy ball method

An early example of k-step methods, also known as inertial-type methods, is the *heavy ball* method of Polyak [56].
Its aim is to minimize a convex function f and it can be phrased as

$$x_k = y_{k-1} - \alpha \nabla f(y_{k-1}) \tag{5.10}$$
$$y_k = x_k + \beta(x_k - x_{k-1}) \tag{5.11}$$

with starting points $x_0, y_0 = x_0 \in \mathbb{R}^n$ and appropriate α, β.
Suppose that f is s l-strongly convex and L-smooth. We denote the condition number of $\nabla^2 f$ by $\kappa = L/l$. If $\alpha = 4/(\sqrt{l} + \sqrt{L})^2$ and $\beta = (\sqrt{L} - \sqrt{l})/(\sqrt{L} + \sqrt{l})$, the following is true:

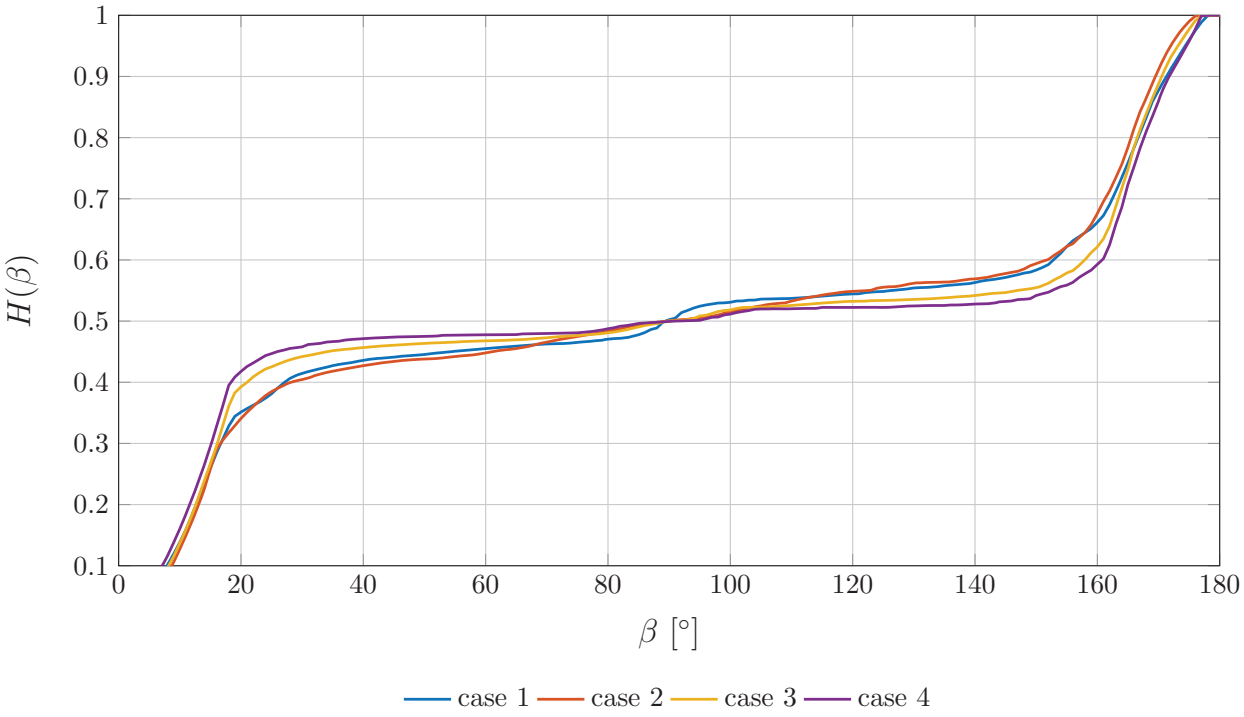

Figure 5.5: Normalized cumulative histogram of $\cos^{-1}(\langle \bar{p}(x^{\hat{k}}_{L-1}), \bar{p}(x^k_l)\rangle)$ for $l = \tilde{l}, ..., L-2$.

$$\|x^{k+1} - x^*\| \leq \left(\frac{\sqrt{\kappa}-1}{\sqrt{\kappa}+1}\right)^k \|x^1 - x^*\|$$

with x^* denoting the unique minimizer of f.
k-step methods are a time-discretization of an ordinary differential equation defining a continuous-time dynamical system (in general are easier to understand than their discrete-time counterparts, see [8]). These methods incorporate gradient information from the last k iterates into the calculation of the iteration step towards the next iterate and can be used to avoid zigzagging behavior. It is shown that methods using such inertial terms progress converge faster than methods using only current gradient information. For a deeper discussion of this matter, see e.g. [2, 52] as well as [28, 29] and the many references therein.

How do we use the idea of the heavy ball method?

Our approach is to use, similar to the heavy ball method, a combination of the gradient information at the current iterate and the momentum information, i.e. gradient information from the previous iterate, as perturbations for algorithmic operators $\boldsymbol{T}$ as defined in (2.24) and show that such an interference can accelerate the convergence of the algorithm.

Formulation as inner perturbation

The inner perturbation scheme (2.28) using the heavy ball perturbation is the following:

$$x^{k+1} = \boldsymbol{T}(x^k + \beta_k b^k) \tag{5.12}$$

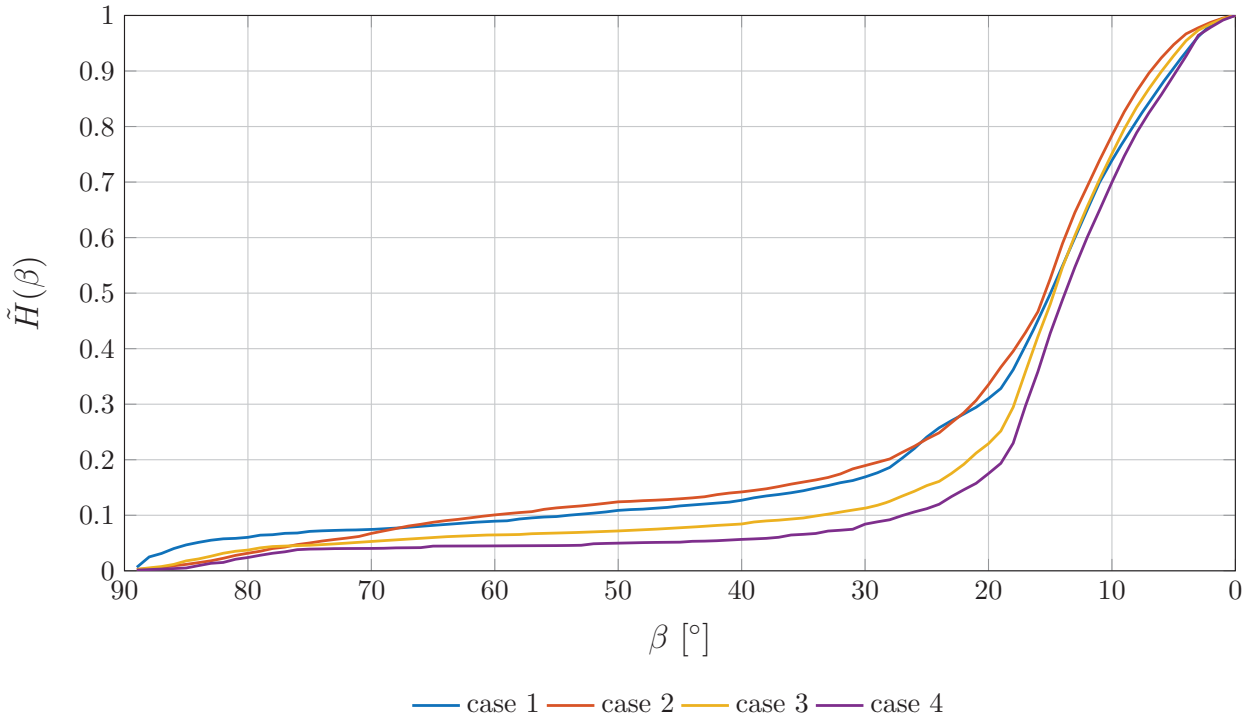

Figure 5.6: Normalized cumulative histogram of $\cos^{-1}(|\langle \bar{p}(x^{\hat{k}}_{L-1}), \bar{p}(x^k_l)\rangle|)$ for $l = \tilde{l}, ..., L-2$.

where

$$b^k = \begin{cases} \lambda_k^{HB} d^{HB} & \text{if } c(x^k) = \text{ true} \\ 0 & \text{otherwise.} \end{cases} \tag{5.13}$$

$\{\beta_k\}_{k=0}^{\infty}$ is a sequence with $\beta_k \in \mathbb{R}_{\geq 0}$ for all $k \geq 0$ and $\sum_{k=1}^{\infty} \beta_k < \infty$, $\{\lambda_k^{HB}\}_{k=0}^{\infty}$ is a bounded user-chosen sequence of step sizes with $\lambda_k^{HB} \geq 0$ for all $k \geq 0$ and $d^{HB} = \bar{p}(x^{k-1}) + \bar{p}(x^k)$, where $p(x)$ is either (2.14) or (2.16). The perturbation direction d^{HB} is chosen like this, similar to iteration rules of k-step methods, in order to make opposing parts of $\bar{p}(x^{k-1})$ and $\bar{p}(x^k)$ cancel each other, because those parts are provoking the zigzagging behavior. Instead we get a direction which contains what both vectors have in common. The function c, which determines, whether perturbations are applied or not, is defined as follows.

$$c(x^k) = \begin{cases} \text{true} & \text{if } \langle \bar{p}(x^{k-1}), \bar{p}(x^k)\rangle \in [-1 + \epsilon_{\min}, -1 + \epsilon_{\max}] \wedge k > 0 \\ \text{false} & \text{otherwise} \end{cases} \tag{5.14}$$

Choosing c like this means, that perturbations are applied, when $\langle \bar{p}(x^{k-1}), \bar{p}(x^k)\rangle$ is close to -1, which translates to $\bar{p}(x^{k-1})$ and $\bar{p}(x^k)$ pointing into almost opposite directions and therefore zigzagging behavior. If that is the case, the convergence of simultaneous and cyclic projection is slow and our aim is to accelerate it by using perturbations.
Recalling Definition 3, we now show that the perturbations (5.13) are bounded.

Lemma 7. *The perturbations $\beta_k b^k$ defined in* (5.13) *are bounded for all $k \geq 0$.*

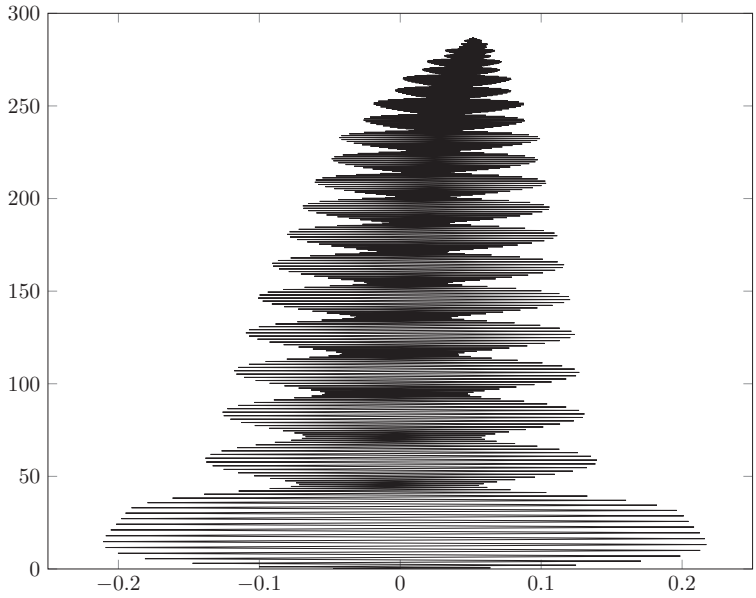

Figure 5.7: Simplified trajectory of iterates in a plane. Subsequent directions $p(x_l^k), p(x_l^{k-1})$ have $\cos^{-1}(\langle \bar{p}(x_l^k), \bar{p}(x_l^{k-1}\rangle) = 150°$. The lengths $\|p(x_l^k)\|$ result from an actual IMRT optimization problem solved via the level set scheme with the unperturbed simultaneous projection method.

Proof.
With $\{\beta_k\}_{k=0}^{\infty}, \{\lambda_k^{HB}\}_{k=0}^{\infty}$ chosen as described in (5.12) and the assumptions it suffices to show that $\|d^{HB}\|$ is bounded.

$$\begin{aligned}\|d^{HB}\| &= \|\bar{p}(x^{k-1}) + \bar{p}(x^k)\| \\ &= \sqrt{\|\bar{p}(x^{k-1})\|^2 + \|\bar{p}(x^k)\|^2 + 2\langle \bar{p}(x^{k-1}), \bar{p}(x^k)\rangle} \\ &= \sqrt{2 + 2(-1+\epsilon)} \leq \sqrt{2\epsilon_{\max}} =: M\end{aligned}$$

□

Formulation as outer perturbation

The outer perturbation scheme (2.26) using the heavy ball perturbation is the following:

$$x^{k+1} = \boldsymbol{T}(x^k) + \beta_k b^k \tag{5.15}$$

where

$$b^k = \begin{cases} \lambda_k^{HB} d^{HB} - \lambda(x^k)p(x^k) & \text{if } \tilde{c}(x^k, x^{k-1}) = \text{true} \\ 0 & \text{otherwise.} \end{cases} \tag{5.16}$$

$\{\beta_k\}_{k=0}^{\infty}$ is a sequence with $\beta_k \in \mathbb{R}_{\geq 0}$ for all $k \geq 0$ and $\sum_{k=1}^{\infty} \beta_k < \infty$, $\{\lambda_k^{HB}\}_{k=0}^{\infty}$ is a user-chosen bounded sequence of step sizes with $\lambda_k^{HB} \geq 0$ for all $k \geq 0$ and $d^{HB} = \bar{p}(x^{k-1}) + \bar{p}(x^k)$, where $p(x)$ is either (2.14) or (2.16). The function $\tilde{c}$ is defined as in (2.25) and (5.14). Recalling Definition 3, we now show that the perturbations (5.16) are bounded.

Lemma 8. *Assume that $\|p(x^k)\| \leq q \in \mathbb{R}$ for all $k \geq 0$. Then the perturbations $\beta_k b^k$ defined in (5.16) are bounded for all $k \geq 0$.*

Proof.
With $\{\beta_k\}_{k=0}^{\infty}$ and $\{\lambda_k^{HB}\}_{k=0}^{\infty}$ chosen as described in (5.15) and the assumptions it suffices to show that $\|b^k\| < \bar{M} \in \mathbb{R}$ for all $k \geq 0$. We have shown before that $\|d^{HB}\| < M \in \mathbb{R}$.

$$\begin{aligned}
\|b^k\|^2 &\leq \|\lambda_k^{HB} d^{HB} - \lambda(x^k)p(x^k)\|^2 \\
&= \|\lambda_k^{HB} d^{HB}\|^2 + \|\lambda(x^k)p(x^k)\|^2 - 2\langle \lambda_k^{HB} d^{HB}, \lambda(x^k)p(x^k)\rangle \\
&\leq (\lambda_k^{HB})^2 M^2 + \lambda(x^k)^2 q^2 - 2\lambda_k^{HB}\lambda(x^k)\left(\langle \bar{p}(x^k), p(x^k)\rangle + \langle \bar{p}(x^{k-1}), p(x^k)\rangle\right) \\
&= (\lambda_k^{HB})^2 M^2 + \lambda(x^k)^2 q^2 - 2\lambda_k^{HB}\lambda(x^k)\left(\|p(x^k)\|(1 + -1 + \epsilon)\right) \\
&= (\lambda_k^{HB})^2 M^2 + \lambda(x^k)^2 q^2 - \underbrace{2\lambda_k^{HB}\lambda(x^k)\|p(x^k)\|\epsilon}_{>0} \\
&< (\lambda_k^{HB})^2 M^2 + 4q^2 =: \bar{M}
\end{aligned}$$

□

5.3.2 The Nesterov perturbation

Nesterov Acceleration Method

The second perturbation we present int his thesis is also inspired by an inertial type method: the Nesterov Acceleration Method. This iteration scheme is structurally very similar to the heavy ball method presented in the last section. It was proposed in [52] and is designed to solve the unconstrained optimization problem

$$\text{Minimize } f(x)$$

where $f : \mathbb{R}^n \to \mathbb{R}$ is a convex function.
The Nesterov Acceleration Method can be phrased as follows: Choose starting points x_0 and $y_0 = x_0 \in \mathbb{R}^n$. Define

$$x_k = y_{k-1} - s\nabla f(y_{k-1}) \tag{5.17}$$

$$y_k = x_k + \frac{k-1}{k+2}(x_k - x_{k-1}). \tag{5.18}$$

When s is a fixed step size with $s < 1/L$, where L is the Lipschitz constant of ∇f, this method has a convergence rate of

$$f(x_k) - f(x^*) = \mathcal{O}\left(\frac{\|x_0 - x^*\|^2}{sk^2}\right)$$

where x^* is any minimizer of f. This convergence rate has been shown to be the optimal rate among all methods, which use only use gradient information of f at each iteration [49]. Since the introduction of Nesterov's scheme, there has been much work on the development of first-order accelerated methods, Theoretical developments can be found in [49, 50, 51] and [64] offers a unified analysis of these ideas.

How do we use the idea of the Nesterov Acceleration Method?

The update rule (5.17) for x_k is structurally similar to simultaneous projection in the sense that it uses only gradient information of y_{k-1}. For the perturbation we present in the following we adopt the momentum term $y_k - x_k$ from (5.18) as perturbation vector b^k.

Formulation as inner perturbation

The inner perturbation scheme (2.28) using the Nesterov perturbation is

$$x^{k+1} = \boldsymbol{T}(x^k + \beta_k b^k) \tag{5.19}$$

where

$$b^k = \begin{cases} \lambda_k^{NE} \frac{k-1}{k+2}(x^k - x^{k-1}) & \text{if } c(x^k) = \text{ true} \\ 0 & \text{otherwise.} \end{cases} \tag{5.20}$$

$\{\beta_k\}_{k=0}^{\infty}$ is a sequence with $\beta_k \in \mathbb{R}_{\geq 0}$ for all $k \geq 0$ and $\sum_{k=1}^{\infty} \beta_k < \infty$, $\{\lambda_k^{NE}\}_{k=0}^{\infty}$ is a user-chosen bounded sequence of step sizes with $\lambda_k^{NE} \geq 0$ for all $k \geq 0$ and c is defined as in (5.14).
As before we now show that the perturbations (5.20) are bounded in the sense of Definition 3 of bounded perturbation resilience.

Lemma 9. *Assume that there exists $q \in \mathbb{R}$ such that $\|p(x^k)\| \leq q$ and $\|p(x^k + \beta_k b^k)\| \leq q$. Then, the perturbations $\beta_k b^k$ defined in* (5.20) *are bounded for all $k \geq 0$.*

Proof.
For all $k \geq 0$ we have $\frac{k-1}{k+2} < 1$. With $\{\beta_k\}_{k=0}^{\infty}$ chosen as described in (5.19) and $\{\lambda_k^{NE}\}_{k=0}^{\infty}$ bounded, it suffices to show that $\|x^k - x^{k-1}\|$ is bounded.
If $c(x^{k-1}) =$ false we have $x^k = \boldsymbol{T}(x^{k-1}) = x^{k-1} + \lambda(x^{k-1})p(x^{k-1})$ and therefore

$$\|x^k - x^{k-1}\| = \|\lambda(x^{k-1})p(x^{k-1})\| \leq 2q.$$

Otherwise we get $\|x^k - x^{k-1}\| = \|\beta_{k-1}b^{k-1} + \lambda p(x^{k-1} + \beta_{k-1}b^{k-1})\|$. We show by induction that this norm is bounded.
$k = 2$ is the first iteration index k for which $c(x^{k-1})$ can possibly be true. If $c(x^2) = c(x^1)$ true we have $x^3 = \boldsymbol{T}(x^2 + \beta_2 b^2)$ and

$$\begin{aligned}\|b^2\| &= \left\|\frac{1}{4}(x^2 - x^1)\right\| \\ &\leq \|x^2 - x^1\| \\ &= \|\lambda(x^1)p(x^1)\| \leq 2q.\end{aligned}$$

Now consider the induction step $k \to k+1$ and assume that $c(x^{k-1}) = c(x^k)$ true.

$$\begin{aligned}\|b^k\| &= \left\|\frac{k-1}{k+2}(x^k - x^{k-1})\right\| \\ &\leq \|x^k - x^{k-1}\| \\ &= \|\boldsymbol{T}(x^{k-1} + \beta_{k-1}b^{k-1}) - x^{k-1}\| \\ &= \|\beta_{k-1}b^{k-1} + \lambda(x^{k-1} + \beta_{k-1}b^{k-1})p(x^{k-1} + \beta_{k-1}b^{k-1})\| \\ &\leq \beta_{k-1}\|b^{k-1}\| + 2q\end{aligned}$$

The induction assumption guarantees that $\|b^{k-1}\|$ and therefore also $\|\beta_{k-1}b^{k-1} + \lambda p(x^{k-1} + \beta_{k-1}b^{k-1})\|$ is bounded.

□

Formulation as outer perturbation

The outer perturbation scheme (2.26) using the Nesterov perturbation is

$$x^{k+1} = \boldsymbol{T}(x^k) + \beta_k b^k \tag{5.21}$$

where

$$b^k = \begin{cases}\lambda_k^{NE}\frac{k-1}{k+2}(x^k - x^{k-1}) - \lambda(x^k)p(x^k) & \text{if } \tilde{c}(x^k, x^{k-1}) = \text{true} \\ 0 & \text{otherwise.}\end{cases} \tag{5.22}$$

$\{\beta_k\}_{k=0}^{\infty}$ is a sequence with $\beta_k \in \mathbb{R}_{\geq 0}$ for all $k \geq 0$ and $\sum_{k=1}^{\infty}\beta_k < \infty$, $\{\lambda_k^{NE}\}_{k=0}^{\infty}$ is a user-chosen bounded sequence of step sizes with $\lambda_k^{NE} \geq 0$ for all $k \geq 0$ and the function $\tilde{c}$ is the same as in (2.25) with c as in (5.14).
As before we now show that the perturbations (5.33) are bounded in the sense of Definition 3.

Lemma 10. *Assume that there exists $q \in \mathbb{R}$ such that $\|p(x^k)\| \leq q$ and $\|p(x^k + \beta_k b^k)\| \leq q$. Then, the perturbations $\beta_k b^k$ defined in (5.22) are bounded for all $k \geq 0$.*

Proof.
With $\{\beta_k\}_{k=0}^{\infty}$ and $\{\lambda_k^{NE}\}_{k=0}^{\infty}$ chosen as described in (5.21) it suffices to show that

$$\|b^k\| = \left\| \frac{k-1}{k+2}(x^k - x^{k-1}) - \lambda(x^k)p(x^k) \right\|$$

is bounded. For all $k \geq 0$ we have $\frac{k-1}{k+2} < 1$.

$$\begin{aligned} &\left\| \frac{k-1}{k+2}(x^k - x^{k-1}) - \lambda(x^k)p(x^k) \right\| \\ \leq &\frac{k-1}{k+2}\|x^k - x^{k-1}\| + \lambda(x^k)\|p(x^k)\| \\ \leq &\|x^k - x^{k-1}\| + 2q \end{aligned}$$

Therefore we need to show that $\|x^k - x^{k-1}\|$ is bounded. We have $\tilde{c}(x^k, x^{k-1}) = \text{true}$ so we know by construction of $\tilde{c}$ that $c(x^{k-1}) = \text{false}$ and therefore $x^k = \boldsymbol{T}(x^{k-1}) = x^{k-1} + \lambda(x^{k-1})p(x^{k-1})$. This yields that

$$\|x^k - x^{k-1}\| = \|\lambda(x^{k-1})p(x^{k-1})\| \leq 2q$$

is bounded. □

5.3.3 The surrogate constraint perturbation

Surrogate constraint methods

Surrogate constraint methods have been proposed by Yang and Murty [66], while aggregation methods using similar approaches have already been presented earlier e.g. in [40, 34]. In the following we will briefly present the general idea of the surrogate constraint method of Yang and Murty [66]. Their approach is to construct an auxiliary, surrogate inequality from a system of inequalities

$$A^\top x \leq b$$

which they aim to solve. They denote the halfspaces which are feasible with respect to the individual inequalities $a_i^\top x \leq b_i$ by $H_i = \{x \in \mathbb{R}^n : a_i^\top x \leq b_i\}$. The surrogate inequality is an aggregation of the original inequalities

$$w_k^\top A^\top x \leq w_k^\top b$$

where w_k is a vector of weights which can depend on the values $a_i^\top x^k - b_i$. w_k is chosen such that its components $w_k^i > 0$ if $a_i^\top x^k > b_i$, which means that only inequalities violated by x^k are contained in the aggregation. They define the halfspace

$$H_{w_k} := \{x \in \mathbb{R}^n : w^\top A^\top x \leq w^\top b\}$$

and calculate the metric projection $\Pi_{H_w}(x^k)$ of the current iterate x^k onto it. Then they set $d(w_k) = \Pi_{H_{w_k}}(x^k) - x^k$ and calculate the next iterate x^{k+1} via

$$x^{k+1} = x^k + \lambda d(w_k)$$

where $\lambda \in [0, 2]$ is a relaxation parameter.
This idea in itself does not alleviate any zigzagging behavior. The surrogate direction $d(w_k)$ is a weighted average of the projections onto the halfspaces H_i corresponding to those inequalities $a_i^\top x \leq b_i$ which are violated. It is possible that

$$\frac{\langle d(w_k), d(w_{k+1})\rangle}{\|d(w_k)\|\|d(w_{k+1})\|} = -1 + \epsilon$$

for $0 < \epsilon \ll 1$ and thus the method exhibits zigzagging behavior.

Dudeks method

In [30] the author presents a method for solving a system of linear inequalities which blends the approach of surrogate constraints with relaxed, averaged projections. This method has the ability to alleviate zigzagging behavior and we describe it in detail here, because we refer to their ideas and results in Section 5.4. In Figure 5.8 we present a sketch that illustrates our description.
Different than [66], they do not aggregate a surrogate inequality from the ones that are violated at the current iterate x^k. Instead, we construct the surrogate halfspace

$$H_{SC} = \{x \in \mathbb{R}^n : \nu^\top (x - x^k) \leq 0\} \tag{5.23}$$

using the normal vector $\nu \in \mathbb{R}^n$ (which is pointing away from H_{SC}). The surrogate halfspace is then used to calculate the next iterate x^{k+1} in the following way (see Figure 5.8).
First they calculate the metric projections $\Pi_{H_i}(x^k)$ of x^k onto those halfspaces H_i that correspond to linear inequalities which are violated by x^k.

$$s^i := \Pi_{H_i}(x^k)$$

Then they calculate the vectors d^i, which point from x^k to the metric projections of $x^k + s^i$ onto the surrogate Halfspace H_{SC}

$$d^i := \Pi_{H_{SC}}(x^k + s^i) - x^k.$$

Next they use weights $w_i(x^k)$ with $w_i(x^k) \geq 0$ and $\sum w_i(x^k) = 1$ to calculate the weighted sum of the vectors d^i.

$$d := \sum w_i d^i$$

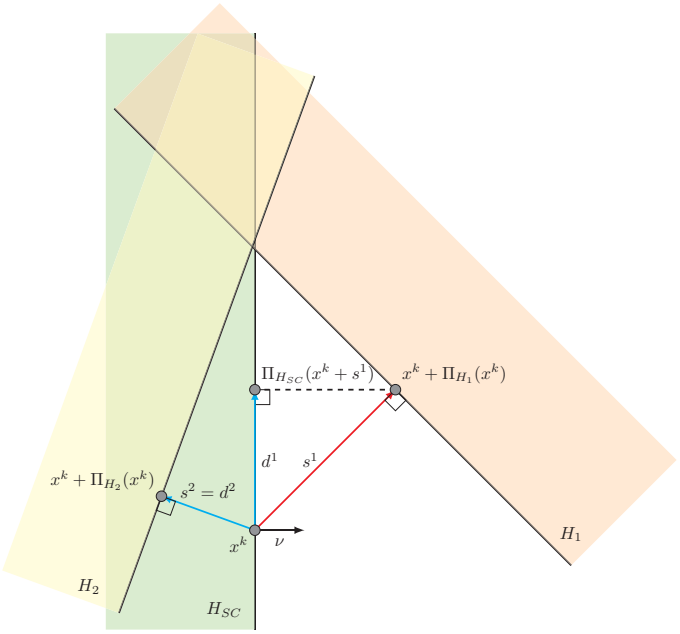

Figure 5.8: Sketch of Dudek's method.

they call d the surrogate constraint direction and get the next iterate via

$$x^{k+1} = x^k + \lambda\theta d$$

where $\lambda \in (0, 2]$ is a relaxation parameter and

$$\theta := \frac{\sum w_i \|s_i\|^2}{\|\sum w_i d_i\|^2}.$$

By this construction, they only use those parts of the vectors s^i for the surrogate constraint direction d, which do not contain any positive parts of the normal vector ν. This property is used to alleviate zigzagging behavior by choosing $\nu = x^{k-1} - x^k$ as the vector pointing into the direction they "came from" in the previous iteration.
In [30], the surrogate constraint method is only formulated for linear feasibility problems. We used their idea as inspiration for the perturbation we present in the following.

How do we use the idea of Dudek's method?

Again, we consider an algorithmic operator $\boldsymbol{T}$ as defined in (2.24).
We modified the idea of [30] in such a manner that we do not project the individual gradients of the violated constraint functions onto the surrogate half-space H_{SC}. Instead, we calculate $p(x^k)$ as defined in (2.13) or (2.15) and then project it onto the half-space H_{SC}.
In Figure 5.9 the vectors $\bar{p}(x^{k-1})$ and $p(x^k)$ are depicted in red. We define the half-spaces

$$H_{SC} := \{x \in \mathbb{R}^n : \langle x - x^k, p(x^{k-1})\rangle \geq 0\} \tag{5.24}$$

$$H_k := \{x \in \mathbb{R}^n : \langle x - (x^k + p(x^k)), p(x^k)\rangle \geq 0\}. \tag{5.25}$$

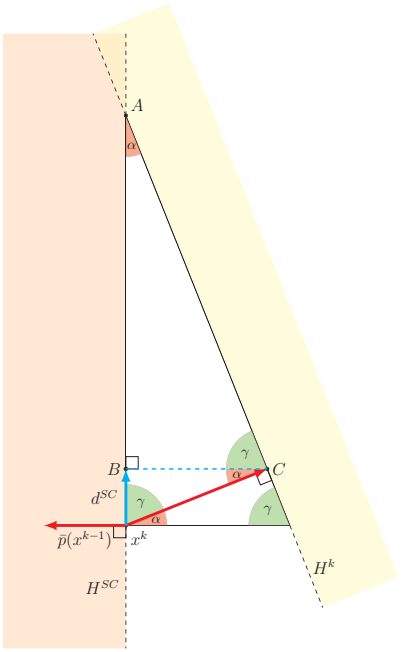

Figure 5.9: The direction d^{SC} (depicted in cyan) of the surrogate constraint perturbation is the vector pointing from x^k to the metric projection of $x^k + p(x^k)$ onto the surrogate half-space H_{SC}.

The vector

$$d^{SC} := \Pi_{H_{SC}}(x^k + p(x^k)) - x^k \tag{5.26}$$

points from x^k to the metric projection of $x^k + p(x^k)$ onto the surrogate half-space H_{SC} (5.24). It is depicted in cyan in Figure 5.9. Projecting $x^k + p(x^k)$ onto H_{SC} eliminates the part of $p(x^k)$ which points into the direction of $-p(x^{k-1})$. This means that $d^{SC} \perp p(x^{k-1})$ and steering the iteration into the direction of d^{SC} reduces zigzagging behavior.
By A we denote the intersection point of H_{SC}, H_k and $span\{p(x^{k-1}), p(x^k))\}$.
Let

$$\alpha := \pi - \cos^{-1}(\langle \bar{p}(x^k), \bar{p}(x^{k-1}) \rangle)$$

be the angle between $-p(x^{k-1})$ and $p(x^k)$ and $\gamma := \pi/2 - \alpha$. Let $B := \Pi_{H^{SC}}(x^k + p(x^k))$ and $C := x^k + p(x^k)$. The triangles ΔCBx^k and ΔCAx^k are similar, so it is true that

$$\frac{\|A - x^k\|}{\|p(x^k)\|} = \frac{\|p(x^k)\|}{\|d^{SC}\|}.$$

Choosing the scaling factor

$$\theta^{SC} = \|p(x^k)\|^2 / \|d^{SC}\|^2 \tag{5.27}$$

we get

$$\frac{\|p(x^k)\|}{\|d^{SC}\|} = \frac{\theta^{SC}\|d^{SC}\|}{\|p(x^k)\|}.$$

These equations yield $\|A-x^k\| = \|\lambda_k^{SC} d^{SC}\|$. The construction of d^{SC} implies that $d^{SC}/\|d^{SC}\| = (A-x^k)/\|A-x^k\|$ and therefore $A - x^k = \lambda_k^{SC} d^{SC}$. This means that the point $x^k + \lambda_k^{SC} d^{SC}$ is actually the same as the point A depicted in Figure 5.9. Note that

$$\begin{aligned} \sin(\alpha) &= \|d^{SC}\|/\|p(x^k)\| && (5.28)\\ \Rightarrow \theta^{SC} &= 1/\sin(\alpha)^2 \\ \Rightarrow \|\theta^{SC} d^{SC}\| &= \|p(x^k)\|/\sin(\alpha). && (5.29) \end{aligned}$$

As before for the heavy ball and Nesterov perturbation, we perturb the iteration sequence generated by $\boldsymbol{T}$ if $\langle \bar{p}(x^k), \bar{p}(x^{k-1})\rangle = -1 + \epsilon$ for $\epsilon \in [\epsilon_{\min}, \epsilon_{\max}] \subset (0,1)$.

Formulation as inner perturbation

The inner perturbation scheme (2.28) using the surrogate constraint perturbation is

$$x^{k+1} = \boldsymbol{T}(x^k + \beta_k b^k) \tag{5.30}$$

where $\{\beta_k\}_{k=0}^{\infty}$ is a sequence with $\beta_k \in \mathbb{R}_{\geq 0}$ for all $k \geq 0$ and $\sum_{k=0}^{\infty} \beta_k < \infty$ and

$$b^k = \begin{cases} \lambda_k^{SC} \theta^{SC} d^{SC} & \text{if } c(x^k) = \text{ true} \\ 0 & \text{otherwise.} \end{cases} \tag{5.31}$$

$\{\lambda_k^{SC}\}_{k=0}^{\infty}$ is a user-chosen bounded sequence of step sizes with $\lambda_k^{SC} \geq 0$ for all $k \geq 0$. Again, c is defined as in (5.14).
As before we now show that the perturbations (5.31) are bounded in the sense of Definition 3 of bounded perturbation resilience.

Lemma 11. *Assume that $\|p(x^k)\| \leq q \in \mathbb{R}$ holds for all $k \geq 0$. Then the perturbations $\beta_k b^k$ as defined in* (5.31) *are bounded for all $k \geq 0$.*

Proof.
With $\{\beta_k\}_{k=0}^{\infty}$ chosen as described in (5.30), it suffices to show that $\|b^k\| \leq M \in \mathbb{R}$ for all $k \geq 0$. Recall that $\alpha = \cos^{-1}(1-\epsilon)$ as in Figure 5.9. We know from (5.29)

$$\begin{aligned} \|b^k\| \leq \|\lambda^{SC} \theta^{SC} d^{SC}\| &\leq 2\|\theta^{SC} d^{SC}\| \\ &= 2\frac{\|p(x^k)\|}{\sin(\alpha)} \\ &\leq 2\frac{q}{\sqrt{2\epsilon_{\min} - \epsilon_{\min}^2}} =: M \end{aligned}$$

□

Formulation as outer perturbation

The outer perturbation scheme (2.26) using the surrogate constraint perturbation is

$$x^{k+1} = \boldsymbol{T}(x^k) + \beta_k b^k \tag{5.32}$$

where

$$b^k = \begin{cases} \lambda_k^{SC}\theta^{SC}d^{SC} - \lambda(x^k)p(x^k) & \text{if } \tilde{c}(x^k, x^{k-1}) = \text{ true} \\ 0 & \text{otherwise.} \end{cases} \tag{5.33}$$

$\{\beta_k\}_{k=0}^{\infty}$ is a sequence with $\beta_k \in \mathbb{R}_{\geq 0}$ for all $k \geq 0$ and $\sum_{k=0}^{\infty}\beta_k < \infty$, $\{\lambda_k^{SC}\}_{k=0}^{\infty}$ is a user-chosen bounded sequence of step sizes with $\lambda_k^{SC} \geq 0$ for all $k \geq 0$ and the function $\tilde{c}$ is the same as in (2.25) with c as in (5.14).
As before we now show that the perturbations (5.33) are bounded in the sense of the Definition 3.

Lemma 12. *Assume that $\|p(x^k)\| \leq q \in \mathbb{R}$ holds for all $k \geq 0$. Then the perturbations $\beta_k b^k$ as defined in* (5.33) *are bounded for all $k \geq 0$.*

Proof.
With $\{\beta_k\}_{k=0}^{\infty}$ chosen as described in (5.32), it suffices to show that $\|b^k\| \leq \bar{M} \in \mathbb{R}$ for all $k \geq 0$. We have shown before that $\|\lambda^{SC}d^{SC}\| \leq M \in \mathbb{R}$.
Let $\beta = \cos^{-1}(\langle \bar{p}(x^{k-1}), \bar{p}(x^k)\rangle)$. We have $d^{SC} \in span\{p(x^{k-1}), p(x^k)\}, d^{SC} \perp p(x^{k-1})$ and $1/\|d^{SC}\|\langle d^{SC}, \bar{p}(x^k)\rangle > 0$. Therefore, $\angle(d^{SC}, p(x^k)) = \beta - \pi/2$, which lies in the open interval $(0, \pi/2)$.

We also know that

$$\begin{aligned} \cos(\beta - \pi/2) &= \sin(\beta) \\ &= \sqrt{1 - \cos(\beta)^2} \\ &= \sqrt{1 - (-1 + \epsilon)^2} \\ &= \sqrt{2\epsilon - \epsilon^2} \end{aligned}$$

$$\begin{aligned} \|b^k\|^2 &\leq \|\lambda_k^{SC}\theta^{SC}d^{SC} - \lambda(x^k)p(x^k)\|^2 \\ &= \|\lambda_k^{SC}\theta^{SC}d^{SC}\|^2 + \|\lambda(x^k)p(x^k)\|^2 - 2\langle \lambda_k^{SC}\theta^{SC}d^{SC}, \lambda(x^k)p(x^k)\rangle \\ &\leq M^2 + \lambda(x^k)^2q^2 - 2\lambda(x^k)\lambda_k^{SC}\|p(x^k)\|\|\theta^{SC}d^{SC}\|\cos(\angle(d^{SC}, p(x^k))) \\ &= M^2 + \lambda(x^k)^2q^2 - \underbrace{2\lambda(x^k)\lambda_k^{SC}\|p(x^k)\|^2\sqrt{2\epsilon - \epsilon^2}/\sin(\alpha)}_{>0} \\ &< M^2 + 4q^2 =: \bar{M} \end{aligned}$$

□

We have shown that the property of boundedness in the sense of Definition 3 is fulfilled by the heavy ball, the Nesterov and the surrogate constraint perturbation, no matter whether they are formulated as inner or outer perturbation. Because both simultaneous and cyclic projection are bounded perturbation resilient, we can use the heavy ball, the Nesterov and the surrogate constraint perturbation together with these methods and retain convergence to a solution of $\boldsymbol{P}^l$, if such a solution exists. [3, Theorem 11 and Corollary 14] states that we preserve the convergence rate of the simultaneous or cyclic projection when we use them with bounded perturbations. In the following section we analyze the convergence behavior of the heavy ball and surrogate constraint perturbation in a theoretical way and present results, which indicate that these perturbations (used within the outer perturbation scheme) are in some cases suited to accelerate the convergence compared to the unperturbed simultaneous projection method.

5.4 Convergence of the perturbed simultaneous projection method

From this section onwards we will assume that the parameters $\{\beta_k\}_{k=0}^{\infty}$ for the perturbations are chosen as in (2.30), i.e.

$$\beta_k = \begin{cases} 1 & k \leq K \\ 0 & k > K \end{cases}$$

with $K = n_{\max}$, which is the maximum number of iterations we allow the projection methods for solving a CFP $\boldsymbol{P}^l$ arising from the perturbed level set scheme described in Section 5.1.

5.4.1 Geometrical analysis

In Figure 5.10 we present a triangle, which we refer to during this section. It is the same triangle we showed in Figure 5.9 in Section 5.3.3. Depicted is the plane $span\{p(x^k), p(x^{k-1})\}$. The line coinciding with the triangle side facing to the right is the line within $span\{p(x^k), p(x^{k-1})\}$, which is perpendicular to the vector $p(x^k)$ and contains the point $x^k + p(x^k)$. The line coinciding with the triangle side facing to the left is the line within $span\{p(x^k), p(x^{k-1})\}$, which is perpendicular to the vector $p(x^{k-1})$ and contains the point x^k. The intersection point of these two lines is denoted by A.
Figure 5.11 shows a magnified part of the simplified trajectory of iterates we presented before in Figure 5.7. In Figure 5.11 an iterate x^k, the vector $p(x^k)$ and (the bottom part of the) triangle described in Figure 5.10 are depicted together with the a part of the simplified trajectory. It gives an intuitive understanding of why methods steering the projection algorithm towards the triangle tip A depicted in Figure 5.10 have great potential to "skip" zigzagging iteration steps and thereby accelerate the convergence.
In the following we will consider the situation that the algorithm has moved from x^{k-1} to $x^k = x^{k-1} + \lambda p(x^{k-1})$ via the unperturbed simultaneous projection method. Now we compare three variants in terms of their progress towards the triangle tip A: the unperturbed simultaneous projection method, the perturbed simultaneous projection method using heavy ball

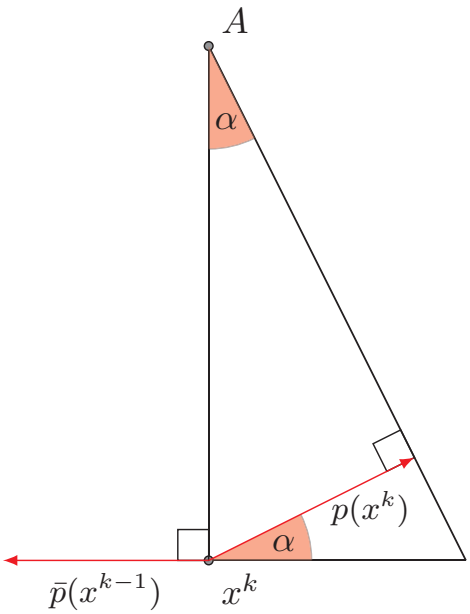

Figure 5.10: Sketch of a triangle constructed from x^k, $p(x^k)$ and $\bar{p}(x^{k-1})$ which we refer to during Section 5.4.1.

perturbation and the perturbed simultaneous projection method using surrogate constraint perturbation.
Let $\beta := \cos^{-1}(\langle \bar{p}(x^k), \bar{p}(x^{k-1}) \rangle)$ and $\alpha := \pi - \beta$.

Unperturbed simultaneous projection

By $x^{SP} = x^k + \lambda p(x^k)$ we denote the next iterate generated by the unperturbed simultaneous projection method.

Figure 5.12 illustrates the progress towards the triangle tip A made by the unperturbed simultaneous projection. It follows immediately from the law of cosines that

$$\|x^{SP} - A\| = \sqrt{\|x^k - A\|^2 + \lambda^2 \|p(x^k)\|^2 - 2\lambda \|p(x^k)\| \|x^k - A\| \cos(\pi/2 - \alpha)}. \tag{5.34}$$

Perturbed simultaneous projection

By $x^{HB} = x^k + 0.5\lambda_k^{HB}(\bar{p}(x^k) + \bar{p}(x^{k-1}))$ we denote the next iterate generated by the perturbed iteration scheme using heavy ball perturbation.

Figure 5.13 illustrates the progress towards the triangle tip A made by the perturbed iteration scheme using heavy ball perturbation. Let $\gamma := \angle(A - x^k, x_{HB}^{k+1} - x^k)$. The triangle $x^k, x^k + 0.5\bar{p}(x^{k-1}), x^k + 0.5(\bar{p}(x^k) + \bar{p}(x^{k-1}))$ is isosceles, because $\|0.5\bar{p}(x^{k-1})\| = \|0.5\bar{p}(x^k)\| = 0.5$. Therefore, $\gamma = \pi/2 - (\pi - \alpha)/2 = \alpha/2$.
We have

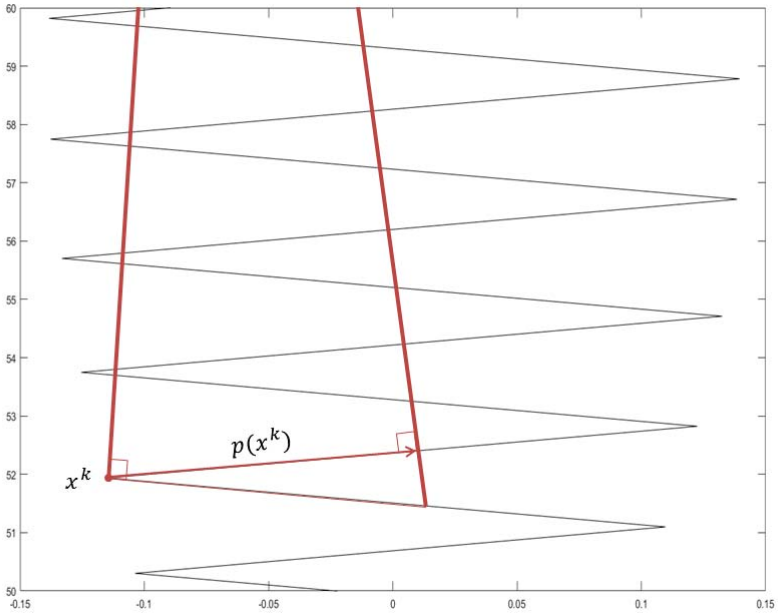

Figure 5.11: A magnified part of the simplified trajectory of iterates depicted in Figure 5.7. The (bottom part of the) triangle depicted in Figure 5.10 with x^k being one of the iterates from the trajectory is drawn in red.

$$\begin{aligned}\|x^{HB} - x^k\| &= \|0.5\lambda_k^{HB}(\bar{p}(x^k) + \bar{p}(x^{k-1}))\| \\ &= 0.5\lambda_k^{HB}\|\bar{p}(x^k) + \bar{p}(x^{k-1})\| \\ &= 0.5\lambda_k^{HB}\sqrt{\|\bar{p}(x^k)\|^2 + \|\bar{p}(x^{k-1})\|^2 + 2\langle\bar{p}(x^k), \bar{p}(x^{k-1})\rangle} \\ &= \frac{\lambda_k^{HB}}{2}\sqrt{2 + 2(-1+\epsilon)} \\ &= \lambda_k^{HB}\sqrt{\frac{\epsilon}{2}}. \end{aligned} \tag{5.35}$$

The distance $\|x^{HB} - A\|$ of course depends on the step size λ_k^{HB}. It attains its minimum if $\langle x^{HB} - A, x^{HB} - x^k\rangle = 0$, which occurs if

$$\|x_{opt}^{HB} - x^k\| = \cos(\alpha/2)\|x^k - A\|, \tag{5.36}$$

which means that

$$\lambda_k^{HB} = \lambda_{opt}^{HB} = \cos(\alpha/2)\|x^k - A\|\sqrt{\frac{2}{\epsilon}}. \tag{5.37}$$

We get

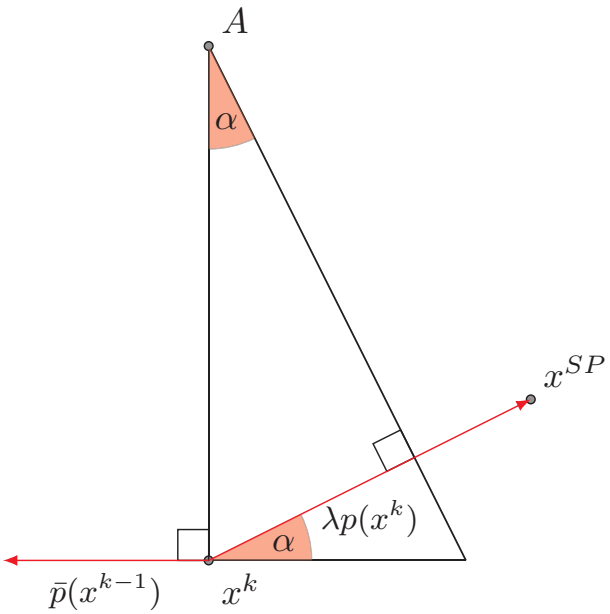

Figure 5.12: Sketch of the simultaneous projection step.

$$\|x_{opt}^{HB} - A\| = \|x^k - A\| \sin(\alpha/2). \tag{5.38}$$

Finally, by $x^{SC} = x^k + \lambda_k^{SC}\theta^{SC}d^{SC}$ with θ^{SC}, d^{SC} as defined in (5.26) and (5.27), we denote the next iterate generated by the perturbed iteration scheme using surrogate constraint perturbation.

Figure 5.14 illustrates the progress towards the triangle tip A made by the perturbed iteration scheme using surrogate constraint perturbation with $\lambda_k^{SC} = 1$. As explained in Section 5.3.3, the surrogate constraint perturbation steers the algorithm immediately to the triangle tip A. Therefore if $\lambda_k^{SC} = 1$ we have

$$\|x^{SC} - A\| = 0.$$

5.4.2 Convergence results

In the literature exist statements about the convergence speed of both the simultaneous projection method and the method introduced by Dudek [30].
Cegielski [13, Theorem 4.4.5] states the following result about the convergence speed of the simultaneous projection method. It is phrased in terms of metric projections Π_{C_i} onto closed convex sets C_i.

Theorem 13. *If* $z \in C := \bigcap_{i\in I} C_i, C \neq \emptyset, \lambda \in (0, 2]$ *and*

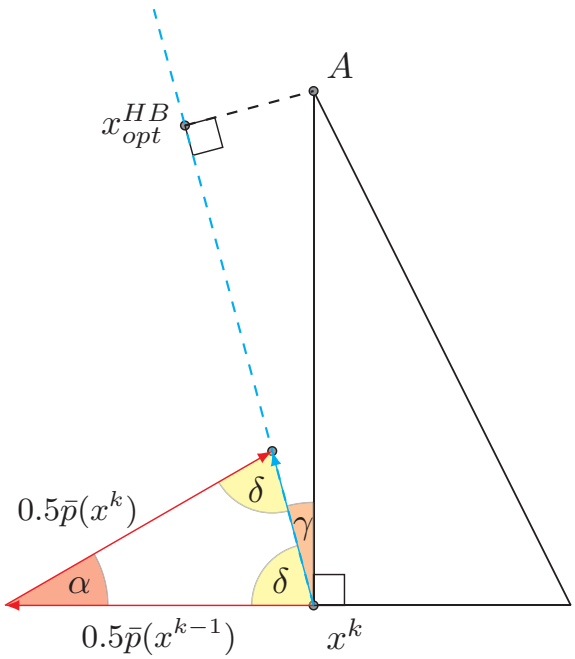

Figure 5.13: Sketch of the heavy ball perturbation step.

$$x^{SP} = x^k + \lambda \sum_{i \in I} w_i(x^k)(\Pi_{C_i}(x^k) - x^k)$$

it holds that

$$\|x^{SP} - z\|^2 \leq \|x^k - z\|^2 - \lambda(2-\lambda) \sum w_i(x^k) \|\Pi_{C_i}(x^k) - x^k\|^2. \tag{5.39}$$

The essential property needed for the proof of this result is that the operators Π_{C_i} are cutters, i.e.

$$\langle \Pi_{C_i}(x) - x, z - x \rangle \geq \|\Pi_{C_i}(x) - x\|^2 \quad \forall z \in C_i, x \in \mathbb{R}^n. \tag{5.40}$$

[13, Corrolary 4.2.6] states that not only metric projections, but also subgradient projections are cutters. Therefore (5.39) also holds for the subgradient projections we introduced in (2.16). To distinguish between metric and subgradient projections, we introduce the notation

$$\tilde{\Pi}_{C_i}(x) - x = -\frac{\max\{0, \varphi_i(x)\}}{\|\xi\|^2} \xi \tag{5.41}$$

where ξ is an arbitrary element of the subdifferential $\partial\varphi_i(x)$ of φ_i at x.

Dudek in [30] states a result about the convergence of their method with a very similar structure to (5.39). Their method, which we describe in detail in Section 5.3.3, is phrased

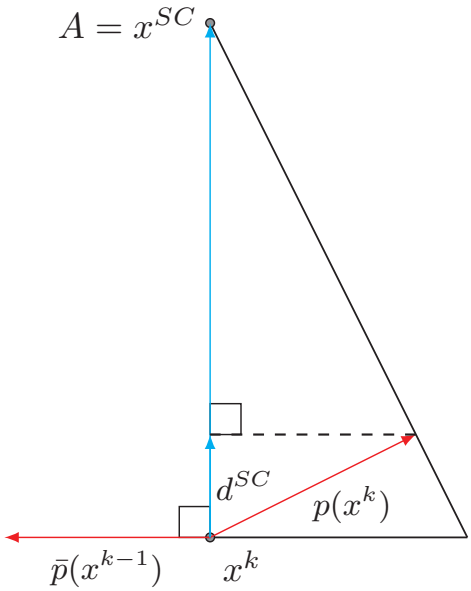

Figure 5.14: Sketch of the surrogate constraint perturbation step.

as an algorithm to solve a system of linear inequalities and the projections considered are metric projections. Nevertheless, the result also applies to subgradient projections, because the proof relies on the fact that the projections are cutters.
Dudeks result phrased in terms of subgradient projection operators $\tilde{\Pi}_{C_i}$ is the following:

Theorem 14. *If* $z \in C := \bigcap_{i\in I} C_i, , C \neq \emptyset, \lambda \in (0, 2], H_{SC}$ *defined as in* (5.23) *and*

$$x^{SC} = x^k + \lambda \frac{\sum_{i\in I} w_i(x^k)\|s^i\|^2}{\left\|\sum_{i\in I} w_i(x^k)d^i\right\|^2} d$$

with

$$\begin{aligned} s^i &= \tilde{\Pi}_{C_i}(x^k) - x^k \\ d^i &= \Pi_{H^{SC}}(\tilde{\Pi}_{C_i}(x^k) - x^k) \\ d &= \sum_{i\in I} w_i(x^k)d^i \end{aligned}$$

it holds that

$$\|x^{SC} - z\|^2 \leq \|x^k - z\|^2 - \lambda(2-\lambda)\sum w_i(x)\|s^i\|^2 \frac{\sum w_i(x)\,\|s^i\|^2}{\left\|\sum w_i(x)d^i\right\|^2}. \tag{5.42}$$

Comparing (5.39) and (5.42) we observe that the reduction $\|x^{k+1} - z\|^2 - \|x^k - z\|^2$ provided by the simultaneous projection and the reduction $\|x^{SC} - z\|^2 - \|x^k - z\|^2$ provided by Dudeks method differs by the factor

$$\delta(x^k) := \frac{\sum w_i(x^k)\|\tilde{\Pi}_{C_i}(x^k) - x^k\|^2}{\|\sum w_i(x^k)\Pi_{H^{SC}}(\tilde{\Pi}_{C_i}(x^k) - x^k)\|^2}. \tag{5.43}$$

We know that for all $k \geq 0$

$$\left\|d^i\right\|^2 + \left\|(x^k + s^i) - \Pi_{H_{SC}}(x^k + s^i)\right\|^2 = \left\|s^i\right\|^2.$$

It follows that

$$\left\|\sum w_i(x^k)d^i\right\|^2 \leq \sum w_i(x^k)\left\|d^i\right\|^2 \leq \sum w_i(x^k)\left\|s^i\right\|^2$$

and thus $\delta(x^k) \geq 1$ for all $k \geq 0$.
The immediate consequence is that the minimal reduction of the distance to any $z \in C$ provided by Dudek's method is at at least as big as the minimal reduction provided by the simultaneous projection method.

New results on the convergence of the perturbed simultaneous projection method

We consider the iteration step $k \to k+1$, which is perturbed using outer perturbations, i.e. we assume that $\tilde{c}(x^k, x^{k-1}) =$ true with the function $\tilde{c}$ as defined in (2.25).

Lemma 15. *If $\langle p(x^{k-1}), \tilde{\Pi}_{C_i}(x^k) - x^k\rangle \leq 0$ for all $i \in I$ then*

$$\sum_{i\in I} w_i(x^k)d^i = \Pi_{H_{SC}}(p(x^k)). \tag{5.44}$$

Proof.
$-\bar{p}(x^{k-1})$ is the normal vector ν to the surrogate half-space H_{SC} (with ν pointing away from H_{SC}).
Let $v = \nu\langle\nu, v\rangle + u$ and $\langle u, \nu\rangle = 0$. From the definition of the metric projection it follows that

$$\Pi_{H_{SC}}(v) = u \Leftrightarrow \langle\nu, v\rangle \geq 0.$$

Now let

$$v^i := \tilde{\Pi}_{C_i}(x^k) - x^k = \nu\langle\nu, v^i\rangle + u^i.$$

The comparison of

$$\begin{aligned}\sum w_i(x^k)d^i &= \sum w_i(x^k)\Pi_{H_{SC}}(\tilde{\Pi}_{C_i}(x^k) - x^k)\\ &= \sum w_i(x^k)u^i\end{aligned}$$

and

$$\begin{aligned} p(x^k) &= \sum w_i(x^k)v^i \\ &= \sum w_i(x^k)(\nu\langle\nu, v^i\rangle + u^i) \\ &= \sum \nu\langle\nu, w_i(x^k)v^i\rangle + w_i(x^k)u^i \\ \Rightarrow \Pi_{H_{SC}}(p(x^k)) &= \sum w_i(x^k)u^i \end{aligned}$$

proves Lemma 15. □

Lemma 15 implies that if $\langle p(x^{k-1}), \tilde{\Pi}_{C_i}(x^k) - x^k\rangle \leq 0$ is fulfilled for all $i \in I$, then the vector d used in Dudek's method is the same as the vector d^{SC} used in the surrogate constraint perturbation. The scaling factor $\sum_{i\in I} w_i(x^k)\|s^i\|^2 / \left\|\sum_{i\in I} w_i(x^k)d^i\right\|^2$, however, is not exactly the same as $\theta^{SC} = \|p(x^k)\|^2/\|d^{SC}\|^2$, which is the scaling factor for d^{SC}. This means that we end up with a slightly different factor $\tilde{\delta}(x^k)$ when we make a statement parallel to Theorem 14 about the result of the surrogate constraint perturbation. We give such a statement in the following, give the exact formula for $\tilde{\delta}(x^k)$ and quantify it more precisely.
Before we present the theorem we briefly explain why the assumption that

$$\langle p(x^{k-1}), \tilde{\Pi}_{C_i}(x^k) - x^k\rangle \leq 0 \quad \forall i \in I$$

is a reasonable one in the context of IMRT optimization.
The simultaneous projection takes all violated constraints into consideration for the computation of the next iterate. In particular when we choose the relaxation parameter $\lambda > 1$ the algorithm tends to (over)fulfill two groups of conflicting clinical goals in an alternating way. Therefore the function gradients contributing to one projection step are very often not considered in the next step, because the corresponding goals are fulfilled in that iteration. In our computations on IMRT cases using the simultaneous projection method we observe two disjoint groups of functions, whose gradients each dominate every other projection step and are opposing to the other group of gradients. Our observations in Section 5.2 provide additional numerical support for this reasoning.

Recall $\beta = \cos^{-1}(\langle\bar{p}(x^k), \bar{p}(x^{k-1})\rangle)$ and $\alpha = \pi - \beta$.

Theorem 16. *If* $\langle p(x^{k-1}), \tilde{\Pi}_{C_i}(x^k) - x^k\rangle \leq 0$ *for all* $i \in I$, $\lambda_k^{SC} \in (0, 2]$ *and*

$$x^{SC} = x^k + \lambda_k^{SC}\theta^{SC}d^{SC}$$

with d^{SC} *and* θ^{SC} *as defined in* (5.26) *and* (5.27) *then*

$$\|x^{SC} - z\|^2 \leq \|x^k - z\|^2 - \frac{\lambda_k^{SC}(2 - \lambda_k^{SC})}{\sin(\alpha)^2}\sum w_i(x^k)\|\tilde{\Pi}_{C_i}(x^k) - x^k\|^2. \tag{5.45}$$

Proof.
From Theorem 14, its proof in [30] and $\theta^{SC} = \|p(x^k)\|^2/\|d^{SC}\|^2$ it follows that

$$\|x^{SC} - z\|^2 \leq \|x^k - z\|^2 - \lambda_k^{SC}(2 - \lambda_k^{SC}) \sum w_i(x^k) \|\tilde{\Pi}_{C_i}(x^k) - x^k\|^2 \left(\frac{\|p(x^k)\|}{\|d^{SC}\|} \right)^2.$$

Let $\langle \bar{p}(x^k), \bar{p}(x^{k-1}) \rangle = -1 + \epsilon = \cos(\beta)$ and $\alpha + \beta = \pi$. The result now follows from

$$\sin(\alpha) = \frac{\|d^{SC}\|}{\|p(x^k)\|}.$$

□

In Section 5.4.1 we have illustrated that x^{SC} coincides with the triangle tip A if $\lambda_k^{SC} = 1$. We have also studied the distance of x^{HB} to A for the case when

$$\lambda_k^{HB} = \lambda_{opt}^{HB} = \|p(x^k)\| \sqrt{2/\epsilon} \cos(\alpha/2) / \sin(\alpha) \tag{5.46}$$

where $\epsilon = \langle \bar{p}(x^k), \bar{p}(x^{k-1}) \rangle + 1$. From these results we deduce the following theorem.

Theorem 17. *If $\langle p(x^{k-1}), \tilde{\Pi}_{C_i}(x^k) - x^k \rangle \leq 0$ for all $i \in I$ then there exists $\tilde{\alpha} \in (0, \pi/3]$ such that if $\alpha = \pi - \cos^{-1}(\langle \bar{p}(x^k), \bar{p}(x^{k-1}) \rangle) < \tilde{\alpha}$ is fulfilled and λ^{HB} is chosen as in (5.46) the following statement holds:*

$$\|x^{HB} - z\|^2 - \left(\|x^k - z\|^2 - \sum w_i \|\tilde{\Pi}_{C_i}(x^k) - x^k\|^2 \right) < 0. \tag{5.47}$$

Proof.
We showed in Section 5.4.1 that for $x^{SC} = x^k + \lambda^{SC}\theta^{SC}d^{SC}$, $\lambda^{SC} = 1$ and $\lambda^{HB} = \cos(\alpha/2)\sqrt{2/\epsilon}\|x^{SC} - x^k\|$ it is true that

$$\begin{aligned}
\|x^{HB} - x^{SC}\| &= \sin(\alpha/2)\|x^{SC} - x^k\| \\
&= \sin(\alpha/2) \left\| \frac{\|p(x^k)\|^2}{\|d^{SC}\|^2} d^{SC} \right\| \\
&= \sin(\alpha/2) \frac{\|p(x^k)\|^2}{\|d^{SC}\|} \\
&= \frac{\sin(\alpha/2)\|p(x^k)\|}{\sin(\alpha)}.
\end{aligned}$$

With this choice of λ^{HB} and λ^{SC} Theorem 16 yields

$$\begin{aligned}
\|x^{HB} - z\|^2 &\leq \|x^{SC} - z\|^2 + \|x^{HB} - x^{SC}\|^2 + 2\|x^{SC} - z\|\|x^{HB} - x^{SC}\| \\
&\leq \|x^k - z\|^2 - \frac{1}{\sin(\alpha)^2} \sum w_i(x^k) \|\tilde{\Pi}_{C_i}(x^k) - x^k\|^2 \\
&\quad + \|x^{HB} - x^{SC}\|^2 + 2\|x^{SC} - z\|\|x^{HB} - x^{SC}\|.
\end{aligned}$$

To examine when the heavy ball perturbation reduces the distance to z even more than the unperturbed simultaneous projection, we consider

$$\begin{aligned}
&\|x^{HB} - z\|^2 - \left(\|x^k - z\|^2 - \sum w_i(x^k)\|\tilde{\Pi}_{C_i}(x^k) - x^k\|^2\right) \\
\leq &\|x^{HB} - x^{SC}\|^2 + 2\|x^{SC} - z\|\|x^{HB} - x^{SC}\| - \frac{\cos(\alpha)^2}{\sin(\alpha)^2}\sum w_i(x^k)\|\tilde{\Pi}_{C_i}(x^k) - x^k\|^2
\end{aligned}$$

$$\begin{aligned}
&\|x^{HB} - x^{SC}\|^2 + 2\|x^{SC} - z\|\|x^{HB} - x^{SC}\| - \frac{\cos(\alpha)^2}{\sin(\alpha)^2}\sum w_i(x^k)\|\tilde{\Pi}_{C_i}(x^k) - x^k\|^2 \\
= &\left(\|p(x^k)\|\frac{\sin(\alpha/2)}{\sin(\alpha)}\right)^2 + 2\|x^{SC} - z\|\|p(x^k)\|\frac{\sin(\alpha/2)}{\sin(\alpha)} - \frac{\cos(\alpha)^2}{\sin(\alpha)^2}\sum w_i(x^k)\|\tilde{\Pi}_{C_i}(x^k) - x^k\|^2 \\
\leq &\left(\|p(x^k)\|\frac{\sin(\alpha/2)}{\sin(\alpha)}\right)^2 + 2\|x^{SC} - z\|\|p(x^k)\|\frac{\sin(\alpha/2)}{\sin(\alpha)} - \frac{\cos(\alpha)^2\|p(x^k)\|^2}{\sin(\alpha)^2} \\
= &\frac{\|p(x^k)\|}{\sin(\alpha)}\left(\frac{\|p(x^k)\|}{\sin(\alpha)}(\sin(\alpha/2)^2 - \cos(\alpha)^2) + 2\|x^{SC} - z\|\sin(\alpha/2)\right).
\end{aligned}$$

For $\alpha < \pi/3$ we have

$$\sin(\alpha/2)^2 - \cos(\alpha)^2 < 0.$$

For all (finite) $\|p(x^k)\|, \|x^{SC} - z\|$ there exists $\tilde{\alpha} \in (0, \pi/3]$ such that for all $\alpha \in [0, \tilde{\alpha})$

$$\left(\frac{\|p(x^k)\|}{\sin(\alpha)}(\sin(\alpha/2)^2 - \cos(\alpha)^2) + 2\|x^{SC} - z\|\sin(\alpha/2)\right) < 0$$

and thus $\|x^{HB} - z\|^2 < \|x^k - z\|^2 - \sum w_i(x^k)\|\tilde{\Pi}_{C_i}(x^k) - x^k\|^2$. □

Theorem 17 implies that under the mentioned assumptions there always exists a value for $\epsilon_{\max}$ with $\epsilon_{\max} > 0$ as parameter for the function and $\tilde{c}$, which guarantees that if $\langle \bar{p}(x^k), \bar{p}(x^{k-1})\rangle < -1 + \epsilon_{\max}$ the minimum reduction achieved by the heavy ball perturbation is larger than the minimum reduction achieved by the simultaneous projection.

5.5 Implementation

The algorithm we used for our computations is implemented according to the pseudo code we present in this section. In Section 5.7 we explain what the methods do in more detail and also consider the computational effort they require.

Algorithm 3 Level set scheme

```
1: x = x^0
2: t = ∞
3: while ¬ problemIsSolved do
4:     [x, feasibleSolutionFound] = solveCFP(t, usePerturbations)
5:     if ¬ feasibleSolutionFound then
6:         problemIsSolved = true
7:     else
8:         t = reduce(φ(x))
9:     end if
10: end while
```

Algorithm 4 solveCFP(t, usePerturbations)

```
1: p = projectionStep(x)
2: x = updateIterate(x, relaxationParameter * p)
3: feasibleSolutionFound = isFeasible(x, t)
4: previousP = p
5: counter = 1
6: numUnperturbedIterations = 1
7: while counter ≤ maxCounter && ¬ feasibleSolutionFound do
8:     p = projectionStep(x)
9:     if usePerturbations then
10:        perturbIteration = iterationIsToBePerturbed(p, previousP,
11:        numUnperturbedIterations)
12:        if perturbIteration then
13:            x = updateIterate(x, perturbationStep(x))
14:            numUnperturbedIterations = 0
15:        else
16:            x = updateIterate(x, relaxationParameter * p)
17:            numUnperturbedIterations++
18:        end if
19:    else
20:        x = updateIterate(x, relaxationParameter * p)
21:        numUnperturbedIterations++
22:    end if
23:    feasibleSolutionFound = isFeasible(x, t)
24:    counter++
25: end while
```

5.6 Results

Now we present our numerical results. These were achieved with an algorithm implemented according to the description in Section 5.1. It uses the outer perturbation scheme (2.26) with the parameters $\{\beta_k\}_{k=0}^{\infty}$ chosen as described in (2.30), i.e.

$$\beta_k = \begin{cases} 1 & k \leq K \\ 0 & k > K \end{cases}$$

with $K = n_{\max}$, which is the maximum number of iterations we allow the projection methods for solving a CFP $\boldsymbol{P}^l$ arising from the perturbed level set scheme described in Section 5.1. The step sizes $\{\lambda_k^{HB}\}$, $\{\lambda_k^{NE}\}$ and $\{\lambda_k^{SC}\}$ of the heavy ball, Nesterov and surrogate constraint perturbation as they are defined in (5.16), (5.22) and (5.33) can differ for each iteration k. In the results we present in this section, however, we chose them as constant for all k and therefore will denote them in the following by $\lambda^{HB}, \lambda^{NE}$ and λ^{SC}.
First we demonstrate the effects of the heavy ball , Nesterov and surrogate constraint perturbation on a linear feasibility problem. In the second part of this section we consider IMRT optimization and solve the arising optimization problems with the same approach using both simultaneous and cyclic projection in an unperturbed and perturbed manner. As the results in this section show, all three perturbations are eminently useful to speed up the convergence of the algorithm towards a solution compared to the unperturbed methods.

5.6.1 Demonstrating the perturbations: A linear feasibility problem

We present a linear feasibility problem and demonstrate the behavior of both the simultaneous and cyclic projection method with and without perturbations when we use them to solve the problem stated below. We show that in this example, the unperturbed versions of the methods often converge slower than the perturbed versions. Furthermore, we demonstrate that the control sequence for the cyclic projection method has an influence on whether the condition triggering the perturbations is fulfilled.

Problem formulation

We consider the system of linear inequalities

$$A \cdot x \leq b \tag{5.48}$$

where

$$A = \begin{pmatrix} -1/\delta_{x_1} & -1/\delta_{x_2} & -1/\delta_{x_3} \\ 1/\delta_{x_1} & -1/\delta_{x_2} & -1/\delta_{x_3} \\ 1/\delta_{x_1} & 1/\delta_{x_2} & -1/\delta_{x_3} \\ -1/\delta_{x_1} & 1/\delta_{x_2} & -1/\delta_{x_3} \end{pmatrix}, b = \begin{pmatrix} -1 \\ -1 \\ -1 \\ -1 \end{pmatrix}$$

and $x = (x_1, x_2, x_3)^T \in \mathbb{R}^3$. In the following, we refer to the inequality $\langle a_i, x \rangle \leq b_i$ by "inequality i", where a_i denotes the i-th row of the matrix A and b_i is the i-th coordinate of b for $i \in \{1, 2, 3, 4\}$.
These linear inequalities define half-spaces. The separating hyperplanes H_i of these half-spaces intersect the x_1-axis at $\pm\delta_{x_1}$, the x_2-axis at $\pm\delta_{x_2}$ and the x_3-axis at δ_{x_3}.
In this example, we choose $\delta_{x_3} = 100$, $\delta_{x_1} = \tan(\beta)\delta_{x_3}/\sin(\alpha)$ and $\delta_{x_2} = \tan(\beta)\delta_{x_3}/\cos(\alpha)$ with $\alpha = 30°$ and $\beta = 5°$.
Next we demonstrate the behavior of simultaneous and cyclic projection with and without perturbations when we use them to solve (5.48).

Table 5.1: Iterations needed in Example 1 to find a feasible solution with $\lambda(x) \equiv 1.9$. SP converges slowly. Using perturbations accelerates the convergence significantly.

	SP	SP + NE	SP + HB			SP + SC
			$\lambda^{HB} = 8$	$\lambda^{HB} = 80$	$\lambda^{HB} = 800$	
K	449	56	58	17	4	4

Results

In what follows, we occasionally (especially in the descriptions and legends of the figures and tables) use abbreviations for the simultaneous projection (SP) and the cyclic projection method (CP) as well as for the heavy ball perturbation (HB) and the surrogate constraint perturbation (SC). CP+HB means for example that cyclic projection was used in the outer perturbation scheme as operator $\boldsymbol{T}$ together with heavy ball perturbation.
For all methods, we choose the starting point $x^0 = (15, 0, 0)^T$ and the parameters $\epsilon_{\max} = 6 \cdot 10^{-2}, \epsilon_{\min} = 10^{-8}, \lambda^{NE} = 1$ and $\lambda^{SC} = 1$. We consider an iterate x^* to be a solution of (5.48), if $\|Ax^* - b\|_\infty \leq 10^{-10}$ and K denotes the number of iterations needed to find x^*.
The choice of λ^{SC} is motivated by maximizing the theoretically predicted reduction in Theorem 16. For λ^{HB}, however, there exists no such guideline. It can only be chosen in an optimal way, if the solution to the problem is already known. We therefore present results for three different values of λ^{HB} to demonstrate the effects of choosing it in an empirical way.

Example 1 First, we use the simultaneous projection as operator $\boldsymbol{T}$ to solve (5.48). We choose $\lambda(x) \equiv 1.9$ to generate a sequence of iterates, which alternates between fulfilling inequalities $\{1, 4\}$ and $\{2, 3\}$. In this way, we obtain a sequence of projection steps $\{p(x^k)\}$ with $\langle \bar{p}(x^k), \bar{p}(x^{k-1}) \rangle \in [-1+\epsilon_{\min}, -1+\epsilon_{\max}]$. If we use the outer perturbation scheme in this situation, perturbations are therefore triggered after every second unperturbed iteration.
The results of our calculations are given in Table 5.1. The unperturbed method exhibits comparably slow convergence speed due to the opposing projection steps, which offer little progress in the direction of the x_3-axis. All three perturbations are able to speed up the iteration process significantly.

Example 2 Next, we solve (5.48) using the unperturbed cyclic projection method as operator $\boldsymbol{T}$ with $\lambda(x) \equiv 1$ and the control sequence $\{j_1(\nu)\}_{\nu=0}^{\infty} = \{1, 2, 3, 4, 1, 2, 3, 4, ...\}$. This results in a sequence $\{p(x^k)\}$ of projection steps, which does not fulfill $\langle \bar{p}(x^k), \bar{p}(x^{k-1}) \rangle \in [-1 + \epsilon_{\min}, -1 + \epsilon_{\max}]$ until the constraint violations fall below the tolerance of 10^{-10}. The outer perturbation scheme using perturbations as defined in (5.16), (5.22) or (5.33) can therefore not be used in a meaningful way with this operator $\boldsymbol{T}$ and choice of parameters. The values of $\langle \bar{p}(x^k), \bar{p}(x^{k-1}) \rangle$ do not reflect the conflict inherent in the system of linear inequalities due to the choice of the control sequence. It takes the unperturbed algorithm 1917 iterations to find a feasible solution x^*.

Example 3 We now change one of the parameters of the cyclic projection and use the relaxation parameter $\lambda(x) \equiv 1.9$ together with the same control sequence as before. This results

Table 5.2: Iterations needed in Example 3 to find a feasible solution with $\lambda(x) \equiv 1.9$ and the control sequence $\{j_1(\nu)\}$. Not all perturbed versions of CP converge faster than unperturbed CP.

	CP	CP+NE	CP + HB			CP + SC
			$\lambda^{HB} = 8$	$\lambda^{HB} = 80$	$\lambda^{HB} = 800$	
K	20	56	34	26	9	4

in a sequence of iterates $\{x^k\}$ and projection steps $\{p(x^k)\}$, which fulfill $\langle \bar{p}(x^k), \bar{p}(x^{k-1}) \rangle \in [-1 + \epsilon_{\min}, -1 + \epsilon_{\max}]$ for some k. Therefore, we are able to use the outer perturbation scheme in a meaningful way with this operator and choice of parameters. The results of our calculations are presented in Table 5.2. We observe that for this choice of control sequence and relaxation parameter, the Nesterov perturbation as well as not all step sizes λ^{HB} result in accelerated convergence behavior. Cyclic projection used as $\boldsymbol{T}$ in the outer perturbation scheme with the surrogate constraint perturbation, however, converges faster than any of the other variants of cyclic projection.

Example 4 Finally, we alter the feasibility problem (5.48) by enlarging the linear inequality system with duplicates of the matrix rows a_i and the values b_i of the right hand side vector. We make this alteration in order to be able to give a control sequence, which both fits Definition 2 and results in the phenomena we will describe in the following. The new matrix $\tilde{A} \in \mathbb{R}^{8\times 3}$ and vector $\tilde{b} \in \mathbb{R}^8$ are given by

$$\begin{aligned} \tilde{A} &:= \left(a_1^T, a_3^T, a_1^T, a_3^T, a_2^T, a_4^T, a_2^T, a_4^T\right)^T \\ \tilde{b} &:= (b_1, b_3, b_1, b_3, b_2, b_4, b_2, b_4)^T. \end{aligned}$$

The system of linear inequalities $\tilde{A}x \leq \tilde{b}$ of course has the same set of solutions as $Ax \leq b$. We solve $\tilde{A}x \leq \tilde{b}$ using the cyclic projection method with $\lambda = 1.9$ and the control sequence $\{j_2(\nu)\}_{\nu=0}^{\infty} = \{1, 2, 3, 4, 5, 6, 7, 8, 1, 2, 3, 4, 5, 6, 7, 8, ...\}$. By repeating pairs of strongly opposing inequalities, we generate a sequence of projection steps $\{p(x^k)\}$, which fulfills $\langle \bar{p}(x^k), \bar{p}(x^{k-1}) \rangle \in [-1 + \epsilon_{\min}, -1 + \epsilon_{\max}]$ for some k. The number of iterations needed by the variants of the cyclic projection to find a feasible solution are given in Table 5.3. Here the surrogate constraint perturbation and all variants of the heavy ball perturbation are able to accelerate the convergence. Again, cyclic projection used in the outer perturbation scheme with the surrogate constraint perturbation was the fastest to converge and again the Nesterov perturbation was unable to accelerate the convergence. In Figure 5.15 we illustrate the norm of the constraint violation $\| \max\{0, Ax^k - b\} \|$ plotted against the iteration index k. HB8, HB80 and HB800 denote the three versions of the heavy ball perturbation using $\lambda^{HB} = 8, 80$ or 800.

Nesterov perturbation Among all of our perturbations the Nesterov perturbation is the least effective for the Examples we present. We illustrate its behavior in Figure 5.16, which shows the norm of the constraint violation caused by the iterates of the unperturbed methods and the perturbed methods using Nesterov perturbation for Examples 1 (Figure 5.16a) and Example 4 (Figure 5.16b). These plots indicate that the Nesterov perturbation tends

Table 5.3: Iterations needed in Example 4 to find a feasible solution with $\lambda(x) \equiv 1.9$ and the control sequence $\{j_2(\nu)\}$. Not all perturbed versions of CP converges faster than unperturbed CP.

	CP	CP+NE	CP + HB			CP + SC
			$\lambda^{HB} = 8$	$\lambda^{HB} = 80$	$\lambda^{HB} = 800$	
K	32	36	29	20	7	3

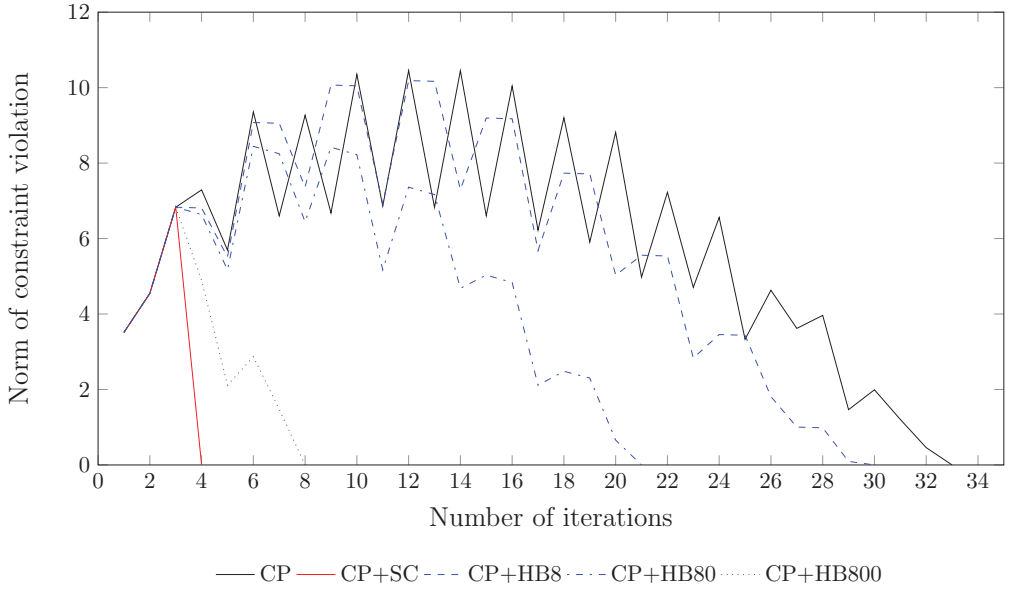

Figure 5.15: Comparison of the constraint violation norm $\|\max\{0, Ax^k - b\}\|$ for perturbed and unperturbed CP in Example 4. CP using SC perturbation is the fastest and unperturbed CP is the slowest to converge to a feasible solution.

to temporarily steer the algorithm into directions, which are unfavorable for fulfilling the constraints. In some cases, however, this interference leads to a faster convergence.

5.6.2 Applying the perturbations in practice: IMRT optimization

The model

In this thesis we choose four IMRT head neck cases for our numerical experiments. In this chapter we consider a model incorporating a reduced set of biological structures and their dose evaluation functions, which focuses on the main conflict between irradiating the tumor volume on the one hand and sparing the myelon and parotids on the other hand. Additionally, we include the healthy tissue not associated with any of the structures mentioned above with the goal to keep the dose in this tissue as low as possible. The dose evaluation functions we use are given in Table 5.4 in detail.
We use a reduced set of biological structures for our calculations, because our focus is to demonstrate the effects of the mathematical methods. Therefore, the treatment plans resulting from our calculations do not fulfill all of the clinical goals a treatment planner would formulate for a full head neck case.
We phrase the IMRT optimization problem in terms of (2.2):

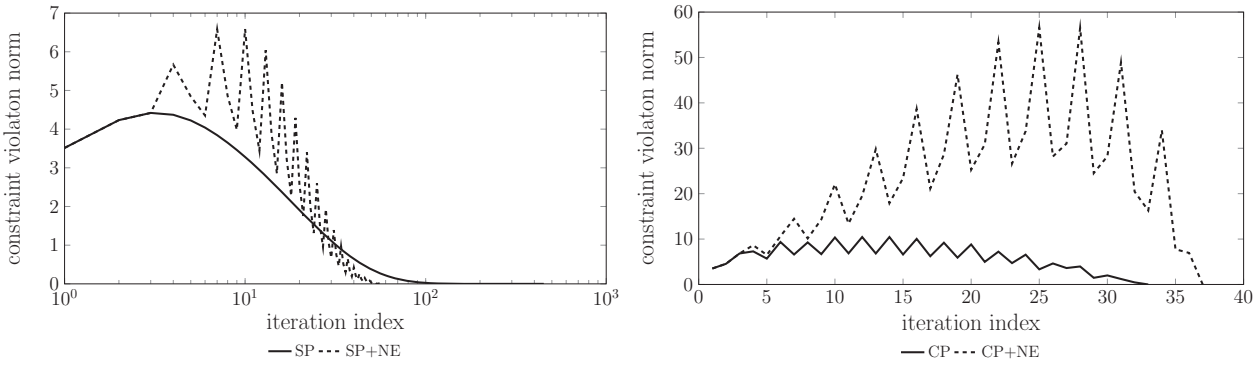

(a) Example 1 **(b)** Example 4

Figure 5.16: Constraint violation norms of the iterates resulting from the unperturbed methods (solid lines) and the perturbed methods using Nesterov perturbation.

Table 5.4: Dose evaluation functions of the considered biological structures.

	structure	function name	parameters
f_1	Left parotis	EUD	$p = 2$
f_2	Right parotis	EUD	$p = 2$
f_3	Myelon	EUD	$p = 2$
f_4	Unclassified healthy tissue	EUD	$p = 2$
f_5	Tumor volume	Tumor conformity	$p = 2, d^{ref} = 60$
g_1	Tumor volume	lower tail penalty	$L = 55$
g_2	Tumor volume	upper tail penalty	$U = 66$
g_3	Myelon	upper tail penalty	$U = 45$

$$\begin{aligned} &\text{Minimize } \Phi(F(x)) \\ &\text{s.t. } g_j(x) \leq 0 \quad j \in J \\ &x \geq 0 \end{aligned} \tag{5.49}$$

where $J = \{1, 2, 3, 4\}, S = \{1, 2, 3, 4, 5\}, F(x) = (f_s)_{s \in S}$. $\Phi(F(x))$ is defined as $\sum_{s \in S} w_s(x) f_s(x)$ with $w_s \in \mathbb{R}_{\geq 0}, \sum_{s \in S} w_s = 1$ and $f_s, g_1, ..., g_3$ as listed in Table 5.4. The function g_4 ensures the positivity of the fluence intensity vector $x \in \mathbb{R}^n$ and is defined as

$$g_4(x) = \frac{1}{n} \sum_{i=1}^{n} \min(x_i, 0)^2$$

where x_i are the coordinates of x.

Results

We use the combination of methods described in Section 5.1 to solve the IMRT optimization problem (5.49) for four different IMRT head neck cases. The underlying dose matrices are again calculated with CERR [27].
We stop the algorithm if the (perturbed or unperturbed) projection method we use is unable to find a feasible solution of the current CFP after $n_{\max} = 10^3$ iterations. Then, the current CFP is assumed to be infeasible and we consider the solution of the previous CFP to be the result of our algorithm. For all our calculations we chose the relaxation parameter $\lambda(x) \equiv 1.9$.
We choose the parameters $\{\beta_k\}_{k=0}^{\infty}$ in (2.26) as described in (2.30), i.e.

$$\beta_k = \begin{cases} 1 & k \leq K \\ 0 & k > K \end{cases}$$

with $K = n_{\max}$.
By $\Phi^*_{\text{method, perturbation}}$ we denote the lowest objective function value, for which the specified projection method used in the outer perturbation scheme with the specified perturbation is able to find a solution within the given maximum number $n_{\max}$ of iterations per CFP $\boldsymbol{P}^l$ as described in (5.1). In the same way we denote by $N_{\text{method, perturbation}}$ the total number of iterations it takes the specified projection method used in the outer perturbation scheme with the specified perturbation to find the solution $x^*_{\text{method, perturbation}}$ with the optimal objective function value $\Phi^*_{\text{method, perturbation}}$.

Initial set of parameters

For our initial set of results we chose $\epsilon_{\max}$ such that $-1+\epsilon_{\max} = \cos(165°)$, which corresponds to $\epsilon_{\max} \approx 0.034$, $\epsilon_{\min} = 10^{-8}, \lambda^{NE} = 1, \lambda^{HB} = 1$ and $\lambda^{SC} = 1$.
Tables 5.5, 5.6, 5.7 and 5.8 present the lowest objective function values achieved by the simultaneous or the cyclic projection method used either in an unperturbed manner or in the outer perturbation scheme with the heavy ball, the Nesterov or the surrogate constraint

perturbation. The values are given with a precision of 10^0. Furthermore, the number of iterations needed to find the solutions are presented. For easier comparison, the percentages with respect to the values corresponding to the unperturbed projection methods are given in brackets.

Note that the optimal objective function values of the perturbed simultaneous projection method $\Phi^*_{\text{SP, HB}}$ and $\Phi^*_{\text{SP, SC}}$ given in Table 5.5 are smaller than the optimal objective function value Φ^*_{SP} of the unperturbed method. The same is true for the cyclic projection method. The optimal objective function values $\Phi^*_{\text{SP, NE}}$ and $\Phi^*_{\text{CP, NE}}$ are in all but one case smaller than the optimal objective function value of the unperturbed methods.

When we use the cyclic projection in the outer perturbation scheme, the condition required to apply the perturbations given in equations (5.20), (5.13) and (5.31) is never met for two of the four IMRT cases. We denote the corresponding values for $\Phi^*_{\text{method, perturbation}}$ and $N_{\text{method, perturbation}}$ by "$-$".

We observe that for all cases $N_{\text{SP, NE}}, N_{\text{SP, HB}}, N_{\text{SP, SC}} < N_{\text{SP}}$, but for some cases $N_{\text{CP, NE}}$, $N_{\text{CP, HB}}$, $N_{\text{CP, SC}} > N_{\text{CP}}$. In these cases, the perturbed method continues beyond solutions with the objective value Φ^*_{CP}, but in total takes more iterations than N_{CP} to get there.

To answer the question whether perturbed methods converge faster, measured at the same objective function value, we present Table 5.10. There we give the number of iterations it takes the perturbed methods to find a solution with an objective function value less or equal than Φ^*_{SP} or Φ^*_{CP}, normalized by N_{SP} and N_{CP}. These values are given with a precision of 10^{-4} and are an indicator for the acceleration of the iteration process caused by the perturbations we used. In the one case where $\Phi^*_{\text{SP, NE}} > \Phi^*_{\text{SP}}$ the value can of course not be calculated and we denote it by "$-$". Note that in all cases the surrogate constraint perturbation is able to accelerate the iteration process even more than the heavy ball perturbation and the Nesterov perturbation.

Figure 5.17 illustrates the progress of the different methods in an exemplary way for case 1. It is notable that perturbations are used rather early in the iteration process when we use simultaneous projection and comparably late when we use cyclic projection. The indices of iterations (counted in a consecutive manner over all $\boldsymbol{P}^l$) in which perturbations are used by the different methods are illustrated in more detail by Figure 5.18 for the same case as in Figure 5.17.

This phenomenon occurs due to the fact that simultaneous projection uses a weighted sum of all function gradients corresponding to violated constraints, whereas cyclic projection uses only gradient information of the next (with respect to the control sequence) violated constraint function.

In our model there are groups of functions which correspond to conflicting goals. By summing the function gradients, simultaneous projection incorporates the information about the conflict between these groups of functions from a very early stage of the iteration process. While this results in strongly opposing subsequent projection steps $p(x^{k-1}), p(x^k)$, and therefore slow convergence, it also triggers the perturbation of the iteration process. When we use cyclic projection, the conflict between the groups of functions only becomes obvious when the subsequently (with respect to the control sequence) violated constraints have opposing function gradients. Figure 5.18 shows that this happens for IMRT cases rather late in the iteration process. The values in Table 5.10 indicate that methods using perturbations early converge faster than methods using them later in the iteration process.

Table 5.9 presents the number of iterations, in which perturbations are used. We observe that

Table 5.5: Lowest objective function values achieved using perturbed and unperturbed SP. In almost all cases perturbed SP reaches solutions with lower function values of Φ than the unperturbed SP.

	Φ^*_{SP}	$\Phi^*_{\text{SP, NE}}$	$\Phi^*_{\text{SP, HB}}$	$\Phi^*_{\text{SP, SC}}$
case 1	3480	3515 (101.01%)	3464 (99.54%)	3387 (97.33%)
case 2	2378	2335 (98.19%)	2356 (99.07%)	2317 (97.43%)
case 3	3129	3032 (96.90%)	3056 (97.67%)	3012 (96.26%)
case 4	3098	2989 (96.48%)	2980 (96.19%)	2941 (94.93%)

Table 5.6: Iteration numbers for perturbed and unperturbed SP. The perturbed SP reaches the solutions within fewer iterations.

	N_{SP}	$N_{\text{SP, NE}}$	$N_{\text{SP, HB}}$	$N_{\text{SP, SC}}$
case 1	7159	1530 (21.37%)	3437 (48.00%)	2155 (30.10%)
case 2	3523	1824 (51.77%)	2340 (66.42%)	1108 (31.45%)
case 3	4773	2398 (50.24%)	3458 (72.45%)	1171 (24.53%)
case 4	4496	1912 (42.53%)	3898 (86.70%)	1292 (28.74%)

in all cases the heavy ball perturbation is applied more often than the surrogate constraint perturbation. Together with $N_{\text{SP, SC}} < N_{\text{SP, HB}}$ and $N_{\text{CP, SC}} < N_{\text{CP, HB}}$, this indicates that in these computations the surrogate constraint perturbation is more effective than the heavy ball perturbation.

Finally in Figure 5.19, we present a cumulative dose volume histogram (DVH) in which we compare the dose distributions calculated for case 1 by the unperturbed simultaneous projection and by the simultaneous projection used in the outer perturbation scheme with the surrogate constraint perturbation. DVHs are a tool used by treatment planners to evaluate the quality of a fluence map and the resulting dose distribution in the patient's body. DVHs show, which percentage of the volume of a certain structure receives a dose greater or equal than the dose value on the horizontal axis. For the tumor volume, a treatment planner might want that 95% of the volume receives at least a dose of 55 Gy and for the myelon, they might want that at most 5% of the volume receives a dose greater than 45 Gy.

The solid lines in Figure 5.19 represent the solution resulting from simultaneous projection without perturbation and the dashed lines correspond to the solution resulting from simultaneous projection with the surrogate constraint perturbation. We observe that the curves for the tumor volume and both parotids do not differ much, but the curves for the myelon are significantly lower for the perturbed method and therefore represent a more desirable dose distribution than the distribution resulting from the unperturbed method.

Varying $\epsilon_{\max}$

In what follows we illustrate the effect of varying the parameter $\epsilon_{\max}$. As before we choose $\epsilon_{\min} = 10^{-8}, \lambda^{NE} = 1, \lambda^{HB} = 1$ and $\lambda^{SC} = 1$. Different than before we choose $\epsilon_{\max}$ such that $-1 + \epsilon_{\max} = \cos(150^\circ)$.

Tables 5.11, 5.12, 5.13 and 5.14 present the lowest objective function values achieved by the

Table 5.7: Lowest objective function values achieved using perturbed and unperturbed CP. In only two of four cases perturbations are used. In these cases the perturbed CP reaches solutions with lower function values of Φ than the unperturbed CP.

	Φ^*_{CP}	$\Phi^*_{\text{CP, NE}}$	$\Phi^*_{\text{CP, HB}}$	$\Phi^*_{\text{CP, SC}}$
case 1	3563	3534 (99.19%)	3490 (97.95%)	3420 (95.99%)
case 2	2424	-	-	-
case 3	3178	3101 (97.58%)	3083 (97.01%)	3052 (96.04%)
case 4	3093	-	-	-

Table 5.8: Iteration numbers for perturbed and unperturbed CP. In only two of four cases perturbations are used. For one IMRT case the iteration numbers rise above N_{CP} for all three perturbations.

	N_{CP}	$N_{\text{CP, NE}}$	$N_{\text{CP, HB}}$	$N_{\text{CP, SC}}$
case 1	6665	3625 (54.39%)	6103 (91.57%)	4044 (60.66%)
case 2	4484	-	-	-
case 3	4238	5094 (120.20%)	5929 (139.90%)	5035 (118.81%)
case 4	5280	-	-	-

simultaneous or the cyclic projection method used either in an unperturbed manner (those values are of course the same as before) or in the outer perturbation scheme with the heavy ball, the Nesterov or the surrogate constraint perturbation. The values are given with a precision of 10^0. Furthermore, the number of iterations needed to find the solutions are presented. For easier comparison, the percentages with respect to the values corresponding to the unperturbed projection methods are again given in brackets.
Note that again the optimal objective function values of the perturbed simultaneous projection method $\Phi^*_{\text{SP, HB}}$ and $\Phi^*_{\text{SP, SC}}$ given in Table 5.11 are smaller than the optimal objective function value Φ^*_{SP} of the unperturbed method. The same is true for the cyclic projection method. The optimal objective function values $\Phi^*_{\text{SP, NE}}$ and $\Phi^*_{\text{CP, NE}}$ are in all but one case smaller than the optimal objective function value of the unperturbed methods.
Different than before the condition required to apply the perturbations given in equations (5.20), (5.13) and (5.31) is always fulfilled in some iterations, even when we use the cyclic projection in the outer perturbation scheme.
We again observe that for all cases $N_{\text{SP, NE}}, N_{\text{SP, HB}}, N_{\text{SP, SC}} < N_{\text{SP}}$. The same applies for

Table 5.9: The number of perturbations used by the perturbed iteration schemes. For all cases HB perturbation is used more often than SC perturbation.

	SP + NE	SP + HB	SP + SC	CP+NE	CP + HB	CP + SC
case 1	263	803	283	275	789	374
case 2	349	534	101	0	0	0
case 3	558	922	166	266	451	349
case 4	455	1074	180	0	0	0

Table 5.10: The fraction of N_{SP} or N_{CP} needed by the perturbed methods to find a solution with objective function value $\leq \Phi^*_{\mathrm{SP}}$ or Φ^*_{CP}. SC perturbation achieves lower values than NE and HB perturbation, in particular if the perturbed method is SP.

	SP + NE	SP + HB	SP + SC	CP + NE	CP + HB	CP + SC
case 1	-	0.4801	0.2122	0.5434	0.7685	0.4308
case 2	0.3684	0.6642	0.2191	-	-	-
case 3	0.2690	0.4324	0.1402	0.9339	0.9122	0.8554
case 4	0.2578	0.4121	0.1417	-	-	-

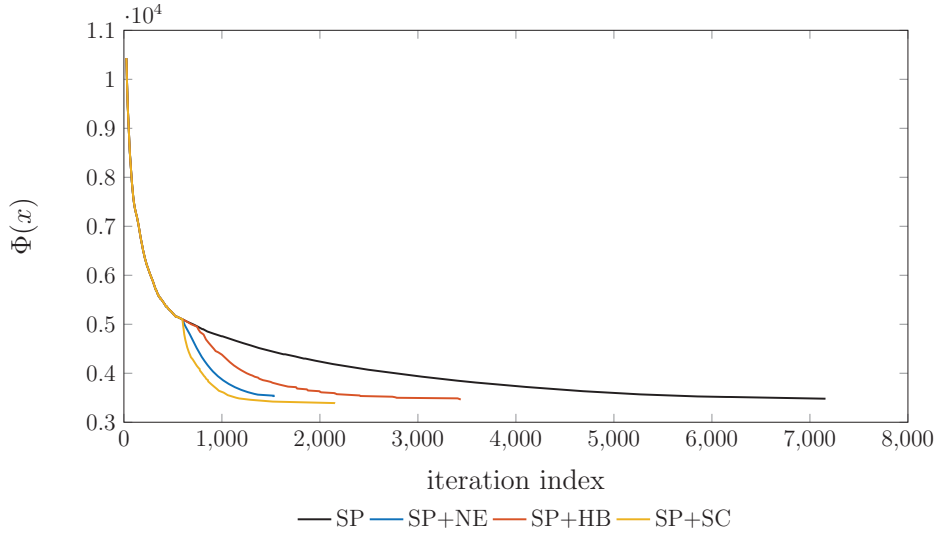

(a) Comparison of perturbed and unperturbed SP.

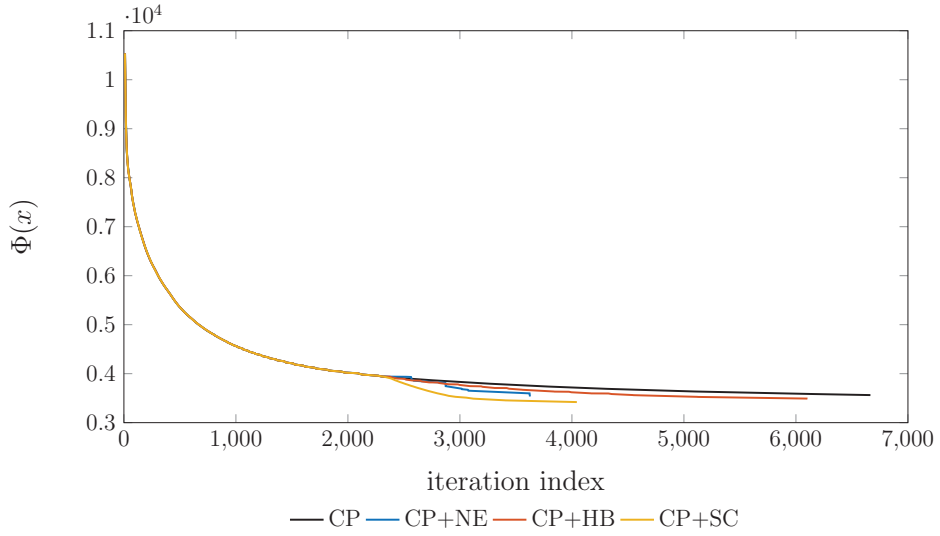

(b) Comparison of perturbed and unperturbed CP.

Figure 5.17: Objective function values achieved by perturbed and unperturbed projection methods plotted against the required number of iterations. SP+SC is the fastest to converge and produces the solution with the lowest objective function value.

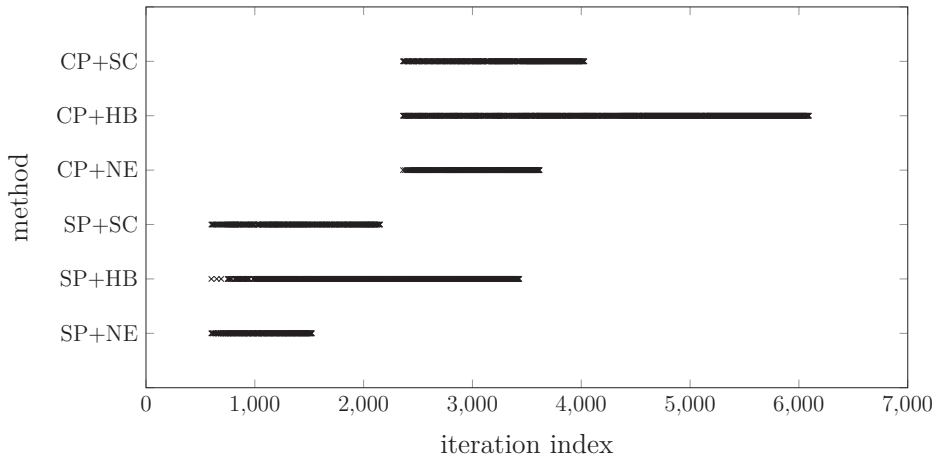

Figure 5.18: Indices of perturbed iterations. Perturbed SP uses perturbations earlier than CP.

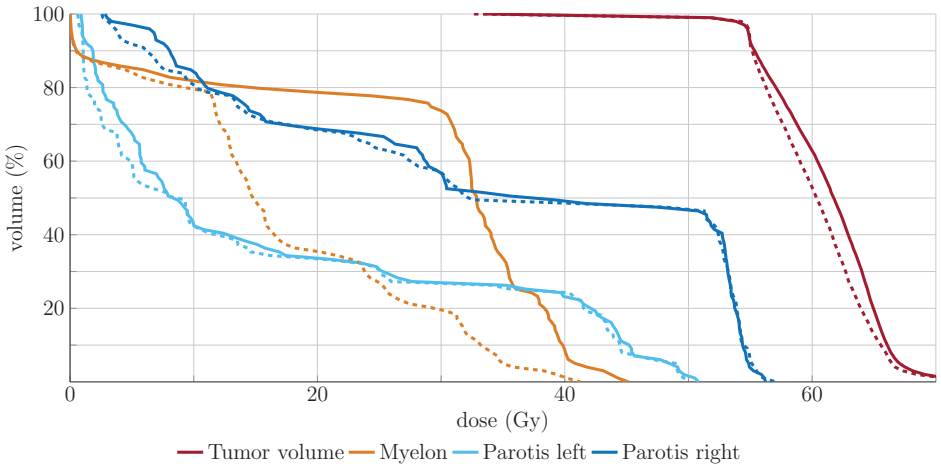

Figure 5.19: Dose volume histogram resulting from solution doses produced by SP (solid lines) and SP+SC (dashed lines).

Table 5.11: Lowest objective function values achieved using perturbed and unperturbed SP. In almost all cases the perturbed SP reaches solutions with lower values of Φ than the unperturbed SP.

	Φ^*_{SP}	$\Phi^*_{\text{SP, NE}}$	$\Phi^*_{\text{SP, HB}}$	$\Phi^*_{\text{SP, SC}}$
case 1	3480	3481 (100.00%)	3460 (99.43%)	3391 (97.44%)
case 2	2378	2326 (97.81%)	2355 (99.03%)	2317 (97.43%)
case 3	3129	3045 (97.32%)	3058 (97.73%)	3025 (96.68%)
case 4	3098	2957 (95.45%)	3002 (96.90%)	2957 (95.45%)

Table 5.12: Iteration numbers for perturbed and unperturbed SP. In all cases the perturbed SP reaches the solutions within fewer iterations than the unperturbed SP.

	N_{SP}	$N_{\text{SP, NE}}$	$N_{\text{SP, HB}}$	$N_{\text{SP, SC}}$
case 1	7159	1572 (21.96%)	3109 (43.43%)	1760 (24.58%)
case 2	3523	1974 (56.03%)	2181 (61.91%)	1390 (39.46%)
case 3	4773	2135 (44.73%)	3247 (68.03%)	1589 (33.29%)
case 4	4496	2680 (59.61%)	2977 (66.21%)	1510 (33.59%)

Table 5.13: Lowest objective function values achieved using perturbed and unperturbed CP. In all cases the perturbed CP reaches solutions with lower values of Φ than the unperturbed CP.

	Φ^*_{CP}	$\Phi^*_{\text{CP, NE}}$	$\Phi^*_{\text{CP, HB}}$	$\Phi^*_{\text{CP, SC}}$
case 1	3563	3532 (99.13%)	3516 (98.68%)	3431 (96.30%)
case 2	2424	2385 (98.39%)	2376 (98.02%)	2369 (97.73%)
case 3	3178	3101 (97.58%)	3080 (96.92%)	3062 (96.35%)
case 4	3093	3032 (98.03%)	3037 (98.19%)	3008 (97.25%)

almost all cases also for the cyclic projection. Only for one case we have $N_{\text{CP, HB}} > N_{\text{CP}}$.
To answer the question whether perturbed methods converge faster, measured at the same objective function value, we present Table 5.15. There we give again the number of iterations it takes the perturbed methods to find a solution with an objective function value less or equal than Φ^*_{SP} or Φ^*_{CP}, normalized by N_{SP} and N_{CP} and with a precision of 10^{-4}. In the one case where $\Phi^*_{\text{SP, NE}} > \Phi^*_{\text{SP}}$ the value can of course not be calculated and we denote it by "$-$". Note that for most of the cases the surrogate constraint perturbation is able to accelerate the iteration process even more than the Nesterov perturbation and the heavy ball perturbation, which is the slowest among the perturbations here.
Table 5.16 presents the number of iterations, in which perturbations are used. We observe that in most cases the surrogate constraint perturbation is applied the fewest times and the heavy ball perturbation the most times. As before we have $N_{\text{SP, SC}} < N_{\text{SP, HB}}$ and $N_{\text{CP, SC}} < N_{\text{CP, HB}}$ which indicates that for this choice of parameters the surrogate constraint perturbation is more effective than the heavy ball perturbation.
Figure 5.20 illustrates the progress of the unperturbed SP and CP as well as the outer perturbation scheme using both projection methods together with the Nesterov, heavy ball and surrogate constraint perturbation in an exemplary way for case 2. It is notable that

Table 5.14: Iteration numbers for perturbed and unperturbed CP. In almost all cases the perturbed CP reaches the solutions within fewer iterations than the unperturbed CP.

	N_{CP}	$N_{\text{CP, NE}}$	$N_{\text{CP, HB}}$	$N_{\text{CP, SC}}$
case 1	6665	2640 (39.61%)	4537 (68.07%)	2316 (34.75%)
case 2	4484	3009 (67.11%)	3513 (78.35%)	2861 (63.80%)
case 3	4238	2859 (67.46%)	4820 (113.73%)	2140 (50.50%)
case 4	5280	2849 (53.96%)	4106 (77.77%)	2719 (51.50%)

Table 5.15: The fraction of N_{SP} or N_{CP} needed by the perturbed methods to find a solution with objective function value $\leq \Phi^*_{\text{SP}}$ or Φ^*_{CP}. In most cases SC perturbation achieves lower values than NE and HB perturbation, in particular if the perturbed method is SP.

	SP + NE	SP + HB	SP + SC	CP + NE	CP + HB	CP + SC
case 1	-	0.4252	0.1298	0.3961	0.5811	0.2215
case 2	0.3398	0.6188	0.3917	0.5256	0.6394	0.3905
case 3	0.2747	0.4121	0.1638	0.4809	0.6300	0.2560
case 4	0.2313	0.3559	0.1419	0.5384	0.5867	0.3072

perturbations are used earlier in the iteration process than with the previous choice of $\epsilon_{\max}$. Again they are applied earlier with the simultaneous projection and comparably later when we use cyclic projection. The indices of iterations in which perturbations are used by the different methods are illustrated in more detail by Figure 5.21 for the same case as in Figure 5.20.

Varying $\lambda^{NE}, \lambda^{HB}$ and λ^{SC}

Next we illustrate the effect of varying the step sizes $\lambda^{NE}, \lambda^{HB}$ and λ^{SC}. As before we choose $\epsilon_{\min} = 10^{-8}$ and $\epsilon_{\max}$ such that $-1 + \epsilon_{\max} = \cos(150°)$.
We experimented with varying $\lambda^{NE}, \lambda^{HB}$ and λ^{SC} with the intention of determining the step sizes which work best for the individual IMRT cases. We chose to perform these experiments only for the perturbed simultaneous projection method, because with this projection method, perturbations are applied earlier in the iteration process and previous results (see e.g. Tables 5.6, 5.8, 5.12 and 5.14) suggest that this is a desirable behavior. We tried the following step

Table 5.16: The number of perturbations used by the perturbed projection methods. For all cases HB perturbation is used more often than NE and SC perturbation. For most cases SC perturbation is used the least often.

	SP + NE	SP + HB	SP + SC	CP+NE	CP + HB	CP + SC
case 1	382	897	428	479	769	411
case 2	539	610	302	607	758	588
case 3	610	971	386	583	899	455
case 4	789	903	367	582	758	610

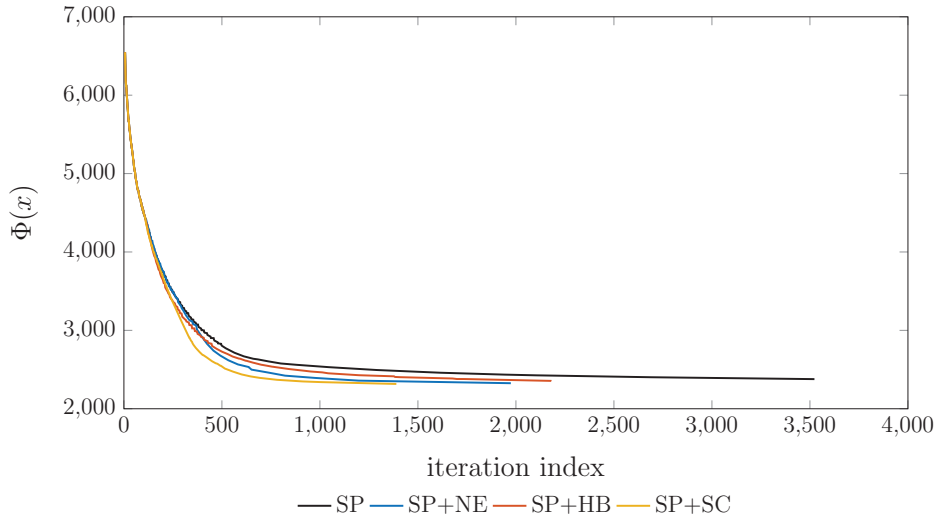

(a) Comparison of perturbed and unperturbed SP.

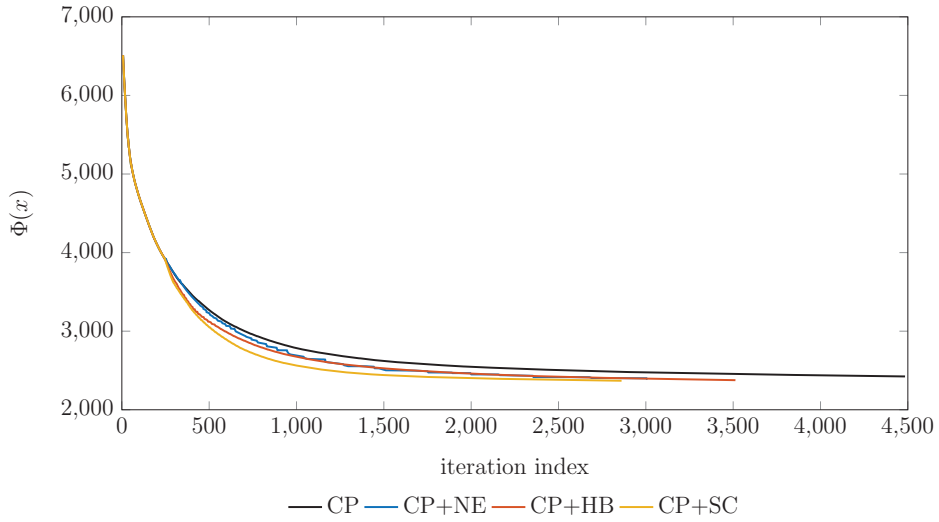

(b) Comparison of perturbed and unperturbed CP.

Figure 5.20: Objective function values achieved by perturbed and unperturbed projection methods plotted against the required number of iterations. SP+SC is the quickest to converge and produces the solution with the lowest objective function value.

size values for all cases:

$$\lambda^{NE} \in \{0.25, 0.5, 0.75, 1, 2\}$$
$$\lambda^{HB} \in \{1, 5, 10, 15, 20, 25, 30\}$$
$$\lambda^{SC} \in \{0.5, 0.8, 1, 2, 3, 5\}$$

For each IMRT case we determined the minimal value of the objective function Φ achieved by any variant of the perturbed simultaneous projection method using any of the step sizes listed above. This value is denoted by Φ^*. We then restricted ourselves to only considering those combinations of perturbations and corresponding step sizes where $\Phi^*_{SP,\text{perturbation}} < \tilde{\Phi}^* = \Phi^*/0.99$, concurring with our choice of reduction strategy for the upper bounds t^l of the CFPs $\boldsymbol{P}^l$, which is described in Section 5.1.

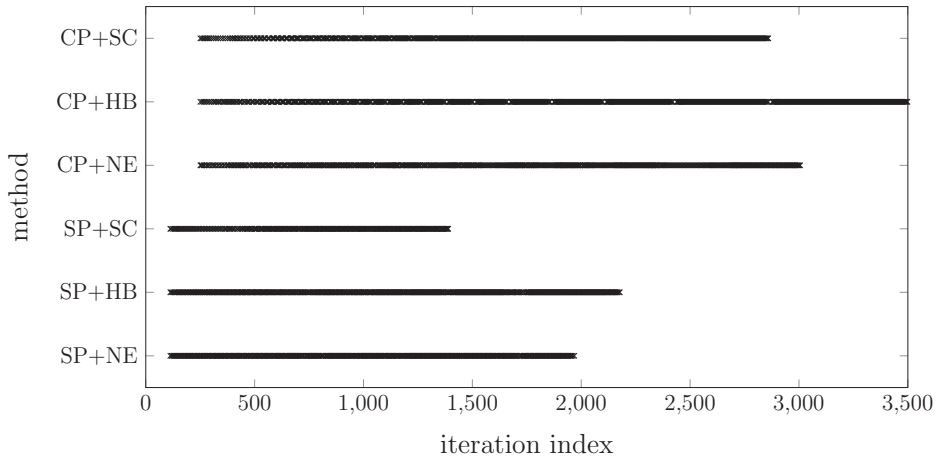

Figure 5.21: Indices of perturbed iterations. SP uses perturbations earlier than CP.

Table 5.17: The values $N_{SP,NE}$ for those step sizes λ^{NE} which result in $\Phi^*_{SP,NE} < \tilde{\Phi}^*$.

λ^{NE}	0.25	0.5	0.75	1	2
case 1					
case 2				1974	
case 3					1746
case 4				2680	

Table 5.18: The values $N_{SP,HB}$ for those step sizes λ^{HB} which result in $\Phi^*_{SP,HB} < \tilde{\Phi}^*$.

λ^{HB}	1	5	10	15	20	25	30
case 1		2191	1423	1794			
case 2		1952		1529			
case 3		1972	1739		1528		
case 4		1942	1847	1359	723		

Table 5.19: The values $N_{SP,SC}$ for those step sizes λ^{SC} which result in $\Phi^*_{SP,SC} < \tilde{\Phi}^*$.

λ^{SC}	0.5	0.8	1	2	3	5
case 1	2290	2126	1760			
case 2			1390	1169	781	
case 3				1479	760	
case 4			1510	1059	1067	

In Tables 5.17 - 5.19 we present an overview of the step sizes, which resulted in solutions that fell among this restriction. If the condition $\Phi^*_{SP,\text{perturbation}} < \tilde{\Phi}^*$ was met for a given step size we gave the corresponding number of iterations in the table. Otherwise we left the space empty.
Among those combinations of perturbations and corresponding step sizes we chose for each perturbation the step size, which resulted in the lowest number of iterations. For case 1 the

Table 5.20: Step sizes $\lambda^{NE}, \lambda^{HB}$ and λ^{SC} chosen individually for each IMRT case.

	λ^{NE}	λ^{HB}	λ^{SC}
case 1	0.5	10	1
case 2	1	15	3
case 3	2	20	3
case 4	1	20	2

Table 5.21: Lowest objective function values achieved using perturbed and unperturbed SP. The perturbed SP achieves smaller objective function values than the unperturbed SP for all perturbations.

	Φ^*_{SP}	$\Phi^*_{\text{SP, NE}}$	$\Phi^*_{\text{SP, HB}}$	$\Phi^*_{\text{SP, SC}}$
case 1	3480	3465 (99.57%)	3408 (97.93%)	3391 (97.44%)
case 2	2378	2326 (97.81%)	2314 (97.31%)	2325 (97.77%)
case 3	3129	3023 (96.61%)	3017 (96.42%)	3022 (96.58%)
case 4	3098	2957 (95.45%)	2961 (95.58%)	2937 (94.80%)

Table 5.22: Iteration numbers for perturbed and unperturbed SP. The iteration numbers of the perturbed SP are significantly smaller than those of the unperturbed SP.

	N_{SP}	$N_{\text{SP, NE}}$	$N_{\text{SP, HB}}$	$N_{\text{SP, SC}}$
case 1	7159	2760 (38.55%)	1423 (19.88%)	1760 (24.58%)
case 2	3523	1974 (56.03%)	1529 (43.40%)	781 (22.17%)
case 3	4773	1746 (36.58%)	1528 (32.01%)	760 (15.92%)
case 4	4496	2680 (59.61%)	723 (16.08%)	1059 (23.55%)

perturbed simultaneous projection using the Nesterov projection was unable to find solutions with $\Phi^*_{SP,NE} < \tilde{\Phi}^*$. In this case we chose the step length λ^{NE}, which gave us the lowest value of $\Phi^*_{\text{SP, NE}}$. The step size values we determined in this way are given in Table 5.20.

Table 5.21 presents the lowest objective function values achieved by the simultaneous projection method used either in an unperturbed manner or in the outer perturbation scheme with the heavy ball, the Nesterov or the surrogate constraint perturbation with the step sizes chosen as described above. The values are again given with a precision of 10^0. Furthermore, the number of iterations needed to find the solutions are presented in Table 5.22. For easier comparison, the percentages with respect to the values corresponding to the unperturbed projection methods are again given in brackets.

The optimal objective function values of the perturbed simultaneous projection method $\Phi^*_{\text{SP, NE}}$, $\Phi^*_{\text{SP, HB}}$ and $\Phi^*_{\text{SP, SC}}$ given in Table 5.5 are smaller than the optimal objective function value Φ^*_{SP} of the unperturbed method. For all cases $N_{\text{SP, NE}}, N_{\text{SP, HB}}, N_{\text{SP, SC}}$ are significantly smaller than N_{SP}.

In Table 5.23 we give again the number of iterations it takes the perturbed methods to find a solution with an objective function value less or equal than Φ^*_{SP} or Φ^*_{CP}, normalized by N_{SP} and N_{CP} and with a precision of 10^{-4}. For all cases the heavy ball and surrogate con-

Table 5.23: The fraction of N_{SP} or N_{CP} needed by the perturbed methods to find a solution with objective function value $\leq \Phi^*_{\mathrm{SP}}$. SC+HB achieves particularly low values.

	SP + NE	SP + HB	SP + SC
case 1	0.3855	0.1280	0.1298
case 2	0.3398	0.1536	0.1414
case 3	0.1724	0.0895	0.0851
case 4	0.2313	0.0854	0.1234

Table 5.24: The number of perturbations used by the perturbed projection methods. For all cases NE perturbation is used more often than HB and SC perturbation.

	SP + NE	SP + HB	SP + SC
case 1	740	370	428
case 2	539	356	132
case 3	505	364	138
case 4	789	150	251

straint perturbation are able to accelerate the iteration process even more than the Nesterov perturbation.

Table 5.24 presents the number of iterations, in which perturbations are used. In contrast to the values resulting from our previously chosen step sizes $\lambda^{NE}, \lambda^{HB}$ and λ^{SC} the heavy ball perturbation is no longer applied the most times. Now the Nesterov perturbation ist applied most often. Together with $N_{\mathrm{SP,\ SC}} < N_{\mathrm{SP,\ NE}}$ and $N_{\mathrm{SP,\ HB}} < N_{\mathrm{SP,\ NE}}$, this indicates that with this choice of parameters the Nesterov perturbation is less effective than the heavy ball and surrogate constraint perturbation.

Figure 5.22 illustrates the progress of the different methods in an exemplary way for case 1. For this choice of step sizes $\lambda^{NE}, \lambda^{HB}$ and λ^{SC} the accelerated decrease of the objective function value $\Phi(x)$ is even more noticeable than previously.

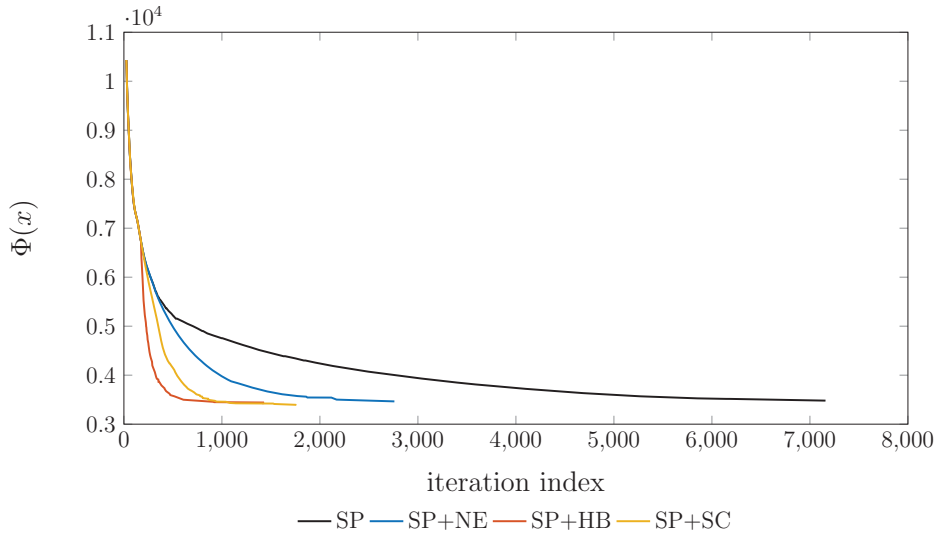

Figure 5.22: Objective function values achieved by perturbed and unperturbed simultaneous projection plotted against the required number of iterations. SP+HB is the quickest to converge while SP+SC produces the solution with the lowest objective function value.

Comparison of theoretical and actual convergence

Finally we compare the theoretically predicted minimum reduction of the distance to a feasible point z by the simultaneous projection and the surrogate constraint perturbation to the reduction that was actually achieved in the process of solving the IMRT optimization problems. Furthermore we compare the reduction achieved in our calculations by the surrogate constraint and heavy ball perturbation to the reductions achieved by the simultaneous projection method. In all our comparisons we considered z to be the solution of the CFP in question. We start with the two comparisons of the actual to the theoretically predicted reduction and continue with the comparisons of perturbed and unperturbed simultaneous projection.
First we recall (5.39) and calculate for each iteration k the distance reduction $\|x^k - z\| - \|x^{SP} - z\|$ to z for the case when the inequality (5.39) is sharp. Next we calculate in the same manner $\|x^k - z\| - \|x_{SP}^{k+1} - z\|$ where $x_{SP}^{k+1} = x^k + \lambda p(x^k)$ is the next iterate generated by the simultaneous projection method.
We consider the ratio

$$r(SP) := \frac{\|x^k - z\| - \|x_{SP}^{k+1} - z\|}{\|x^k - z\| - \|x^{SP} - z\|}$$

for all iteration indices k in all CFPs $\boldsymbol{P}^l$ where $l = 1, ..., L-1$ and denote by $h(r, SP)$ the number of values $r(SP)$ for which $r(SP) \leq r$. In Figure 5.23 we present the quotient

$$H(r, SP) := h(r, SP)/K_{\text{total}},$$

in an exemplary manner for one of the IMRT cases where K_{total} is the total number of iterations over all CFPs $\boldsymbol{P}^l$ for $l = 1, ..., L-1$.
Next we recall (5.45) and calculate for each perturbed iteration the distance reduction $\|x^k - z\| - \|x^{SC} - z\|$ to z for the case when the inequality (5.45) is sharp. We calculate in the same manner $\|x^k - z\| - \|x_{SC}^{k+1} - z\|$ where $x_{SC}^{k+1} = x^k + \lambda^{SC}\theta^{SC}d^{SC}$.

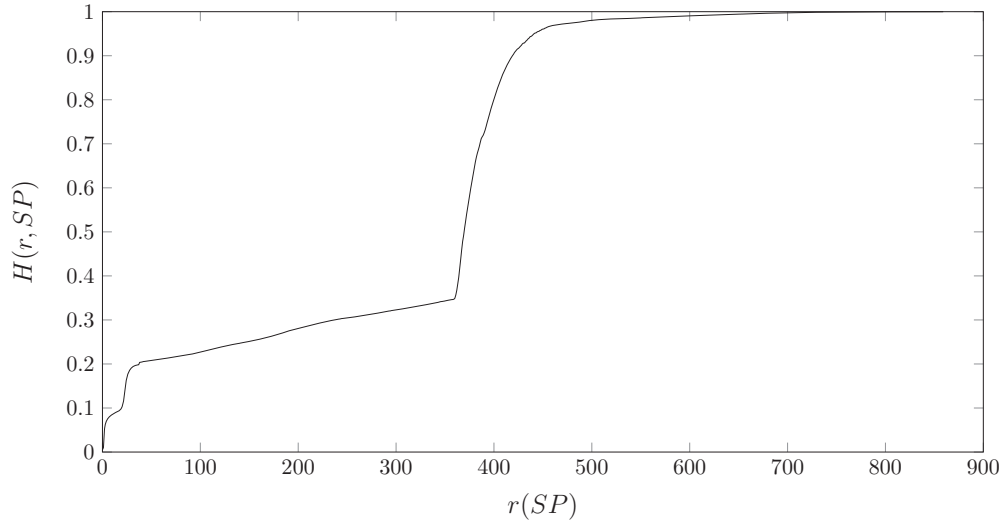

Figure 5.23: Normalized cumulative histogram of the ratio $r(SP)$.

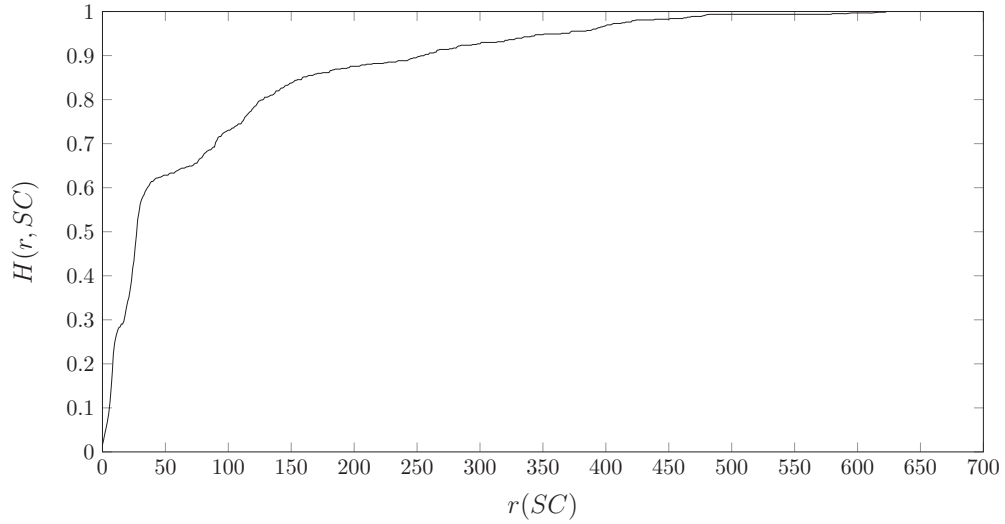

Figure 5.24: Normalized cumulative histogram of the ratio $r(SC)$.

Similar to before we consider the ratio

$$r(SC) := \frac{\|x^k - z\| - \|x_{SC}^{k+1} - z\|}{\|x^k - z\| - \|x^{SC} - z\|}$$

for all perturbed iterations k in all CFPs $\boldsymbol{P}^l$ where $l = 1, ..., L-1$. We denote by $h(r, SC)$ the number of values $r(SC)$ for which $r(SC) \leq r$. In Figure 5.24 we present the quotient

$$H(r, SC) := h(r, SC)/K_{\text{total}},$$

in an exemplary manner for one of the IMRT cases where K_{total} is the total number of perturbed iterations over all $\boldsymbol{P}^l$ for $l = 1, ..., L-1$.
We observe that both inequalities (5.39) and (5.45) are not sharp for the vast majority of iterations in our IMRT optimization process. The actual progress achieved by the unperturbed simultaneous projection is bigger than the minimum progress predicted by (5.39) and

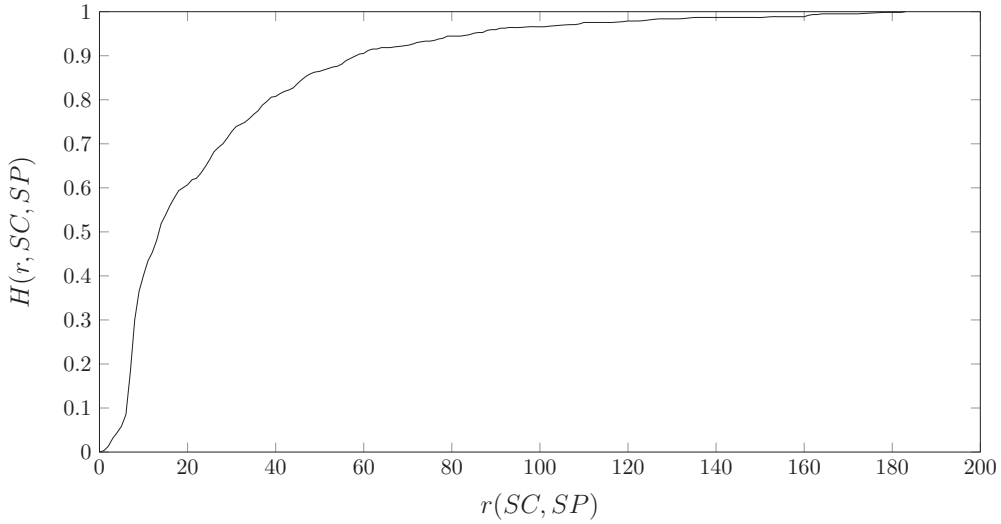

Figure 5.25: Normalized cumulative histogram of the ratio $r(SC, SP)$.

the same is true for the perturbed simultaneous projection using the surrogate constraint perturbation in comparison with (5.45).
Additionally we compare for all perturbed iterations the reduction achieved by the perturbed iterate to the reduction that would have been achieved in that iteration by the unperturbed simultaneous projection.
We consider the ratios

$$r(SC, SP) := \frac{\|x^k - z\| - \|x_{SC}^{k+1} - z\|}{\|x^k - z\| - \|x_{SP}^{k+1} - z\|}$$

and

$$r(HB, SP) := \frac{\|x^k - z\| - \|x_{HB}^{k+1} - z\|}{\|x^k - z\| - \|x_{SP}^{k+1} - z\|},$$

where $x_{HB}^{k+1} = x^k + 0.5(\bar{p}(x^k) + \bar{p}(x^{k-1}))$, for all perturbed iterations k in all CFPs $\boldsymbol{P}^l$ with $l = 1, ..., L-1$.
We denote by $h(r, SC, SP)$ the number of values $r(SC, SP)$ for which $r(SC, SP) \leq r$ and by $h(r, HB, SP)$ the number of values $r(HB, SP)$ for which $r(HB, SP) \leq r$.
In Figure 5.25 we present the quotient

$$H(r, SC, SP) := h(r, SC, SP)/K_{\text{total}}$$

and in Figure 5.26 the quotient

$$H(r, HB, SP) := h(r, HB, SP)/K_{\text{total}},$$

in an exemplary manner for one of the IMRT cases where K_{total} is the total number of iterations where the perturbation in question was applied.
The progress provided by the surrogate constraint perturbation in an iteration of the perturbed simultaneous projection scheme is bigger than the progress that would have been achieved by the simultaneous projection in that iteration. This is not always true for the

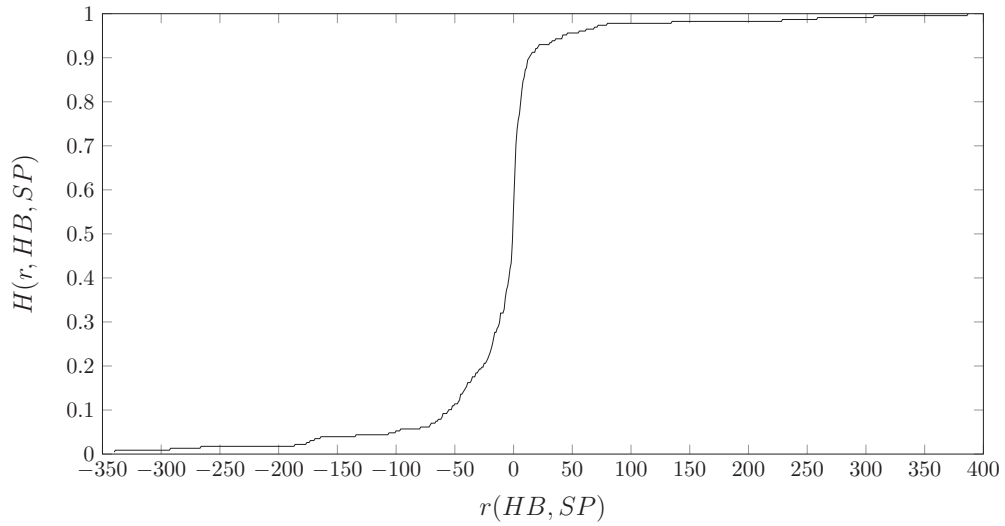

Figure 5.26: Normalized cumulative histogram of the ratio $r(HB, SP)$.

heavy ball perturbation. It happens in about 50% of the iterations that $\|x^k - z\| - \|x_{HB}^{k+1} - z\| < 0$, which means that applying the heavy ball perturbation increased the distance to z in that iteration. The decrease of the overall iteration numbers presented in the previous part of this section, however, indicates that applying the heavy ball perturbation steers the algorithm into a favorable direction, even if it increases the distance to z in the short term.

5.7 Computational effort

The results in Section 5.6 demonstrate that the perturbed iteration scheme using the simultaneous projection method as operator $\boldsymbol{T}$ needs less iterations in Algorithm 4 to find feasible solutions of the CFPs $\boldsymbol{P}^l$. In this section we explore what extra computational effort per iteration is necessary to apply the perturbations. We compare the computational effort in terms of floating point operations (FLOPs), which are needed for one iteration of Algorithm 4, i.e. executing code lines 7-24 one time. We juxtapose the unperturbed simultaneous projection and the perturbed iteration scheme using simultaneous projection with heavy ball, surrogate constraint or Nesterov perturbation.
In this section we denote the length of the decision variable vector x^k by n_b (number of beamlets), the size of the dose matrix $\boldsymbol{D}$ by $n_v \times n_b$ where n_v is the number of voxels, the number of functions φ_i by n_f and the number of objective functions accumulated in Φ, which we choose as $\Phi(F(x)) = \sum_{s \in S} f_s(x)$, by n_o.
In the following we list the methods occurring in Algorithm 4 and their computational effort. We take into account the results known from previously executed methods. A detailed List of the FLOPs needed to perform each operation is given in Table 5.25.

1. projectionStep

To calculate the projection step of the simultaneous projection method, we need to

(1a) calculate the values of the functions φ_i , which consists of

(1a.i) calculating the dose $d = \boldsymbol{D}x^k$

(1a.ii) calculating $(d - d^{ref})^2$

(1a.iii) calculating $\frac{1}{|\mathcal{O}_i|}\sum(d - d^{ref})^2$

(1a.iv) calculating $\sum_{s\in S} f_s(x)$

(1b) calculate the gradients of the functions φ_i , which consists of

(1b.i) calculating $\boldsymbol{D}^T(d - d^{ref})$

(1b.ii) calculating $2\boldsymbol{D}^T(d - d^{ref})$

(1b.iii) calculating $\sum_{s\in S} \nabla f_s(x)$

(1c) calculate $p = -\sum w_i(\varphi_i(x^k)/\|\nabla\varphi_i(x^k)\|^2)\nabla\varphi_i(x^k)$ with $w_i = \varphi_i(x^k)/\sum_{j\in I}\varphi_j(x^k)$, which consists of

(1c.i) calculating $w_i = \varphi_i(x^k)/\sum_{j\in I}\varphi_j(x^k)$ ($2n_f - 1$ FLOPs)

(1c.ii) calculating $-\sum w_i \frac{\varphi_i(x^k)}{\|\nabla\varphi_i(x^k)\|^2}\nabla\varphi_i(x^k)$ ($4n_b n_f + n_f - n_b$ FLOPs)

2. iterationIsToBePerturbed

To evaluate the condition whether the iteration is to be perturbed we need to

(2a) calculate the norms of $p(x^k)$ and $p(x^{k-1})$

(2b) calculate the inner product of $p(x^k)$ and $p(x^{k-1})$ and divide it by $\|p(x^k)\| \cdot \|p(x^{k-1})\|$

3. perturbationStep

The number of FLOPs needed to calculate the perturbation steps is different for each perturbation.

(3.I) **Heavy ball perturbation (HB):**

(3.I.a) Divide $p(x^k)$ and $p(x^{k-1})$ by their norms

(3.I.b) Add $\bar{p}(x^k)$ and $\bar{p}(x^{k-1})$

(3.II) **Surrogate constraint perturbation (SC):**

(3.II.a) Calculate $d^{SC} = p(x^k) - \frac{\langle p(x^k), p(x^{k-1})\rangle}{\langle p(x^{k-1}), p(x^{k-1})\rangle}p(x^{k-1})$

(3.II.b) Calculate $\theta^{SC} = \frac{\langle p(x^k), p(x^k)\rangle}{\langle d^{SC}, d^{SC}\rangle}$

(3.II.c) Multiply θ^{SC} and d^{SC}

(3.III) **Nesterov perturbation (NE):**

(3.III.a) Calculate the step length $(k-1)/(k+2)$

(3.III.b) Subtract $x^k - x^{k-1}$

4. updateIterate

Updating the iterate takes only two vector operations

(4a) Multiply the projection or perturbation step with the relaxation parameter/ step length

(4b) Add the result to x^k

5. isFeasible

$2n_v(n_b + 1) + n_o - 1$
To determine whether an iterate is feasible we need to

(5) calculate the values of the functions $\varphi_i(x^k)$, see the first step of the calculation of the projection step. We have described this process in detail in (1a).

In Table 5.26 we summarize our comparison and give the number of floating point operations needed for each method as well as this number expressed in the $\mathcal{O}$-notation. We observe that the computational effort does not differ in the $\mathcal{O}$-notation, because only the scalar multiplier of n_b and in the constant summand changes for different methods. In the same way as before in Section 5.6 we denote e.g. by SP+NE the perturbed simultaneous projection using the Nesterov perturbation.
To give an impression of the magnitude we choose to first give the summands which include the parameter n_v, which is the largest one for our application. Next come those of the remaining summands which contain n_b, the second largest parameter, then the ones containing n_o, then those containing n_f and finally constants.
We quantify the amount of extra computational effort caused by the perturbations by calculating the actual number of FLOPs for one of the cases considered by us in an exemplary manner. In Table 5.27 we present the amount of extra computational effort expressed in terms of percent of the number of FLOPs needed for the unperturbed simultaneous projection. In this case we have $n_v = 50961, n_b = 1785, n_o = 6$ and $n_f = 5$. For SP+HB for example we calculated

$$100 \cdot (\text{FLOPs(SP+HB)} - \text{FLOPs(SP)})/\text{FLOPs(SP)}$$

where FLOPs(method) is the number of FLOPs required for one iteration of the method in question according to the expression in Table 5.26. The values presented in Table 5.27 illustrate that the extra effort needed for a perturbed iteration step vanishes in comparison to the effort for one iteration of the unperturbed simultaneous projection.

5.8 Discussion

In this chapter we phrased a convex multicriteria optimization problem as a convex single criteria optimization problem by accumulating the objective functions in a weighted sum. We solved the single criteria problem by transforming it into a sequence of convex feasibility problems via the level set scheme. We then used either the simultaneous or the cyclic subgradient projection method to solve the feasibility problem. We exploited the fact that both projection methods are bounded perturbation resilient and modified the iteration scheme of the projection methods with perturbations which we developed using ideas of the Nesterov

Table 5.25: A detailed list of the number of FLOPs needed to perform each operation.

operation	FLOPs
1a.i	$n_v(2n_b - 1)$
1a.ii	$2n_v$
1a.iii	n_v
1a.iv	$n_o - 1$
total 1a	$2n_v(n_b + 1) + n_o - 1$
1b.i	$n_b(2n_v - n_f)$
1b.ii	n_v
1b.iii	$(n_o - 1)n_b$
total 1b	$(2n_v - n_f + n_o - 1)n_b + n_v$
1c.i	$2n_f - 1$
1c.ii	$4n_b n_f + n_f - n_b$
total 1c	$4n_b n_f + 3n_f - n_b - 1$
total 1	$2n_v(n_b + 1) + n_o - 1 + (2n_v - n_f + n_o - 1)n_b + n_v + 4n_b n_f + 3n_f - n_b - 1$ $=n_v(4n_b + 3) + n_b(3n_f + n_o - 2) + 3n_f + n_o - 2$
2a	$2(2n_b - 1) + 2$
2b	$2n_b - 1 + 2$
total 2	$6n_b + 1$
3.I.a	$2n_b$
3.I.b	n_b
total 3.I	$3n_b$
3.II.a	$2n_b + 1$
3.II.b	$2n_b$
3.II.c	n_b
total 3.II	$5n_b + 1$
3.III.a	3
3.III.b	n_b
total 3.III	$n_b + 3$
4.a	n_b
4.b	n_b
total 4	$2n_b$
total 5	$2n_v(n_b + 1) + n_o - 1$

Table 5.26: Computational effort in terms of floating point operations (FLOPs) needed for one iteration in Algorithm 4 using the unperturbed simultaneous projection (SP) or the perturbed iteration scheme with the simultaneous projection and heavy ball (SP+HB), surrogate constraint (SP+SC) or Nesterov perturbation (SP+NE).

method	FLOPs	$\mathcal{O}$
SP	$n_v(6n_b+5)+n_b(n_o+3n_f)+2n_o+3n_f-3$	$\mathcal{O}(n_v n_b + n_b n_o + n_b n_f)$
SP+HB	$n_v(6n_b+5)+n_b(n_o+3n_f+9)+2n_o+3n_f-2$	$\mathcal{O}(n_v n_b + n_b n_o + n_b n_f)$
SP+SC	$n_v(6n_b+5)+n_b(n_o+3n_f+11)+2n_o+3n_f-1$	$\mathcal{O}(n_v n_b + n_b n_o + n_b n_f)$
SP+NE	$n_v(6n_b+5)+n_b(n_o+3n_f+7)+2n_o+3n_f+1$	$\mathcal{O}(n_v n_b + n_b n_o + n_b n_f)$

Table 5.27: The additional amount of FLOPs required for the perturbed simultaneous projection variants in terms of percent of the number of FLOPs required for the unperturbed simultaneous projection.

method	extra effort [% of FLOPs(SP)]
SP+HB	$2.9420 \cdot 10^{-03}$
SP+SC	$3.5960 \cdot 10^{-03}$
SP+NE	$2.2888 \cdot 10^{-03}$

Acceleration Method [52], the heavy ball method by Polyak [56] and a method by Dudek [30], which blends the idea of surrogate constraint methods with relaxed, averaged projections. All of the algorithms they propose are not designed for solving a convex nonlinear feasibility problem. Dudek's method for example is even phrased only in the context a system of linear inequalities. Nonetheless, all of the methods contain approaches to accelerate convergence and reduce zigzagging behavior, which we incorporated in the perturbations formulated by us.

We proved that these perturbations are bounded, which allows us to use them together with the simultaneous and cyclic subgradient projection method in the sense of their bounded perturbation resilience. We also proved that the minimum progress achieved in one iteration by the perturbed simultaneous subgradient projection method using the surrogate constraint perturbation is significantly bigger than the minimum progress achieved by the unperturbed simultaneous subgradient projection method if subsequent projection steps are strongly opposing. Furthermore we showed that there always exist parameters for the heavy ball perturbation such that the minimum progress achieved by the perturbed simultaneous subgradient projection method using the heavy ball perturbation is at least as big as the minimum progress achieved by the unperturbed simultaneous subgradient projection method.

Our numerical results demonstrate that in the majority of cases the perturbed projection methods converge faster than their unperturbed counterparts, both for the linear feasibility problems we discussed and those arising from IMRT treatment planning. In IMRT optimization applying perturbations early in the iteration process, as it is done for the simultaneous projection, yields better results than applying them later, like for the cyclic projection.

We present results for three different parameter choices, which illustrate both the effect of changing the threshold of when perturbations are applied and the step sized used by them.

Even for our initial naive choice of parameters the perturbed methods offer a significant improvement in the majority of cases compared to their unperturbed counterpart.
In our computations the perturbed versions of the simultaneous projection method yield the biggest improvement in both iteration numbers and objective function values of the solutions. Less improvement is achieved by the perturbed versions of the cyclic projection method. The perturbed simultaneous projection method using the surrogate constraint perturbation surpasses the objective function value achieved by the unperturbed simultaneous projection method after 9-40% (with an average of 17%) of the number of iterations needed by the unperturbed method. For the heavy ball perturbation this range is 9-66% (with an average of 35%) and the Nesterov perturbation needs 17-37% (with an average of 29%) of the number of iterations needed by the unperturbed method. The least improvement is achieved by the cyclic projection using the heavy ball perturbation. This method surpasses the objective value achieved by the unperturbed cyclic projection after 58-91% (with an average of 69%) of the iterations needed by the unperturbed method. For a few combination of IMRT cases and parameter choices the overall convergence was delayed by using perturbed projection methods.
We considered the extra computational effort needed for the perturbed iteration scheme and illustrated that for our IMRT optimization problems this value is only marginally higher than the effort needed for the unperturbed iteration scheme. Together with the fact that in the vast majority of our experiments the perturbed methods are able to lower the number of iterations significantly, our approach offers clear advantages in terms of computational effort.
We did not derive any rules for choosing the step sizes of the perturbations or the threshold, which determines whether perturbations are applied in a given iteration. Our results indicate, however, that these values can be chosen from experiments on similar problems in a reliable way. Also a result on the convergence behavior of the Nesterov perturbation remains an open task.

6 Conclusions and perspective

Mathematical optimization in IMRT treatment planning has been an area of long-lasting and prosperous research, which has enabled great advances in clinical practice. Its findings have helped, for example, to improve the treatment plan quality and to present a previously unknown multitude of pareto optimal treatment options to the planner. They then have the opportunity to choose from this multitude the treatment plan which fits best for the individual patient. However, some characteristics of IMRT optimization problems, like the ill-conditionedness of the problem and the strong conflict between the clinical goals, are still challenging to optimization solvers.

In this thesis a general convex multicriteria optimization problem is phrased either as convex single criteria constrained optimization problem or in a lexicographic manner as a sequence of convex single criteria constrained optimization problems. Each single criteria optimization problem is then translated into a sequence of convex feasibility problems via the the level set scheme. Different projection methods are presented as algorithmic operators to solve the feasibility problems and difficulties we face using this approach in IMRT optimization are illustrated, which result from the aforementioned characteristics of IMRT problems. We propose to exploit the bounded perturbation resilience of the projection methods in order to implement two ways of using perturbations to mitigate these difficulties.

In Chapter 4 we use superiorization, which is a special case of perturbations. It is implemented in order to steer the lexicographic optimization process towards a solution of an optimization level, which is favorable with respect to the objective function of the next optimization level. Thereby we accelerate the convergence of the overall procedure. Two sets of superiorization parameters determined in an experimental way are presented: One is tailored individually for each IMRT case we considered and chosen such that it accelerates the convergence for the respective optimization problem the most. Using these parameters results in an acceleration of at least 7.9% and at most 33.8% with an average of 15.6% in terms of numbers of multiplications of the dose matrix and the fluence vector, which we used as units for measuring progress here, because those multiplications constitute the main computational effort. Then the question if similar optimization problems might benefit from superiorization with a common set of parameters is explored. We propose such a set for the IMRT cases we considered and are able to accelerate the convergence with it by at least 4.6% and at most 11.4% with an average of 8.9%.

In Chapter 5 we use perturbations as anti-zigzag strategy. Three variants of perturbations, which we developed based on methods in the literature, are introduced: The Nesterov perturbation, the heavy ball perturbation and the surrogate constraint perturbation. We prove that these perturbations are bounded and can therefore be used together with projection methods in the sense of their bounded perturbation resilience. In Section 5.4 theoretical results on the convergence of the perturbed simultaneous subgradient projection method using the surrogate constraint and heavy ball perturbation are developed. We prove that the worst case progress made by a surrogate constraint perturbation step is at least as big

as the worst case progress achieved by the simultaneous subgradient projection method and even significantly bigger if subsequent steps taken by the simultaneous subgradient projection method are strongly opposing. The perturbed and unperturbed cyclic and simultaneous subgradient projection method are then applied to IMRT optimization and we demonstrate that the perturbed simultaneous subgradient projection method converges significantly faster than its unperturbed counterpart for all variants of perturbations. The perturbed method arrives at a solution at least 13.3% and at most 84.1% faster than its unperturbed counterpart with an average of 58.5%. The cyclic subgradient projection method is accelerated by using perturbations in the majority of, but not in all cases. It achieved an acceleration of up to 65.3% with an average of 24.9% compared to the unperturbed method. Finally the computational effort needed for the perturbed and unperturbed simultaneous subgradient projection method is considered. It turns out that the effort for the perturbed method is less than $4 \cdot 10^{-3}$% higher than for its unperturbed counterpart in the IMRT cases we considered.
An interesting direction for future research could be to improve the strategy to detect whether a convex feasibility problem is inconsistent, which in general is a nontrivial task. In both of our approaches this difficulty is not addressed. Detecting inconsistency in the way we implemented it, i.e. by exceeding a maximum number of iterations, is computationally expensive and does not give any kind of guarantee, that the feasibility problem is indeed inconsistent. Using other strategies for detecting inconsistency might provide more insight on the quality of the solutions found by the algorithmic operators used to solve the convex feasibility problems.
As a perspective, it would be very interesting to find out if our strategies are applicable to areas other than IMRT optimization in an equally successful way. In particular the Nesterov, heavy ball or surrogate constraint perturbation could prove to be useful for other optimization problems where the algorithmic operator used to solve them both is bounded perturbation resilient and exhibits zigzagging behavior.

Scientific career

04/2015 – 04/2019	PhD in Mathematics at the Technical University of Kaiserslautern (funded by a scholarship of the Fraunhofer ITWM and the Technical University of Kaiserslautern)
09/2014 – 03/2015	ProSAT at the Technical University of Kaiserslautern
10/2006 – 12/2013	Diploma in Mathematics at the University of Bremen Title of the diploma thesis: *Asymptotical analysis of electroimpedancetomography with small inhomogenities*

Akademischer Werdegang

04/2015 – 04/2019	Promotionsstudium in Mathematik an der Technischen Universität Kaiserslautern (finanziert von einem Stipendium des Fraunhofer ITWM und der Technischen Universität Kaiserslautern)
09/2014 – 03/2015	ProSAT an der Technischen Universität Kaiserslautern
10/2006 – 12/2013	Diplomstudium Mathematik an der Universität Bremen Titel der Diplomarbeit: *Asymptotische Analysis zur Elektroimpedanztomographie von kleinen Einschlüssen*

Publication list of the author

Parts of this thesis have been submitted or published in the following articles.

[4] E Bonacker, A Gibali, KH Küfer, and P Süss.
Speedup of lexicographic optimization by superiorization
and its applications to cancer radiotherapy treatment.
Inverse Problems, 33(4):044012, 2017.

[5] E Bonacker, A Gibali, and KH Küfer.
Accelerating two projection methods via perturbations
with application to intensity-modulated radiation therapy.
Applied Mathematics and Optimization, 2019.
https://doi.org/10.1007/s00245-019-09571-4

Bibliography

[1] M Alber, G Meedt, F Nüsslin, and R Reemtsen. On the degeneracy of the IMRT optimization problem. *Medical Physics*, 29(11):2584–2589, 2002.

[2] H Attouch, Z Chbani, J Peypouquet, and P Redont. Fast convergence of inertial dynamics and algorithms with asymptotic vanishing viscosity. *Mathematical Programming*, 168(1-2):123–175, March 2018.

[3] C Bargetz, S Reich, and R Zalas. Convergence properties of dynamic string-averaging projection methods in the presence of perturbations. *Numerical Algorithms*, 77(1):185–209, Jan 2018.

[4] M Bazaraa, H Sherali, and C Shetty. *Nonlinear Programming: Theory and Algorithms*. John Wiley & Sons, third edition, 2006.

[5] DP Bertsekas. *Nonlinear Programming: 2nd Edition*. Athena Scientific, 1999.

[6] E Bonacker, A Gibali, K-H Küfer, and P Süss. Speedup of lexicographic optimization by superiorization and its applications to cancer radiotherapy treatment. *Inverse Problems*, 33(4):044012, 2017.

[7] T Bortfeld and W Schlegel. Optimization of beam orientations in radiation therapy: some theoretical considerations. *Physics in Medicine & Biology*, 38(2):291, 1993.

[8] J M Borwein, S B Lindstrom, B Sims, A Schneider, and M P Skerritt. Dynamics of the douglas-rachford method for ellipses and p-spheres. *Set-Valued and Variational Analysis*, 26(2):385–403, Jun 2018.

[9] A Brahme. Dosimetric precision requirements in radiation therapy. *Acta Radiologica. Oncology*, 23:379–391, 1984.

[10] RE Burkhard, H Leitner, R Rudolf, T Siegl, and E Tabbert. Discrete optimization model for treatment planning in radiation therapy. In H Hutten, editor, *Science and Technology for Medicine, Biomedical Engineering in Graz*. Pabst, 1995.

[11] D Butnariu, R Davidi, GT Herman, and IG Kazantsev. Stable convergence behavior under summable perturbations of a class of projection methods for convex feasibility and optimization problems. *IEEE Journal of Selected Topics in Signal Processing*, 1(4):540–547, 2007.

[12] F Carlsson and A Forsgren. Iterative regularization in intensity-modulated radiation therapy optimization. *Medical Physics*, 33(1):225–234, 2006.

[13] A Cegielski. *Iterative Methods for Fixed Point Problems in Hilbert Spaces*. Springer-Verlag Berlin Heidelberg, 2013.

[14] Y Censor. Weak and strong superiorization: Between feasibility-seeking and minimization. *Analele Stiintifice ale Universitatii Ovidius Constanta, Seria Matematica*, 23, 10 2014.

[15] Y Censor. Superiorization and perturbation resilience of algorithms: a continuously updated bibliography. *arXiv preprint arXiv:1506.04219*, 2015.

[16] Y Censor and Zenios S A. *Parallel Optimization: Theory, Algorithms, and Applications*. Oxford University Press, 1997.

[17] Y Censor, MD Altschuler, and WD Powlis. On the use of Cimmino's simultaneous projections method for computing a solution of the inverse problem in radiation therapy treatment planning. *Inverse Problems*, 4(3):607–623, 1988.

[18] Y Censor, W Chen, and H Pajoohesh. Finite convergence of a subgradient projections method with expanding controls. *Applied Mathematics & Optimization*, 64(2):273–285, Oct 2011.

[19] Y Censor, T Elfving, and GT Herman. Averaging strings of sequential iterations for convex feasibility problems. *Studies in Computational Mathematics*, 8:101–113, 12 2001.

[20] Y Censor, GT Herman, and M Jiang. Superiorization: theory and applications. *Inverse Problems*, 33(4):040301, mar 2017.

[21] Y Censor and D Reem. Zero-convex functions, perturbation resilience, and subgradient projections for feasibility-seeking methods. *Mathematical Programming*, 152(1):339–380, Aug 2015.

[22] PL Combettes. Hilbertian convex feasibility problem: Convergence of projection methods. *Applied Mathematics and Optimization*, 35(3):311–330, May 1997.

[23] PL Combettes and J Luo. An adaptive level set method for nondifferentiable constrained image recovery. *IEEE Transactions on Image Processing*, 11(11):1295–1304, 2002.

[24] C Cotrutz, M Lahanas, C Kappas, and D Baltas. A multiobjective gradient-based dose optimization algorithm for external beam conformal radiotherapy. *Physics in Medicine and Biology*, 46(8):2161–2175, jul 2001.

[25] R Davidi, Y Censor, RW Schulte, S Geneser, and L Xing. Feasibility-seeking and superiorization algorithms applied to inverse treatment planning in radiation therapy. *Contemporary Mathematics*, 636:83–92, 2015.

[26] A R De Pierro and A N Iusem. A finitely convergent "row-action" method for the convex feasibility problem. *Applied Mathematics and Optimization*, 17(1):225–235, Jan 1988.

[27] JO Deasy, AI Blanco, and VH Clark. Cerr: A computational environment for radiotherapy research. *Medical Physics*, 30(5):979–985, 2003.

[28] Q-L Dong, A Gibali, D Jiang, and S-H Ke. Convergence of projection and contraction algorithms with outer perturbations and their applications to sparse signals recovery. *Journal of Fixed Point Theory and Applications*, 20(1):16, Jan 2018.

[29] Q-L Dong, A Gibali, D Jiang, and Y Tang. Bounded perturbation resilience of extragradient-type methods and their applications. *Journal of Inequalities and Applications*, 2017(1):280, Nov 2017.

[30] R Dudek. Iterative method for solving the linear feasibility problem. *Journal of Optimization Theory and Applications*, 132(3):401–410, 2007.

[31] E Garduño and GT Herman. Superiorization of the ml-em algorithm. *IEEE Transactions on Nuclear Science*, 61(1):162–172, 2014.

[32] A Gibali, K-H Küfer, D Reem, and P Süss. A generalized projection-based scheme for solving convex constrained optimization problems. *Computational Optimization and Applications*, 70(3):737–762, Jul 2018.

[33] A Gibali, K-H Küfer, D Reem, and P Süss. A generalized projection-based scheme for solving convex constrained optimization problems. *Computational Optimization and Applications*, 70(3):737–762, 2018.

[34] F Glover. A multiphase-dual algorithm for the zero-one integer programming problems. *Operations Research*, 13(6):879–893, 1965.

[35] OCL Haas, KJ Burnham, and JA Mills. *Adaptive error weighting scheme to solve the inverse problem in radiotherapy*. Coventry University, 1997.

[36] HW Hamacher and K-H Küfer. Inverse radiation therapy planning: A multiple objective optimization approach. *Discrete Applied Mathematics*, 118(1-2):145–161, 2002.

[37] GT. Herman. Superiorization for image analysis. In RP. Barneva, VE Brimkov, and J Šlapal, editors, *Combinatorial Image Analysis*, pages 1–7, Cham, 2014. Springer International Publishing.

[38] GT Herman, E Garduño, R Davidi, and Y Censor. Superiorization: An optimization heuristic for medical physics. *Medical Physics*, 39(9):5532–5546, 2012.

[39] A Holder. Partitioning multiple objective solutions with applications in radiotherapy design. *Technical Report54, Trinity University Mathematics*, 2001.

[40] AS Householder and FL Bauer. On certain iterative methods for solving linear systems. *Numerische Mathematik*, 2(1):55–59, 1960.

[41] W Jin, Y Censor, and M Jiang. A heuristic superiorization-like approach to bioluminescence tomography. *IFMBE Proceedings*, 39:1026–1029, 01 2013.

[42] S Kim, H Ahn, and S-C Cho. Variable target value subgradient method. *Mathematical Programming*, 49(1):359–369, 1990.

[43] K Kiwiel. The efficiency of subgradient projection methods for convex optimization, part i: General level methods. *SIAM Journal on Control and Optimization*, 34(2):660–676, 1996.

[44] K Kiwiel. The efficiency of subgradient projection methods for convex optimization, part ii: Implementations and extensions. *SIAM Journal on Control and Optimization*, 34(2):677–697, 1996.

[45] K-H Küfer, A Scherrer, M Monz, F Alonso, H Trinkaus, T Bortfeld, and C Thieke. Intensity-modulated radiotherapy – a large scale multi-criteria programming problem. *OR Spectrum*, 25(2):223–249, May 2003.

[46] M Lahanas, E Schreibmann, and D Baltas. Multiobjective inverse planning for intensity modulated radiotherapy with constraint-free gradient-based optimization algorithms. *Physics in Medicine and Biology*, 48(17):2843–2871, 2003.

[47] EK Lee, T Fox, and I Crocker. Simultaneous beam geometry and intensity map optimization in intensity-modulated radiation therapy. *International Journal of Radiation Oncology*Biology*Physics*, 64(1):301 – 320, 2006.

[48] K Miettinen. *Nonlinear Multiobjective Optimization*. Kluwer Academic Publishers, 1999.

[49] Y Nesterov. *Introductory Lectures on Convex Optimization: A Basic Course*, volume 87 of *Applied Optimization*. Kluwer Academic Publishers, 2004.

[50] Y Nesterov. Smooth minimization of non-smooth functions. *Mathematical Programming*, 103(1):127–152, 2005.

[51] Y Nesterov. Gradient methods for minimizing composite functions. *Mathematical Programming*, 140(1):125–161, 2013.

[52] Y E Nesterov. A method for solving the convex programming problem with convergence rate o$(1/k^2)$. *Doklady Akademii Nauk SSSR*, 269:543–547, 1983.

[53] A Niemierko. Reporting and analyzing dose distributions: a concept of equivalent uniform dose. *Medical Physics*, 24:103–110, 1997.

[54] U Oelkfe and C Scholz. *Dose Calculation Algorithms*, pages 187–196. Springer Berlin Heidelberg, Berlin, Heidelberg, 2006.

[55] Cancer Care Ontario. Dose objectives for head and neck imrt treatment planning recommendation report, Feb 2014. URL: `https://www.cancercareontario.ca/sites/ccocancercare/files/guidelines/full/DoseObj_HN_IMRT_TrtmtPlngRec_0.pdf`.

[56] B T Polyak. Some methods of speeding up the convergence of iteration methods. *USSR Computational Mathematics and Mathematical Physics*, 4(5):1 – 17, 1964.

[57] H Romeijn, R Ahuja, J Dempsey, and A Kumar. A column generation approach to radiation therapy treatment planning using aperture modulation. *SIAM Journal on Optimization*, 15(3):838–862, 2005.

[58] H Romeijn, J Dempsey, and J Li. A unifying framework for multi-criteria fluence map optimization models. *Physics in Medicine and Biology*, 49(10):1991–2013, 2004.

[59] A Scherrer. *Adaptive approximation of nonlinear minimization problems - The adaptive clutering method in inverse radiation therapy planning*. PhD thesis, Department of Mathematics, Technische Universität Kaiserslautern, 2006.

[60] W Schlegel and A Mahr. 3D conformal radiation therapy - multimedia introduction to methods and techniques. Springer, 2001.

[61] DM Shepard, MC Ferris, GH Olivera, and TR Mackie. Optimizing the delivery of radiation therapy to cancer patients. *SIAM Review*, 419:721–744, 1999.

[62] W Su, S Boyd, and EJ Candès. A differential equation for modeling nesterov's accelerated gradient method: Theory and insights. *Journal of Machine Learning Research*, 17(153):1–43, 2016.

[63] P Süss. *A primal-dual barrier algorithm for the IMRT planning problem*. PhD thesis, Department of Mathematics, Technische Universität Kaiserslautern, 2008.

[64] P Tseng. On accelerated proximal gradient methods for convex-concave optimization, 2008. URL: `https://www.mit.edu/~dimitrib/PTseng/papers/apgm.pdf`.

[65] S Webb. *The physics of conformal radiotherapy*. IOP Publishing Ltd., 1997.

[66] K Yang and KG Murty. New iterative methods for linear inequalities. *Journal of Optimization Theory and Applications*, 72(1):163–185, 1992.

[67] Y Yu. Multiobjective decision theory for computational optimization in radiation therapy. *Medical Physics*, 24(9):1445–1454, 1997.

[68] X Zhao, KF Ng, C Li, and J-C Yao. Linear regularity and linear convergence of projection-based methods for solving convex feasibility problems. *Applied Mathematics & Optimization*, 78(3):613–641, Dec 2018.

This thesis is motivated by the treatment planning problem in intensity modulated radiation therapy (IMRT). We tackle the multicriteria optimization problem arising from this application by transforming it into a sequence of convex feasibility problems via the level set scheme and then solve each feasibility problem using projection methods. Some characteristics of the IMRT treatment planning problem are challenging to this strategy. Ill-conditionedness and the correlation of the objective functions often lead to zigzagging behavior by the projection methods and therefore slow convergence of the overall optimization procedure. To mitigate these disadvantages, we exploit the bounded perturbation resilience of the projection methods. We introduce three new perturbations designed to avoid the zigzagging behavior and combine them with the projection methods. We study both the theoretical and computational impact of the suggested perturbed iteration schemes. We demonstrate our methods on linear examples and also apply them to nonlinear optimization problems arising from IMRT treatment planning on real cases.

ISBN 978-3-8396-1529-4

9 783839 615294

FRAUNHOFER VERLAG